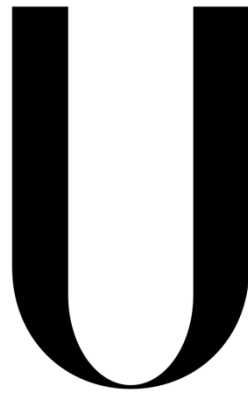


Universidade de Lisboa

Faculdade de Ciências

Departamento de Física



LISBOA

---

UNIVERSIDADE  
DE LISBOA

# Selective functionalization of electrospun fibres

André Francisco Oliveira Girão

Dissertação

Mestrado Integrado em Engenharia Biomédica e Biofísica

Perfil em Engenharia Clínica e Instrumentação Médica

2013



Universidade de Lisboa

Faculdade de Ciências

Departamento de Física



LISBOA

---

UNIVERSIDADE  
DE LISBOA

# Selective functionalization of electrospun fibres

André Francisco Oliveira Girão

Dissertação orientada pelo Professor Doutor Lorenzo Moroni e pelo  
Professor Doutor Hugo Alexandre Ferreira

Mestrado Integrado em Engenharia Biomédica e Biofísica

Perfil em Engenharia Clínica e Instrumentação Médica

2013



the more I see, the less I know

---

# Acknowledgments

---

First of all, I would like to thank Professor Clemmens van Blitterswijk and Associate Professor Roman Truckenmüller for the opportunity of study in the Department of Tissue Regeneration at MIRA, institute of for biomedical technology and technical medicine of the University of Twente. My sincere appreciation is also extended to Associate Professor Lorenzo Moroni for have received me into his research group and proposing me this exciting project.

I owe my deepest gratitude to Maqsood Ahmed and Paul Wieringa for their teachings, patience and most important for their friendship. It was a great honor for me work and learn with Max and Paul during my master studies at University of Twente.

This work would not have been possible without the support and friendship of Professor Hugo Ferreira. I am grateful for his supervision and for having inspired me to look for new and exciting opportunities outside the University of Lisbon.

I was never by myself during my academic journey because my friends were always with me to make me feel at home. Thank you Andreia, Gil, João, Mariana, Melissa, Neuza and Patrícia. I know that you will never let me walk alone.

Finally, I would like to express my gratitude to my parents and sister for their motivation, support and kindness.

---

# Resumo

---

A engenharia de tecidos é uma área multidisciplinar da engenharia biomédica que articula conceitos da química, física, engenharia e medicina com o objetivo de recuperar ou substituir uma função perdida de determinado órgão ou tecido. Um dos principais desafios desta área da biotecnologia é a criação de matrizes tridimensionais biocompatíveis e biodegradáveis que sejam capazes de garantir um suporte físico e bioquímico adequado à regeneração celular. Assim, as características mecânicas, químicas e biológicas destas matrizes devem ser adaptadas ao ambiente celular que se pretende reproduzir, dando origem quer à resposta celular específica das células cultivadas na matriz, quer à otimização da resposta fisiológica do próprio organismo.

Com efeito, dependendo da função a que se destina, as matrizes usadas em engenharia de tecidos variam tanto no biomaterial que lhes dá origem como na técnica de fabricação utilizada. As vantagens dos polímeros face aos outros materiais tais como biocompatibilidade, biodegradação, alta porosidade e boas propriedades mecânicas, tornam-nos no tipo de material mais utilizado na construção de matrizes tridimensionais. É o caso do copolímero PolyActive, já aprovado pela Food and Drug Administration (FDA) e utilizado em múltiplas aplicações em engenharia de tecidos, com especial destaque para a regeneração óssea. A versatilidade deste polímero está estreitamente relacionada com o rácio dos segmentos químicos que o constituem, um segmento hidrofílico de Politereftalato de etileno (PEOT) e outro hidrofóbico de Poli(tereftalato de butileno) (PBT), que ao ser modificado permite o controlo das propriedades mecânicas e químicas do material. Por outro lado, a eletrofiação é uma técnica de fabricação que tem crescido em termos de popularidade pois permite o fabrico de matrizes fibrosas capazes de simular detalhadamente a topografia das fibras de colagénio que compõem a matriz extracelular natural.

Tendo tudo isto em conta, neste estudo foram construídas matrizes tridimensionais de PolyActive por eletrofiação capazes de modular e guiar a resposta celular a partir de recursos topográficos e bioquímicos. A topografia das matrizes foi controlada com a introdução de elétrodos capazes de influenciar o campo elétrico e, assim, alinhar as fibras de PolyActive durante o processo de eletrofiação, que ocorreu num ambiente controlado para garantir a reprodução das propriedades das fibras. Já a incorporação de biomoléculas na superfície das fibras foi conseguida a partir da investigação de duas estratégias distintas.

Numa das abordagens, matrizes fibrosas de dois tipos de PolyActive (1000PEOT70PBT30 e 300PEOT55PBT45) foram expostas a irradiação ultravioleta (UV) com o objetivo de introduzir grupos químicos na superfície das fibras capazes de aumentar a adesão de biomoléculas. As diferenças entre superfícies tratadas e não

tratadas com UV foram analisadas com recurso às técnicas de espectroscopia de infravermelho médio com transformada de Fourier acoplada ao acessório de reflexão total atenuada (ATR-FTIR) e de fotoeletrões excitados por raios X (XPS). Os resultados mostram que os grupos funcionais resultantes da interação da superfície das fibras com o UV dependem do rácio PEOT/PBT e do conteúdo de Polietilenoglicol (PEG) presente no copolímero. Assim, as fibras de 1000PEOT70PBT30 (PA 1000) apresentaram um grande número de grupos carboxilo e hidroxilo na sua superfície devido à degradação do segmento de PEOT e da sua grande cadeia polimérica de PEG após 40 minutos de exposição à radiação UV. Por sua vez, a matriz fibrosa de 300PEOT55PBT45 (PA 300), quando sujeita ao mesmo período de irradiação UV, originou p-benzoquinonas na superfície das suas fibras devido ao alto teor cristalino da sua estrutura. Em ambos os casos, o tratamento UV aumentou as áreas de adesão das proteínas oriundas do meio de cultura celular e por conseguinte a adesão celular tornou-se também mais eficiente. Porém, a resposta celular é dependente não só das características das matrizes, mas também da linha celular utilizada. Por exemplo, as células Schwann de rato mostraram não só preferência pelas áreas ativadas pelo UV, mas também se mostraram sensíveis a pequenas alterações do alinhamento das fibras resultantes das diferenças entre os dois copolímeros. Foi também utilizada uma máscara de níquel para controlar espacialmente a introdução de novos grupos químicos nas superfícies das matrizes fibrosas de PA 300 e PA 1000.

A segunda estratégia apresentada consistiu na eletrofiação de fibras de PA 300 com grupos químicos incorporados para uma funcionalização posterior. Basicamente, uma solução polimérica composta por PA 300 e PEG com determinados grupos funcionais numa proporção 4:1 foi sujeita ao processo de eletrofiação, originando fibras de PA 300 com os grupos funcionais do PEG na sua superfície. Esta abordagem inovadora e inédita possibilitou a seleção dos grupos funcionais localizados na superfície das matrizes fibrosas e consequentemente o controlo do tipo de biomoléculas que vão aderir às fibras. Neste estudo foram utilizados dois tipos de PEG funcionalizado: PEG com terminais alcinos ((bis)PEG-Alkyne), que possibilitam a cicloadição azida-alcino com biomoléculas que tenham a função azida; e PEG com grupos terminais de N-hidroxisuccinimida ((bis)PEG-SVA), que facilitam a ligação com proteínas. As superfícies das matrizes de PA 300 + (bis)PEG-SVA e de PA 300 + (bis)PEG-Alkyne foram analisadas recorrendo às técnicas de ATR-FTIR e XPS. No primeiro caso, os resultados provaram a existência de N-hidroxisuccinimida na superfície das fibras, que depois foi confirmada com recurso a microscopia de fluorescência; relativamente às matrizes de PA 300 + (bis)PEG-Alkyne, apesar das técnicas de espectrometria não produzirem resultados conclusivos, foi possível confirmar a presença de alcinos na superfície das fibras a partir das imagens de microscopia de fluorescência.



O sucesso da segunda abordagem permite abrir as portas ao aparecimento de novas metodologias de design e fabricação de matrizes biofuncionais, já que torna possível a simulação e controlo do ambiente bioquímico que influencia as respostas celulares de uma forma simples e eficiente.

---

# Abstract

---

The principal objective of a new generation of tissue engineering scaffolds is to reproduce the spatial and biochemical microenvironmental characteristics of the natural extracellular matrix (ECM) with the purpose of modulating the cell response and consequently enhance tissue repair. There is an enormous variety of scaffolding approaches that highly depend on the biomaterial selection, on the fabrication technique used and on the specific function of the scaffold.

In this study, bioactive electrospun scaffolds made of PolyActive (Poly(ethylene oxide terephthalate) / Poly(buylene terephthalate) (PEOT/PBT)) copolymer, capable of combining a spatially organized structure with bioactive factors, was developed. The design and fabrication strategies used to create the scaffolds allow the tailoring of the scaffold's function by manipulating the introduction of specific chemical groups on its surface for further selective immobilization of complex biomolecules, resulting in the desired cell response.

In one approach, the surface of both 300PEOT55PBT45 (PA 300) and 1000PEOT70PBT30 (PA 1000) electrospun fibres were modified via UV exposure, resulting in the introduction of specific functional groups able to improve the protein adsorption process and consequently increase the available areas for cell attachment. A spatial definition of protein adsorption was accomplished by exposing the fibres via patterned mask.

An alternative strategy consisted of electrospinning PA 300 fibres with incorporated chemical groups for later functionalization. Alkyne and NHS-esters functional groups were successfully incorporated on the surface of the electrospun fibres via the introduction of specific PEG linkers ((bis)PEG-alkyne and (bis)PEG-SVA) in the electrospinning blend solution. This innovative methodology can be adopted for multiple tissue engineering applications since specific chemical groups can be introduced onto the surface of electrospun fibres, leading to a meticulous selection of the biochemical elements that will be adsorbed and consequently to a detailed control of the cell behaviour.

**Keywords:** tissue engineering scaffold; PolyActive; electrospinning; UV irradiation; (bis)PEG-SVA; (bis)PEG-Alkyne; protein adsorption; click chemistry; Attenuated Total Reflectance Fourier Transform Infrared (ATR-FTIR); X-ray Photoelectron Spectroscopy (XPS).

# Table of contents

List of acronyms .....	13
List of figures .....	14
List of tables .....	16
1. Introduction .....	17
1.1. Materials .....	17
1.1.1. PolyActive .....	19
1.2. Fabrication Techniques .....	26
1.2.1. Electrospinning .....	27
1.3. Scaffold function .....	30
2. State of the Art .....	31
2.1. Surface Modification of electrospun fibres .....	31
2.2. Electrospun fibres for the delivery of bioactive molecules .....	34
2.3. Fabrication of electrospun fibres with the defined structure .....	36
3. Aim .....	39
4. Materials and methods .....	40
4.1. Electrospinning .....	40
4.1.1. PA 300 .....	40
4.1.2. PA 300 + (bis)PEG-SVA .....	40
4.1.3. PA 300 + (bis)PEG-Alkyne .....	41
4.1.4. PA 1000 .....	41
4.2. UV treatment .....	41
4.3. Analysis techniques .....	41
4.3.1. NMR .....	41
4.3.2. ATR-FTIR .....	42
4.3.3. XPS .....	43
4.4. Protein adsorption tests .....	43
4.5. Click Chemistry tests .....	44
4.6. Cell culture .....	44
5. Functionalization of PolyActive electrospun fibres by UV exposure .....	46
5.1. Scaffolds characterization .....	46
5.2. Protein adsorption tests .....	61

5.3.	Cell response .....	65
6.	Electrospinning PA fibres with functional groups .....	69
6.1.	PolyActive + (bis)PEG-SVA electrospun fibres.....	69
6.1.1.	(bis)PEG-SVA/Amine reaction .....	69
6.1.2.	Scaffold characterization.....	71
6.1.3.	Protein adsorption .....	75
6.2.	PolyActive + (bis)PEG-Alkyne electrospun fibres .....	76
6.2.1.	(bis)PEG-Alkyne/Azide reaction .....	76
6.2.2.	Scaffold characterization.....	78
6.2.3.	Click Chemistry tests .....	81
7.	Discussion .....	84
8.	Conclusion .....	91
9.	References.....	92

# List of acronyms

3 D	Three dimensional
ATR-FTIR	Attenuated Total Reflectance Fourier Transform Infrared
BSA	Bovine serum albumin
CHCl <sub>3</sub>	Chloroform
cm	Centimetre
Cu(I)	Copper(I)
ECM	Extracellular Matrix
EDC	1-ethyl-3-(3-dimethylaminopropyl) carbodiimide
FBS	Fetal Bovine Serum
FDA	Food and Drug Administration
FITC-BSA	Albumin-fluorescein isothiocyanate conjugate from bovine
HO <sup>·</sup>	Hydroxyl radical
HFIP	1, 1, 1, 3, 3, 3-hexafluoro-2-propanol
NHS	N-hydroxysuccinimide
nm	Nanometre
NMR	Nuclear Magnetic Resonance
PA	PolyActive
PA 300	300PEOT55PBT45
PA 1000	1000PEOT70PBT30
PBS	Phosphate buffered saline
PBT	Poly(buylene terephthalate)
PEG	Polyethylene glycol
PEO	Polyethylene oxide
PEOT	Poly(ethylene oxide terephthalate)
PO <sup>·</sup>	Alkoxy radical
POO <sup>·</sup>	Alkylperoxy radical
POOOO-P	Tetraoxides
POOH	Hydroperoxide
μm	Micrometre
UV	Ultraviolet irradiation
V	Volume
w	weight
wt %	Weight percent
XPS	X-ray Photoelectron Spectroscopy

# List of figures

- Figure 1 Chemical structure of PEOT/PBT copolymers. Page 19.
- Figure 2 Hydrolysis mechanism of PEOT/PBT in water. Page 21.
- Figure 3 Oxidation of PEO: formation of alkoxy radicals via photo ( $h\nu$ ) and thermal ( $\Delta$ ) conditions. Page 22.
- Figure 4 Oxidation of PEO: formation of the final products via three different pathways. Page 23.
- Figure 5 Photo-oxidative reactions of PEOT. Page 24
- Figure 6 Formation of Hydroperoxides on PBT. Page 25.
- Figure 7 Two different pathways for the Formation of mono and di-hydroxy-substituted compounds. Page 25.
- Figure 8 Schematic of the electrospinning process. Page 28.
- Figure 9 Surface modification scheme for galactose conjugation to PCLEEP electrospun nanofiber scaffold. Page 34.
- Figure 10 Coaxial electrospinning process. Page 37.
- Figure 11 ATR-FTIR spectra of PA 1000 and PA 300. Page 47.
- Figure 12 H-NMR spectra of PA 1000 and PA 300. Page 48.
- Figure 13 FTIR spectra of PA 1000 at various UV exposure times. Page 49.
- Figure 14 FTIR spectra of PA 300 at various UV exposure times. Page 49.
- Figure 15 Degradation pathways of phenol under the UV irradiation. Page 50.
- Figure 16 FTIR spectra of the C-H aromatic zone after various UV exposure times. Page 51.
- Figure 17 FTIR spectra of the C-O-C zone after various UV exposure times. Page 52.
- Figure 18 FTIR spectra of the C-O zone after various UV exposure times. Page 53.
- Figure 19 FTIR spectra of the C-O zone after various UV exposure times. Page 54.
- Figure 20 FTIR spectra of the C-H zone after various UV exposure times. Page 55.
- Figure 21 FTIR spectra of the O-H zone after various UV exposure times. Page 56.
- Figure 22 Spectra of the relative changes in different peak areas of the PA 1000 after various UV exposure times. Page 57.
- Figure 23 Spectra of the relative changes in different peak areas of the PA 300 after various UV exposure times. Page 57.
- Figure 24 C1s peaks of PA 300. Page 60.
- Figure 25 C1s peaks of PA 1000. Page 60.
- Figure 26 Mechanism of covalent attachment of carboxylic acid with protein via EDC/NHS complex. Page 62.
- Figure 27 Representative fluorescence microscope images of PA 300. Page 63.
- Figure 28 Representative fluorescence microscope images of PA 1000. Page 63.
- Figure 29 Fluorescent microscope observations of PA 300. Page 64.
- Figure 30 Fluorescent microscope observations of PA 1000. Page 64.
- Figure 31 Fluorescent microscope observations of PA 300 + UV (40min / Mask) + BSA and PA 1000 + UV (40min/ Mask) + BSA. Page 65.
- Figure 32 Rat Schwann Cells staining. Page 66.
- Figure 33 Rat Schwann Cells staining: PA 1000 + 40min UV irradiation. Page 66.

- Figure 34 Rat Schwann Cells staining: PA 1000 + 40min UV irradiation (UV Mask). Page 67.
- Figure 35 Rat Schwann Cells staining. Page 67.
- Figure 36 Rat Schwann Cells staining: PA 300 + 40min UV irradiation. Page 68.
- Figure 37 Rat Schwann Cells staining: PA 300 + 40min UV irradiation (UV Mask). Page 68.
- Figure 38 Molecular structure of (bis)PEG-SVA. Page 69.
- Figure 39 Reaction of (bis)PEG-SVA with amines on proteins. Page 70.
- Figure 40 H-NMR spectrum of (bis)PEG-SVA. Page 71.
- Figure 41 ATR-FTIR spectrum of PA300 + (bis)PEG-SVA. Page 71.
- Figure 42 Comparison between the ATR-FTIR spectra of PA 300 and PA 300 + (bis)PEG-SVA. Page 72.
- Figure 43 Comparison between the ATR-FTIR spectra of PA 300 and PA 300 + (bis)PEG-SVA. Page 72.
- Figure 44 Comparison between the ATR-FTIR spectra of PA 300 and PA 300 + (bis)PEG-SVA. Page 73.
- Figure 45 C1s peaks of PA 300 + (bis)PEG-SVA. Page 74.
- Figure 46 Fluorescent microscope observations of PA 300 + (bis)PEG-SVA. Page 75.
- Figure 47 Two alternative pathways to the Huisgen 1,3-dipolar cycloaddition reaction: thermal and Cu(I) catalyzed. Page 77.
- Figure 48 Molecular structure of (bis)PEG-Alkyne. Page 77.
- Figure 49 H-NMR spectrum of (bis)PEG-Alkyne. Page 77.
- Figure 50 ATR-FTIR spectrum of PA300 + (bis)PEG-Alkyne. Page 78.
- Figure 51 Comparison between the ATR-FTIR spectra of PA 300 and PA 300 + (bis)PEG-Alkyne. Page 79.
- Figure 52 Comparison between the ATR-FTIR spectra of PA 300 and PA 300 + (bis)PEG-Alkyne. Page 79.
- Figure 53 Comparison between the ATR-FTIR spectra of PA 300 and PA 300 + (bis)PEG-Alkyne. Page 79.
- Figure 54 C1s peaks of PA 300 + (bis)PEG-Alkyne. Page 81.
- Figure 55 Fluorescent microscope observations of PA 300 + (bis)PEG-Alkyne after incubation in a Azidedye /PBS solution. Page 82.
- Figure 56 Fluorescent microscope observations of the negative control PA 300 after incubation in a Azide-dye / PBS solution. Page 82.
- Figure 57 Fluorescent microscope observations of the negative control PA 300 + (bis)PEG-Alkyne before incubation in a Azide-dye / PBS solution. Page 83.
- Figure 58 Incorporation of functionalized PEG linkers on the surface of electrospun scaffolds by two different strategies. Page 88.
- Figure 59 Segregation of a mixed cell population. Page 90.

# List of tables

Table 1	PEO content (wt%) of PEOT/PBT copolymers produced with PEG of different molecular weights at diverse soft to hard segment ratios. Page 20.
Table 2	Relative Changes in the C-H aromatic peak area for PA1000 and PA 300 during UV exposure. Page 51.
Table 3	Relative Changes in the C-O-C peak area for PA1000 and PA 300 during UV exposure. Page 52.
Table 4	Relative Changes in the C-O peak area for PA1000 and PA 300 during UV exposure. Page 53.
Table 5	Relative Changes in the C=O peak area for PA1000 and PA 300 during UV exposure. Page 53.
Table 6	Relative Changes in the C-H peak area for PA1000 and PA 300 during UV exposure. Page 54.
Table 7	Relative Changes in the O-H peak area for PA1000 and PA 300 during UV exposure. Page 56.
Table 8	PA 1000 elemental composition before and after 40 minutes of UV irradiation. Page 58.
Table 9	PA 300 elemental composition before and after 40 minutes of UV irradiation. Page 58.
Table 10	Fractions of various functional groups from PA 1000 C1s peaks. Page 59.
Table 11	Fractions of various functional groups from PA 300 C1s peaks. Page 59.
Table 12	Comparison between the ATR-FTIR peak areas of PA 300 and PA 300 + (bis)PEG-SVA. Page 73.
Table 13	PA 300 + (bis)PEG-SVA elemental composition. Page 73.
Table 14	Fractions of various functional groups from PA 300 + (bis)PEG-SVA C1s peaks. Page 74.
Table 15	Comparison between PA 300 and PA 300 + (bis)PEG-SVA functional groups from N1s peaks. Page 75.
Table 16	Comparison between the ATR-FTIR peak areas of PA 300 and PA 300 + (bis)PEG-Alkyne. Page 80.
Table 17	PA 300 + (bis)PEG-Alkyne elemental composition. Page 80.
Table 18	Fractions of various functional groups from PA 300 + (bis)PEG-Alkyne C1s peaks. Page 81.



# 1. Introduction

Tissue engineering is an interdisciplinary area that applies the principles of clinical medicine, mechanical engineering and materials science to increase and optimize the body's natural response after tissue or organ damage. This field relies extensively in the use of 3D scaffolds able to provide suitable microenvironments that should mimic the natural extracellular matrix, providing both topographical and chemical cues to enhance cell adhesion, proliferation and differentiation towards new tissue formation.

Currently, there are two major tissue engineering approaches. The most popular strategy follows the idea that the new tissue should come from an implant with pre-cultured cells. In this approach, the seeded cells are usually isolated from the host target tissue and they should proliferate in an appropriate 3D dimensional scaffold, before implantation. The other strategy explains that, immediately after injury, an acellular scaffold should be implanted into the defect area. This particular scaffold should be functionalized with specific biomolecules able to recruit progenitor cells towards the injured area, and then promote their proliferation and differentiation with the purpose of regenerating the wounded tissue. Both strategies can also be combined since a functionalized scaffold can be useful in an *ex-vivo* situation by inducing cell seeding, proliferation and differentiation in order to encourage tissue formation after implementation *in vivo*. In this approach it is expected that the scaffold could continue to release signalling molecules with the purpose of enhancing the regeneration of the defect area, even after implementation [1].

In the light of these strategies, to achieve success in tissue engineering, it is necessary to combine and balance the role of cells, scaffolds and biomolecules. To accomplish that, it is crucial that the scaffold not only provides the physical support, but also the chemical agents that will modulate the injury microenvironment. Generally, the scaffold for tissue engineering should present good levels of biocompatibility and biodegradability as well as an architecture and mechanical properties adapted to its specific purpose. So, there are three main topics that should be considered during the scaffold design: choice of the material, manufacturing technology and the final function of the scaffold.

## 1.1. Materials

The choice of a suitable material is a crucial step in the development of scaffolds for tissue engineering applications since the selected material will be responsible for facilitating the generation of a useful size and volume of tissue, allow

an efficient delivery of molecular and mechanical signals to the cells and it should also support the cells and optimize their function within the scaffold. In fact, as the goal of the scaffold is to mimic the advantageous characteristics of the natural extracellular matrix (ECM), the scaffolding material should present physical, chemical and biological properties that enhance biocompatibility and biodegradability in order to avoid unwanted host tissue reaction of the immune system and the damage of the tissues via toxic products, respectively [2,3,4].

Some of the most common categories of biomaterials used in the fabrication of scaffolds for tissue engineering are ceramics, natural polymers and synthetic polymers.

Ceramic scaffolds are mostly used in bone regeneration applications, such as grafting in bone replacement and coating metal implants, because of their mechanical stiffness, low elasticity and hard brittle surface. The most frequent biomedical ceramic is hydroxyapatite (HA) because of its structural and chemical similarity to the mineral phase of the native bone that assures biocompatibility as well as osteoblast differentiation and proliferation. However, ceramics also proved to be difficult to shape for implementation and tricky to adapt to other clinical applications due their brittleness and porous network structure [5,6,7].

In contrast to the ceramic scaffolds, polymers offer design flexibility since the composition, structure and arrangement of their constituent macromolecules can be adapted to different functions. Generally, polymers present appropriate properties for tissue engineering applications like biocompatibility, high surface-to-volume ratio, high porosity, biodegradation and good mechanical features [8]. There are two main types of polymers used as biomaterials: natural polymers and synthetic polymers.

The natural polymers have a very elevated potential for achieving clinical success because they normally exhibit high levels of biocompatibility, biodegradability and low immunogenicity, which consequently enhance the cells performance in the biological systems. They can be classified as proteins (e.g. collagen and gelatin), polysaccharides (e.g. alginate and chitosan) or polynucleotides (DNA, RNA) [8,9]. Natural biomaterials, especially collagen based biomaterials, have been successfully used to support growth of axons and also to deliver multiple cell types into the nervous system after injury. Indeed, the importance of collagen in nerve regeneration applications can be exemplified by the three conduits made of collagen type I for peripheral nerve system regeneration already approved by the FDA (Food and Drug Administration): NeuraGen®, Neuroflex™ and NeuroMarix™ [10]. Besides nerve tissue engineering, natural polymers are currently used in several areas of tissue engineering such as bone tissue engineering [11] and they are also utilized as DNA carriers for gene delivery applications [12].

Relative to the natural polymers, synthetic polymers offer some advantages which includes great design flexibility, reproducibility under controlled conditions and the control of both physical and chemical material properties like porosity, biodegradability and biocompatibility. In addition to this, they are cheaper and represent a more consistent source of raw materials than natural polymers; however there is a higher risk of rejection due the reduced biocompatibility comparing with natural polymers. Typically, the synthetic polymers used in tissue engineering applications are either hydrophobic biodegradable polyesters, such as polyglycolide (PGA), polylactide (PLA), poly( $\epsilon$ -caprolactone) (PCL), or hydrophilic biodegradable polymers like Polyethylene oxide (PEO). Synthetic polymers can be easily combined in order to generate new biomaterials with desirable properties; in this way it is possible to create a material able to conjugate the mechanical properties of the hydrophobic polyesters with the cell affinity of the hydrophilic polymers. For example, poly-dl-lactic-co-glycolic acid (PLGA) is a very versatile and well studied synthetic copolymer that has shown very good performances in mimicking the microenvironment that supports the cells. Some applications include bone [13] and nerve tissue engineering [14]. In fact, some copolymers like Degrapol® and PolyActive® have already found clinical use and are both already FDA approved.

### 1.1.1. PolyActive

The wide range of mechanical properties like elasticity, toughness and strength in combination with easy processability and high levels of biocompatibility offered by the copolymers of poly(ethylene oxide terephthalate)-poly(buylene terephthalate) (PEOT/PBT), make this class of copoly(ether ester)s one top candidate for tissue engineering applications [15,16].

Like other segmented block copolymers, the properties of PEOT/PBT, are determined by the characteristics of the constituting segments: the hydrophilic poly(ethylene oxide terephthalate) segment adds the soft elastomeric, hydrogel-like behaviour into the copolymer while the hydrophobic poly(buylene terephthalate) introduces rigidity (Figure 1)[16,17].

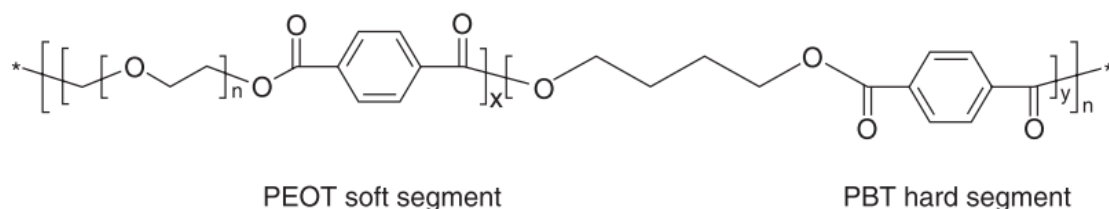


**Figure 1.** Chemical structure of PEOT/PBT copolymers. Adapted from [15].

Deschamps et al. [16,18] have described the preparation of PEOT/PBT as a two step polycondensation of polyethylene glycol (PEG), 1,4-butanediol and dimethyl

terephthalate (DMT) in the presence of titanium tetrabutoxide as catalyst and Irganox 1330 as antioxidant. Firstly there is a transesterification of PEG, DMT and 1,4-butanediol under a nitrogen atmosphere at 180°C, then after two hours, the pressure slowly decreases (from 1000 to 0.1mbar) and the temperature is, at the same time, increased to 240°C in order to enable polycondensation. The composition of the block copolymers is designated as **a**PEOT**b**PBT**c**, where **a** is the starting PEG molecular weight, **b** the weight percentage of PEOT and **c** the percentage of the PBT hard segments. The soft segments weight contribution (**b**) is related not only with the contribution of PEO (polyethylene-oxide) and the terephthalate ester units (T) present in the soft segments, but also with the starting PEG molecular weight (Table 1).

The variations in the soft and hard segments ratio and in the PEG's molecular weight used during the PEOT/PBT copolymers synthesis have different effects on the phase separation of the system and consequently in the tailoring of characteristics such as wettability [19,20], swelling [20], biodegradation rate [16,18], protein adsorption [19] and mechanical properties [16,20]. As the different macromolecules of block copolymers are covalently linked, the macrophase separation is unable to occur; however, microphase separation can still happen [16]. Therefore, the phase separation will be more distinct if there is an increase in PEOT length and in the PBT sequence with further crystallization of these blocks or in the polymers that contain high molecular weight PEG [16].

	Soft/hard segment ratio (wt/wt)					
	100/0	70/30	60/40	55/45	30/70	0/100
PEG 300	100	49	42	38	21	0
PEG 1000	100	62	53	49	26	0
PEG 4000	100	68	58	53	29	0

**Table 1.** PEO content (wt%) of PEOT/PBT copolymers produced with PEG of different molecular weights at diverse soft to hard segment ratios. Adapted from [16].

The swelling capacity and other polymer features like the flexible and plastic behaviour are highly influenced by controlling the polymer mesh size, that is, the effective length of the soft segment between the physical crosslinks. Thus a larger PEO content will result in a larger network mesh size and consequently in an improvement in the swelling ability and viscoelastic parameters. In contrast, decrease of the elastic moduli of the polymer will be noted [17,20].

The PEOT/PBT copolymers have been also extensively investigated in terms of *in vitro* and *in vivo* biocompatibility [18,21] and there are two major types of

degradation process that can occur: hydrolysis of the ester bonds and oxidation of the ether bonds [16]. Because of the PEOT/PBT molecular structure, the degradation mechanisms rates varies from very low for low PEG molecular weight and high PBT content to high for larger contents of PEOT and longer PEO segments [21].

During the hydrolytic degradation of the PEOT/PBT block copolymers in an aqueous media (Figure 2), the hydrophilic domain is more accessible to water uptake; this is because the ester bond present in the PEOT segment (ester A) is more liable to be attacked by water due the great hydrophobicity of the PBT segments [22]. Firstly, the hydrolysis will cause chain scissions of the PEOT segments and consequently provoke an entanglement of the remaining chain molecules, which will then reorganize themselves from a disordered state to an ordered state [22]. The continuous water absorption and the presence of carboxyl acids, that are resulted from the reaction, will initiate new chain scission events and eventually the ester bond in the crystalline region (ester B) will be also attacked by water; ultimately, the whole molecule is broken into pieces [16,22].

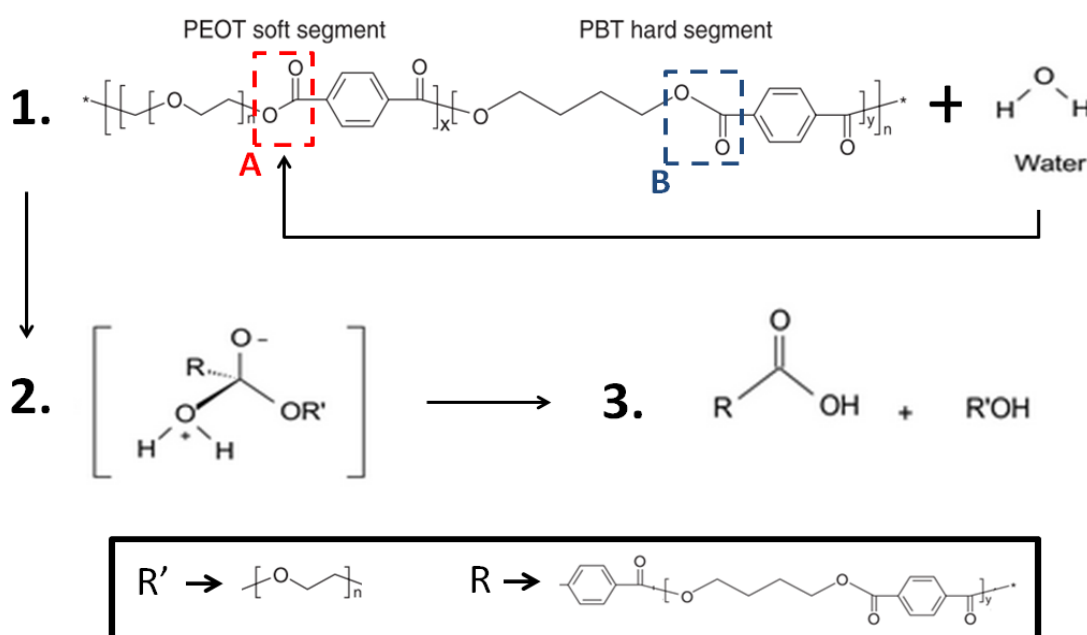


**Figure 2.** Hydrolysis mechanism of PEOT/PBT in water: **1)** The ester bond in the PEOT segment is attacked by water; **2)** The H from H<sub>2</sub>O joins to the oxygen atom in the OR' part of the original ester and the OH part of the H<sub>2</sub>O joins to R; **3)** The products of the reaction are a carboxyl acid and an alcohol.

Unlike hydrolysis, the PEOT/PBT oxidation mechanism can easily occur in the presence of air and, similarly to other polymers containing PEO, it originates scission of the polymer chain via free radical reactions [16]. These radicals are usually produced by photonic activation of chromophores, which can be present either as internal (in-chain) impurities such as hydroperoxides or carbonyls, or external impurities like

polymerization catalyst residues or pollutants from the atmosphere [23,24]. Another possible sources of chromophores include unsaturated groups like C=O or C=C [25,26].

When the formation of the chromophoric radical occurs in the PEO segment, it will lead to the formation of a macroradical in the polymer backbone by hydrogen abstraction of the carbon atoms in the  $\alpha$ -position to the oxygen. The macroradical will then react with atmospheric  $O_2$  and produce an alkylperoxy radical ( $POO\cdot$ ). After that, a new abstraction of a labile hydrogen from the same neighbouring macromolecule can lead to the formation of a hydroperoxide ( $POOH$ ) that will be decomposed by thermal and photo degradation to generate an alkoxy radical ( $PO\cdot$ ) and a hydroxyl radical ( $HO\cdot$ ) (equation 1)[23,27]. An alternative pathway that describes the formation of the alkoxy radical is the recombinations of the alkylperoxy radicals following the Russell type mechanism [23,27,28]. This bimolecular recombination is described by the equation 2, where the peroxy radicals recombine and produce unstable tetraoxides ( $P-O-O-O-P$ ). At the end of the reaction mechanism, the  $P-O-O-O-P$  decomposes to give two alkoxy radicals in a cage and an oxygen molecule (Figure 3) [23,27].

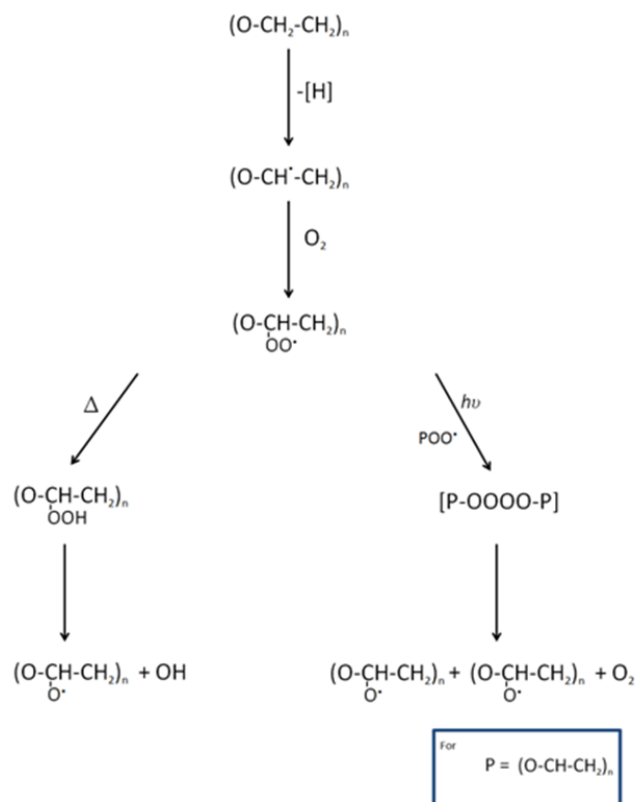
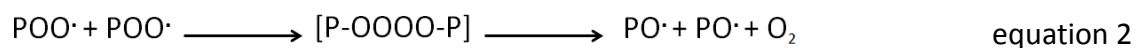
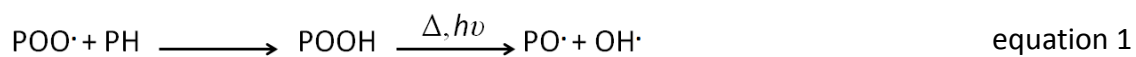


**Figure 3.** Oxidation of PEO: formation of alkoxy radicals via photo ( $h\nu$ ) and thermal ( $\Delta$ ) conditions.

The reaction presented in equation 2 is more common during photo-oxidation of PEO; on the other hand equation 1 usually happens when the PEO thermo-oxidation occurs. After the formation of the alkoxy radical, the oxidation process may proceed by three different pathways, depending on the environment conditions:  $\beta$ -scission, reaction with a hydroxyl radical and hydrogen abstraction reaction of alkoxy radical (Figure 4) [23,29].

The  $\beta$ -scission of the radical leads to the formation of formate end groups that can be produced directly from the scission or from a supplementary pathway, where the oxidation of the macroradicals generated from the scission will lead to the formation of primary hydroperoxides. These primary hydroperoxides because of the thermal and photo-degradation will also produce formates [23].

Other alternative route leads to the formation of ester functions because of the reaction of alkoxy radicals with hydroxyl radicals under thermo-oxidative conditions. Alternatively, the alkoxy radical can be involved in a hydrogen abstraction reaction which will form a thermal unstable hemiacetal that will be decomposed to alcohols and carboxylic acids [23,29].

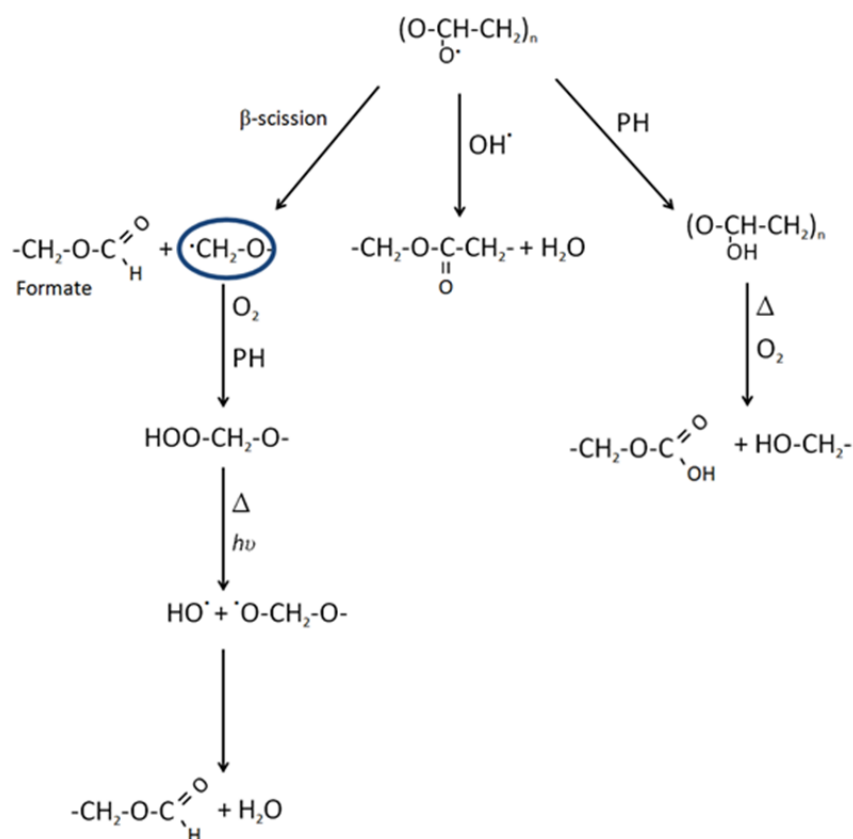


**Figure 4.** Oxidation of PEO: formation of the final products via three different pathways.

Morlat et al. [23] have studied the PEO oxidation mechanism and concluded that the photo-oxidative conditions favour the  $\beta$ -scission of the alkoxy radicals and consequently the generation of formates in a ratio of 5:1 against chain esters. On the

other hand, under thermo-oxidative conditions the production ratio of formates and esters are similar [23,30].

Besides the PEO oxidation mechanism, the PEOT segment can offer an alternative oxidation mechanism via the terephthalate ester units (Figure 5). The key event in this degradation process is also the scission of the polymer main chain that generates carboxyl end groups, volatile products such as CO and CO<sub>2</sub> and it can also produce mono or dihydroxy terephthalates [31].

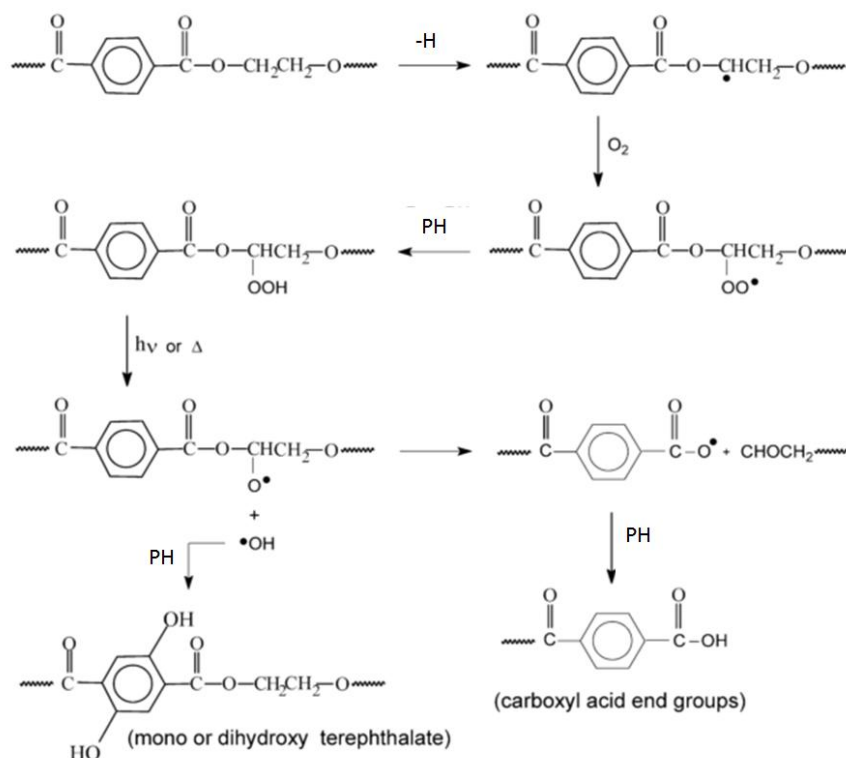
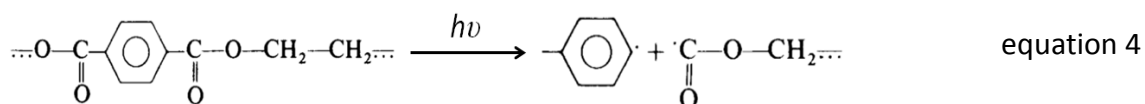
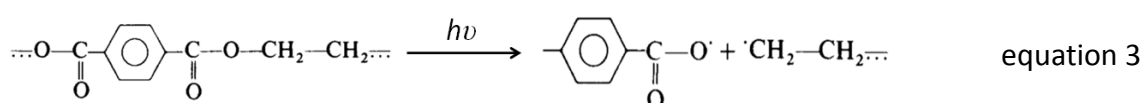
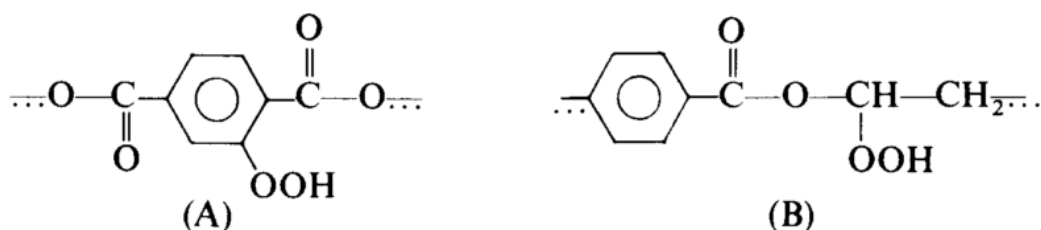
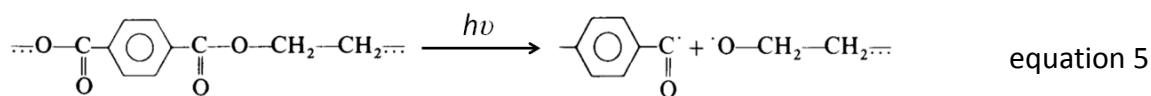


Figure 5. Photo-oxidative reactions of PEOT.

Relative to the PBT segment, the oxidation process is a complex mechanism in which both photolytic and photo-oxidative reactions interfere [32,33]. The activation of the chromophore groups can lead to three direct photo-scission processes (equations 3, 4 and 5) that will generate primary radicals [32]. These radicals are able to provoke the oxidation of the carbon atom located in the  $\alpha$ -position to the oxygen ester by abstraction of labile hydrogen atoms, leading to the formation of hydroperoxides. During photo-oxidation, there is also possible that some hydroperoxides are formed on the aromatic rings (Figure 6) [32,33].







**Figure 6.** Formation of Hydroperoxides on PBT. **a)** on the aromatic ring; **b)** on the  $\alpha$ -position to the oxygen ester. Adapted from [35].

In both cases presented in Figure 6, the homolysis of the hydroperoxides O-O bond generates alkoxy and hydroxyl radicals [33,34]. The alkoxy radicals located on the aromatic ring are able to participate in a hydrogen abstraction reaction involving the polymer chain that will lead to the formation of mono and di-hydroxy-substituted compounds [33,35]. These compounds can also be produced if the hydroxyl radicals, originated from the O-O homolysis at the ester's  $\alpha$ -carbon, react with the aromatic rings of the PBT segment (Figure 7) [33]. The characteristic yellowing of the samples containing PBT can be related to the formation of these compounds and with their further degradation [36].

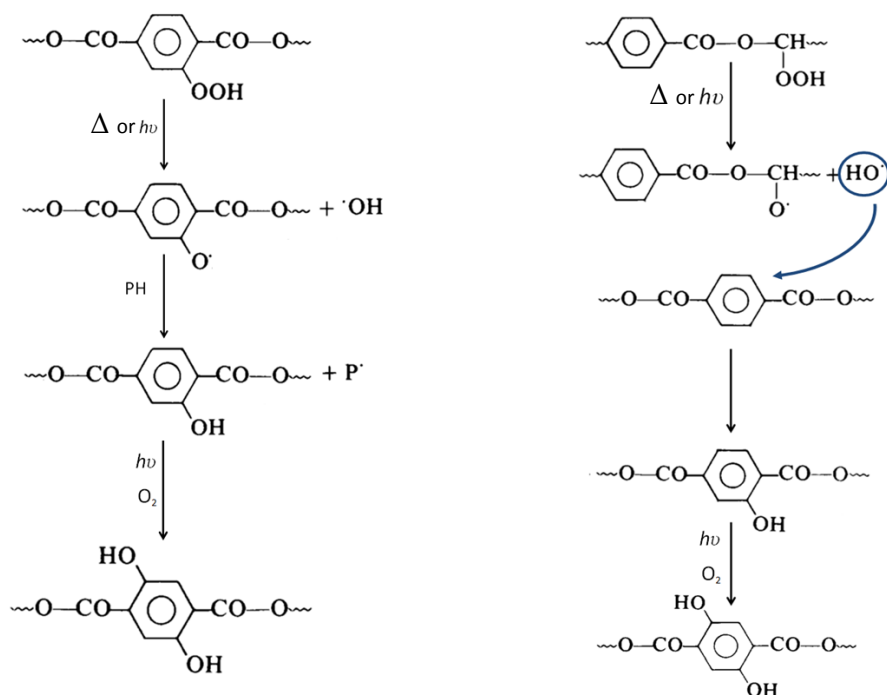


**Figure 7.** Two different pathways for the Formation of mono and di-hydroxy-substituted compounds. Adapted from [35].

The alkoxy radicals produced by the degradation of the unstable hydroperoxides in the carbon  $\alpha$ -position will follow a similar chain of reactions showed in the Figure 5 [32].

In summary, the PEOT/PBT copolymers are excellent candidates as scaffolds in the engineering of both hard and soft tissues because of the easy adaptable properties described above and the good results in the *in vivo* and *in vitro* biocompatibility tests, which have allowed the FDA approval for clinical applications as cement stopper and bone filler in orthopaedic surgery (PolyActive®) [15,18,20].

## 1.2. Fabrication Techniques

There are several techniques to shape polymers into advantageous, complex and reproducible scaffolds that exhibit useful properties for specific tissue engineering applications. The selection of one fabrication technique deeply depends on the desired purpose of the scaffold and the bulk and surface properties of the material.

Fibrous scaffolds are very popular since they can successfully mimic the architecture of the native extracellular matrix at the nanoscale level. In fact, the diameter of the nanofibres that form the scaffold apparatus ranges from 1 to 1000 nm, matching the size scale of extracellular matrix fibres such as collagen (50 to 500 nm). In addition to this, the combination of the high surface area to volume ratio with the microporous structure of the nanofibres enhances cell adhesion, proliferation, migration and differentiation [8,37,38]. There are three production methods that are commonly used to produce fibrous scaffolds: phase separation, self assembly and electrospinning.

Phase separation is a method used to build scaffolds by thermally inducing the separation of a homogeneous polymer solution into a multiphase system, which comprises a polymer-poor phase (low polymer concentration) and a polymer-rich phase (high polymer concentration). Generally, phase separation begins with a polymer dissolution that is followed by a liquid-liquid phase separation process. Then, the upper critical temperatures originate both polymer-poor phase and polymer-rich phase via polymer gelation. At the end, the polymer-rich phase solidifies to form a matrix and the polymer-poor phase originates pores due the solvent removal. The fibre diameter can be modulated by selecting appropriate gelling temperature (high temperatures lead to microfibres and lower temperatures originate nanofibers); on the other hand, the polymer concentration influences the mechanical properties (tensile modulus and tensile strength) of the fibres. Although the phase separation technique do not require specialized equipment and assures the desired shape for the scaffold, it can only be performed by a limited number of polymers (e.g. PLGA and chitosan) and it offers little control over the pre size distribution [37,38,39].

The self assembly process can be defined as an autonomous organization of components such as biomolecules into complex structures due to noncovalent bonds or weak covalent interactions such as electrostatic, van der Waals and hydrophobic interactions. So, in order to build fibrous scaffolds it is necessary that small units like proteins assemble into nanofibres with high aspect ratio, which can mimic the *in vivo* microenvironment of the cells. In fact, this approach can be applied *in vivo* in order to create a nanofibre system able to connect neighbouring cells and consequently organize a three dimensional network capable of mechanically support them. For example, a peptide amphiphile (PA)-based-self-assembling system allows the generation of thermally stable protein-like nanofibres with the purpose of mimicking the extracellular matrix; one possible application of this system uses the changes of the microenvironment pH to induce self assembly processes for bone tissue engineering. However, self assembly is not a very common approach for tissue engineering purposes as it is limited to few polymers and it has low economic viability [37,38,39].

Electrospinning is the most popular fabrication technique to create fibrous since it simpler and more cost effective, compared with both self assembly and phase separation. Because of that, the electrospinning principles will be discussed in detail in the following section.

### **1.2.1. Electrospinning**

Electrospinning is a fairly time- and cost-efficient technique that is used to produce ultrafine micro or nanofibres with considerable surface areas and porosity, flexibility in surface functionalities and advanced mechanical performance (stiffness and tensile strength).

The equipment needed for the electrospinning process includes a syringe pump, a high voltage source and a collector. The procedure is relatively simple and it basically involves the formation of polymer fibres due to electrostatic repulsion of a polymer solution (Figure 8). At the beginning of the process, the polymer solution is held to the needle tip of the syringe (spinneret) via surface tension. Then, the introduction of an electric field originates mutual charge repulsion within the polymer solution that is directly opposite to the surface tension. Upon reaching a critical voltage, the electrostatic force generates localized charges that counterbalance with the surface tension of the polymer solution at the spinneret tip, leading to droplet elongation and stretching until a conical shape known as the Taylor cone is formed, and a continuous jet is ejected. Initially, the polymer jet travels directly towards the grounded collecting plate; however, it will deviate from the most direct path, resulting in a spiralling and further stretching, when the charge density (that increases with the increasing distance from the spinneret) overcomes the surface tension. Finally, the

polymer jet thins in air because of the elongation and the evaporation of the solvent, leading to the formation of electrospun fibres on the target [37,38,40].

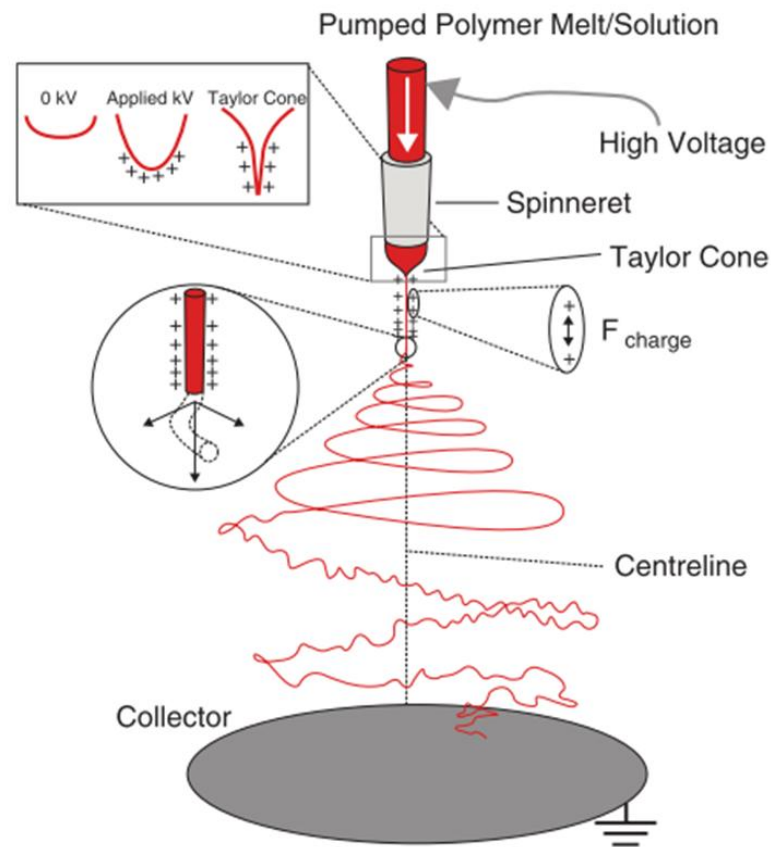


**Figure 8.** Schematic of the electrospinning process. Adapted from [40].

Electrospinning can be performed using a wide range of polymers. In fact, several synthetic polymers like poly(lactic acid) (PLLA), poly(lactic-co-glycolic acid, poly(e-caprolactone) (PCL) and Polyethylene glycol (PEG) have been successfully used to electrospin nanofibres for several tissue engineering applications. For instance, Shin et al. [41] have construct a nanofibre-based PLGA scaffold with the potential of enhanced articular cartilage reconstruction. In another example, hBM-MSCs were able to produce cartilaginous extracellular matrix after being successfully cultured in PCL electrospun nanofibres for cartilage tissue engineering purposes [42].

Natural polymers such as collagen or chitosan can also be electrospun; however they are usually blended with synthetic polymers or salts in order to increase the solution viscosity and consistency [38,40]. For example, Jeong et al. [43] have electrospun composite alginate/ chitosan by adding PEO to the polymer solution. The authors used the ability of this synthetic polymer to increase the polymer chain entanglements and decrease the conductivity of the charged polysaccharide solutions in order to aid the electrospinning process.

The sizes of the electrospun fibres are typically between 200 nm and 5 mm, depending on the conditions. In fact, fibre morphology can be easily controlled by adapting the parameters of the electrospinning process. These parameters can be classified in system parameters, process parameters and ambient parameters [37,40].

The system parameters are mainly associated with the solution properties such as viscosity/polymer concentration, conductivity, surface tension and polymer molecular weight. Generally, increasing the viscosity of the solution by increasing polymer concentration leads to the formation of uniform fibres (without beads and junctions) with larger diameter. Variations in the conductivity by adding salt normally result in small diameter fibres with fewer beads present. A decrease on beading can also be accomplished with higher molecular weight polymers. The effects described above can be very difficult to isolate due the inter-connected relationship between all the polymer solution parameters. For example, it is very common that the conductivity variations affect the viscosity of the polymer solution [37,44,45].

On the other hand, the process parameters are related with the controlled variables such as flow rate, electric field strength, distance between the spinneret and the collector, needle tip design and collector composition and geometry. The effects on the fibre morphology after an increase on the applied voltage are increased beading and decreased diameter. On the other hand, increasing distance from the collector can result in decreased fibre diameter and decreased fibre wetness due the longer evaporation time of the solvent from the nanofibres. Contrary, when the flow rate increases, there are an increment in fibre wetness and bead formation [37,44,45].

The ambient parameters like humidity and temperature are also important for tailoring the nanofibres. As the increasing of the temperature leads to a decrease of the polymer viscosity, the electrospun fibres usually present a smaller diameter. The humidity can affect the morphology of the fibre by the appearance of pores. Although there are studies that corroborate these results, these parameters are poorly understood because their effects depend on the type of polymer, polymer-solvent combination, molecular weight and polymer hydrophilicity [44,45].

Overall, electrospinning has been distinguished as an efficient and versatile technique for the fabrication of polymer micro or nanofibres. In fact, the electrospun scaffolds can be tailored in order to mimic the native extracellular matrix and consequently support the attachment and proliferation of a large variety of cell types. Regardless, it can be a big challenge to engineer scaffolds with complex structures using only the electrospinning approach.

### 1.3. Scaffold function

The term “bioactive scaffold” is currently applied in the tissue engineering field to describe a scaffold capable of not only supporting the cells physically and mechanically, but also enhancing cell adhesion, migration and proliferation as well as phenotype choice via biochemical agents. The goal of these scaffolds is to recreate the functions of the extracellular matrix in a temporally and spatially organized structure [1].

In this way, the function of an optimal scaffold would be providing cell guidance and all aspects of cell response in a similar way as the ECM. Generally, the functions of the ECM include providing structural support and mechanical properties for cells to reside, bioactive cues to enable cells to respond to various signals of their environment, a flexible physical environment to allow a quick and efficient remodelling in case of tissue dynamic process like wound healing and it also act as reservoir of biomolecules and mediates their release. Currently, the scaffolds are able to closely mimic all this features due the physical and chemical characteristics of the materials used and also the microfabrication techniques selected. As explained above, electrospinning can efficiently produce nanofibres with similar dimensions as the collagen fibres from the natural extracellular matrix [46,47].

In terms of bioactivity, scaffolds can be adapted to interact with the cellular components and consequently facilitate and regulate their actions in a dynamic way. In order to accomplish that, the chemistry of the surface should not be only dependent on the properties of the bulk material, but also on the incorporation of biological cues like cell-adhesive ligands (e.g. fibronectin) to promote cell attachment [46]. For example, the surface properties of the poly-acrylonitrile methyl acrylate (PAN-MA) electrospun scaffold were improved by fibronectin adsorption, which proved to influence both the Schwann cells migration and the neurite outgrowth from dorsal root ganglion culture [48]. The scaffolds could also be used as reservoirs or delivery structures for biomolecules such as growth factors. Both hydrogels and electrospun fibres are very popular examples of this type of approach [1,46]. In fact, Holland et al. [49] have managed to create a oligo(poly(ethylene glycol)fumarate / gelatin (OPF/gelatin) hydrogel able to simultaneously deliver insulin-like growth factor-1 (IGF-1) and transforming growth factor- $\beta$ 1 (TGF-  $\beta$ 1) in a controlled manner to cartilage tissue engineering applications. Similarly, Wang et al. [50] have accomplished to release recombinant human bone morphogenetic protein (rhBMP-2) from an electrospun scaffold for bone tissue engineering applications. Besides the biological cues, it is also important that the scaffold provides physical cues like topography to modulate cell morphology and alignment [46]. In tissue engineering approaches, the incorporation of biological and mechanical cues on the surface of the scaffold usually occurs after application of some specific surface modification technique.

## 2. State of the Art

The combination of natural and synthetic polymers can optimize the physical and biological properties of the electrospun scaffolds, as well as mimic the morphology of the extra cellular matrix. However, in order to reach advanced biological and therapeutic applications, the surface of the fibres should be able to immobilize some active agents such as proteins and therapeutic genes without compromising the bulk properties.

For tissue engineering purposes, the role of the immobilized biomolecules on the nanofibres surface should be comparable to the function of the biochemical cues present *in vivo* during tissue regeneration, which is enhancing the specific phenotype and organization of the cells. According to this, several techniques of surface modification such as plasma and radiation treatment are being used on the surface of the electrospun scaffolds to directly enhance cell attachment and proliferation via protein and peptides adsorption. A complementary approach can be followed in the event of the adsorbed biomolecules are further released into the cell environment in a controllable and localized way to promote cell differentiation and proliferation.

In addition to the tissue regeneration proposes, the nanofibre meshes could be also used in drug delivery applications since the highly interconnected open nanoporous structure provides an extremely high surface area to volume ratio that results in a considerable drug loading amount per unit mass.

The electrospinning modality can also influence the properties of the surface by inducing diversification on the performance of the scaffolds. Indeed, the electrospinning technique can be adapted in order to control the composition of the core-shell structure of the fibres or to modulate the surface patterning by topographic cues.

In this way, it is important to understand which techniques are commonly used on surface functionalization and what advantages each one brings into tissue engineering applications (section 2.1). The biomolecule delivery approach will be presented in section 2.2 and the applications that come from different electrospinning modalities will be explained in section 2.3.

### 2.1. Surface Modification of electrospun fibres

The main goal of the surface modification techniques is introduce functional groups on the surface of the electrospun fibres able to immobilize secondary bioactive molecules, guaranteeing at same time good biocompatibility levels and the preservation of the fibres morphology and their bulk properties [51,52].

Gas plasma treatment is a common, suitable and versatile technique that is mainly employed to generate functional groups such as hydroxyl, carboxyl and amino groups on the polymer surface. Normally, it results in an increase of the surface wettability without changing the bulk properties of the material or causing degradation; moreover, it can be used in complex shaped surfaces and it is a solvent free technology [51,53].

Plasma is a high energy state of matter, in which an oxygen or nitrogen containing gas or an inert gas is partially ionized [51,53]. There are two major categories of plasma: the thermal plasmas that cannot be used for biomedical polymers functionalization due to the high temperatures of the gas; and the non thermal plasmas that can be utilized in tissue engineering applications since the combination of low gas temperature and high electron temperature is able to originate chemical and physical changes on the surface without causing any thermal damage [53].

For tissue engineering applications the appropriate selection of the gas (oxygen, air or ammonia) used in the plasma treatment is a critical topic because it decides the functional groups that will be introduced on the target surface and consequently the specific biomolecules that can be covalently immobilized (e.g. collagen, gelatin, laminin and fibronectin) [54,55]. Poly(L-lactic acid)-co-poly( $\epsilon$ -caprolactone) electrospun fibres treated with air plasma were able to immobilize collagen on their surface and consequently improve the attachment, spreading and viability of the coronary artery endothelial cells [56]; in a similar example, Argon plasma treatment was used by Duan et al. [57] in order to build a collagen coated poly( $\epsilon$ -caprolactone) electrospun scaffolds capable of enhancing the attachment, spreading and proliferation of human dermal fibroblasts. In other cases, electrospun PLLA nanofibres pre-treated with plasma were used to adsorb laminin [58] and cationized gelatin [59] for neural and cartilage tissue engineering applications, respectively.

The wet chemical processes like hydrolysis and aminolysis are also suitable approaches to create new functionalities on the surface of biomedical polymers. The procedure involves the reaction between the scaffold and liquid reagents under basic or acidic conditions to generate functional groups by random chemical scission of the ester linkages on the backbone chain located on the surface. Indeed, the degraded and water insoluble polymer fragments, that result from the wet chemical process, are able to generate carboxylic, hydroxyl and amino groups [51,53,54]. Although this process is relatively simple since it does not require specialized equipment, the results are often non specific and non reproducible [53]. So, the duration of the hydrolysis and the concentration of the hydrolysing agents are essential to optimally produce



functional groups without altering significantly the bulk properties of the scaffold [51,54].

The applications of the wet chemical process concerning electrospun fibres are mostly related with bone tissue engineering applications. One example was developed by Jim et al. [60] who were able to create a suitable environment for the proliferation and function of osteoblasts using an electrospun poly( $\epsilon$ -caprolactone) (PCL) fibrous scaffold treated by a controlled hydrolysis in a NaOH medium.

The use of radiation is another method used in tissue engineering applications to modify biomedical polymer surfaces. The most common category of irradiation technique uses ultraviolet light (UV); however there are other types of radiation able to introduce chemical groups on scaffolds' surfaces such as gamma radiation, ozone treatment and ozone combined with UV irradiation. The goal of the radiation approach is to generate reactive areas that can become functional groups or can be used to initiate grafting of monomers or graft polymerization. In fact, radiation is a simple and clean surface modification method since it does not require chemical additives or catalysts, though the dependence on the energy source can lead to nonspecific and non permanent degradation of the polymer backbone [51,53].

The surface modification via UV irradiation is commonly used in tissue engineering applications due its direct effect on protein adsorption and consequently on the cell adhesion process [61]. For example, Welle et al. [62] were able to modify the surface of electrospun Poly(propyl carbonate) (PPC) fibres via deep UV irradiation in order to increase the adsorption of proteins that stimulate cell adhesion. The study showed positive results with both L929 fibroblasts and primary rat hepatocytes cell lines. The UV irradiation can be also used to photo-reduce the  $\text{Ag}^+$  ions within cellulose acetate (CA) nanofibres to build antimicrobial separation filters [63]. Basically, the CA nanofibres electrospun from a combined CA /  $\text{AgNO}_3$  solution were irradiated with UV light with the purpose of producing Ag nanoparticles on their surface.

The relevance of the graft polymerization induced by UV irradiation in the construction of advanced and specific electrospun scaffolds was discussed by Chua et al. in several reports. In one example, the polyethersulfone (PES) electrospun nanofibre scaffold was firstly carboxylated by UV-initiate poly(acrylic acid) (PAAc) grafting and then functionalized with amino groups to facilitate the adhesion and expression of umbilical cord blood hematopoietic stem/progenitor cells (HSPCs) [64]. In another approach followed by the same author [65], a nanofibre scaffold functionalized with galactose was used to study the attachment, the phenotype and the functional maintenance of rat hepatocytes. This strategy is summarized in the Figure 9: initially the Poly(acrylic acid) (PAAc) was grafted onto the surface of the electrospun poly( $\epsilon$ -caprolactone-co-ethyl ethylene phosphate) (PCLEEP) scaffold via UV irradiation; then, the surface carboxyl ( $\text{COOH}$ ) groups were covalently conjugated

with 1-O-(60-aminohexyl)-D-galactopyranoside (AHG) via N-hydroxysulfosuccinimide (sulfo-NHS) / 1-ethyl-3-(3-dimethylaminopropyl) carbodiimide (EDC) complex in order to allow cells attachment through galactose - asialoglycoprotein receptor (ASGPR) interactions.

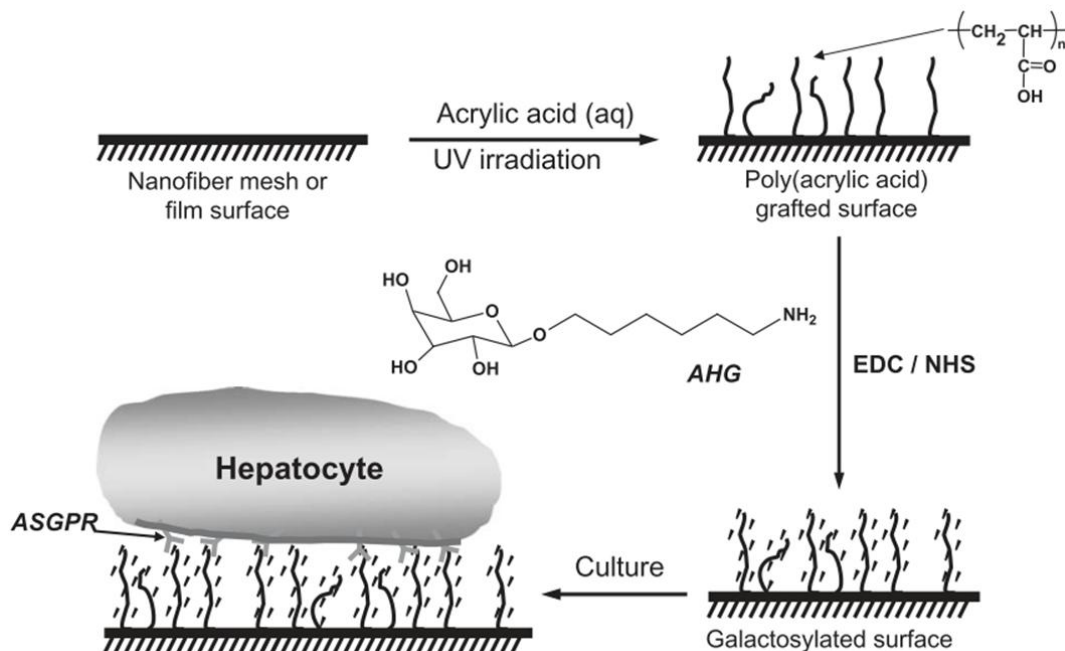


**Figure 9.** Surface modification scheme for galactose conjugation to PCLEEP electrospun nanofiber scaffold Adapted from [65].

Besides the UV irradiation treatment, there are other valid options like gamma irradiation that can be used on surface modification procedures. For instance, it can be used to graft Acrylic acid (AAc) on Poly(L-lactic co-poly-ε-caprolactone) (PLCL) for further immobilization of gelatin; this strategy was applied in a study of the adhesion, spreading and proliferation of human mesenchymal stem cells (hMSCs) by Shin et al. [66]. Using a similar electrospun scaffold, but utilizing photo-grafting Arg-Gly-Asp (RGD) containing peptide instead of gelatin, it was possible study the adhesion and proliferation of the MC3T3-E1 pre-osteoblastic cells [67].

## 2.2. Electrospun fibres for the delivery of bioactive molecules

The surface of the electrospun scaffolds can be chemically functionalized with the purpose of achieving sustained delivery of bioactive molecules. This means that instead of having proteins immobilized on the surface to enhance cell adhesion, the scaffolds should ensure the bioactivity of the incorporated biomolecules and fit their release profile within the adequate time frame [1]. The signalling molecules used depend on the function of the scaffold: cell division can be stimulated by mitogens; the

migration, proliferation and differentiation can be accomplished by the release of proteins such as growth factors and the control generation of tissue form can be due to the morphogens action [68].

Although growth factor delivery scaffolds are usually fabricated using hydrogels due their defined three-dimensional polymer networks that allows easy incorporation of proteins, their limitations like poor mechanical properties, cell death in the depths of the scaffold and the impossibility of having a controlled release over a long time period [69,70] have turned electropun fibres into a viable alternative for protein delivery approaches. Indeed, the electrospun scaffolds can easily act as a drug carrier since their structural characteristics allow good dissolution rate, relative ease of drug incorporation and limited time for dug crystallization [71].

Besides the protein release issue, electrospun scaffolds could also be adapted for gene delivery. The differences between the scaffolds are related with the particularities of both delivery systems: contrary to the growth factors, which act extracellularly by binding to cell surface receptors, target genes must enter into the host genome of endogenous cells, transforming them into bio-activated actors able to produce therapeutic proteins. So, the target genes are usually packed within vectors (viral and non-viral) before incorporation into the scaffold in order to protect the genes from degradation [1].

Physical surface adsorption is a simple approach to load biomolecules into electrospun scaffolds. Basically, the fibres are dipped into an aqueous phase (solution or emulsion) containing biomolecules, which consequently attach to the scaffold via electrostatic forces. For example, BMP-2 was released by a poly(D,L-lactide-co-glycolide)/hydroxyl-lapatite (PLGA/HAp) electrospun scaffold to enhance bone regeneration after being successfully adsorbed by the fibres [72]. The PLGA/Hap electrospun scaffold also proved to be very promising as a DNA delivery device since it was also tested for encapsulation of BMP-2 plasmid DNA/chitosan nanoparticles. The DNA/chitosan nanoparticles released from the PLGA/Hap fibres proven to have a remarkable intracellular effect in the human marrow stem cells (hMSCs) by improving their attachment, viability and transfection efficiency of DNA [73].

In another method named blend electrospinning, biomolecules are mixed within the polymer solution in order to electrospin a hybrid scaffold. As this strategy localizes the biomolecules (e.g. proteins) within the fibres of the scaffolds, it allows more sustained release profiles compared to physical adsorption [1,51]. The common protein release from blend electrospun scaffolds is divided in two periods: during the first 24 hours a burst release occurs due a certain fraction of proteins that are located on the surface of the scaffold; after this period, a sustained release close to a linear mode is observed because of either the protein diffusion process or the polymer degradation process combined with protein diffusion. So, different polymers with

specific properties will originate unique release behaviours [1]. Besides the release profile, the preservation of the biological activity of the biomolecules is a very important prerequisite in designing electrospun scaffolds with the purpose of delivery [51]. For example, basic fibroblast growth factors were introduced into PLGA fibres and their release favoured bone marrow stem cell attachment, proliferation and differentiation [70]. Blend electrospinning was also used to build a PEO/ Bovine serum albumin (BSA) scaffold [74] and a PLLA / laminin electrospun scaffold capable of enhance PC12 cell viability and neurite outgrowth [58].

## **2.3. Fabrication of electrospun fibres with the defined structure**

The function of the electrospun scaffolds can be modulated through the use of several innovative electrospinning techniques that permit the fabrication of multi-layered electrospun fibres and the control of topographic cues.

The core-shell structure is a very useful nanofibre scaffold shape because this structure is capable of containing bioactive agents such as proteins, drugs and enzymes within the core and consequently control their release kinetics. The electrospinning modality used to fabricate this kind of scaffold is called coaxial electrospinning, in which both polymer solution and biological solution are coaxial and simultaneously electrospun without direct mixing by using two aligned syringes (Figure 10). As explained in the section 1.2.1, during coaxial electrospinning, it is necessary to apply appropriate parameters in order to fabricate a suitable electrospun scaffold. Therefore, several factors like feeding rate of the inner and outer fluids, interfacial tension and viscoelasticity of the two solutions can influence the process output by affecting the entrapment of components in the core part and the dimensions of both inner and outer diameters [1,51].

Coaxial electrospinning was recently used for both tissue engineering and drug delivery applications since the release profile includes an initial burst released followed by a sustained release period, which is analogous to the one from blend electrospun scaffolds presented in the previous section. However, the initial burst release from the coaxial electrospun fibres is inferior in volume and consequently more prolonged because of the core characteristics that work as a reservoir system with a biodegradable polymer barrier able to control the biomolecules diffusion rate [1,51]. For example, Sahoo et al. [70] have showed that PLGA coaxial nanofibres are capable of sustaining the release of bFGF from its core for two weeks, a much longer period than the release profile of basic fibroblast growth factors incorporated in a PLGA / bFGF blend scaffold. The release kinetics of proteins from coaxial electrospun scaffolds was thoroughly studied by Zhang et al. [75] that have encapsulated fluorescent-labeled

BSA protein along with PEG in PCL nanofibres with variable dimensions. The report indicated that the release rate is fibre size dependent, which means that smaller-sized fibres have a faster release than the larger ones. These results were able to provide basis for further design and optimization of protein delivery from coaxial electrospun fibres for several tissue engineering applications. For instance, the coaxial electrospun methodology was successfully applied in the building of a composite poly(lactic acid-caprolactone) / nerve growth factor (P(LLA-CL)/NGF) nerve conduit able to promote sciatic nerve regeneration in rats [76].

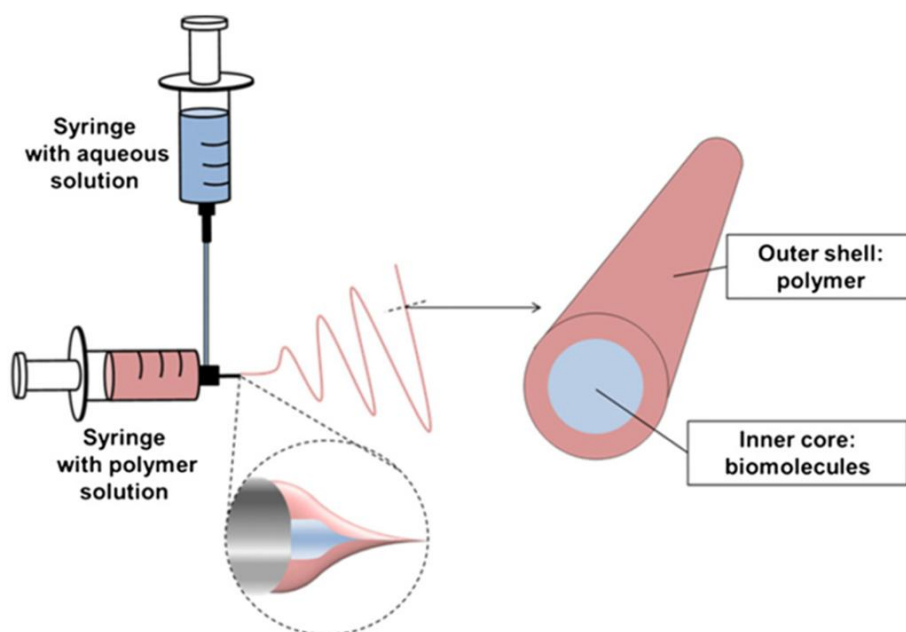


**Figure 10.** Coaxial electrospinning process. Adapted from [51].

Besides the chemical rearrangement of the electrospun fibres, the physical organization and orientation of the fibres also play important roles during the design of the scaffold. This is because the scaffolds should replicate the natural structure of the extracellular matrix, which contains components that are arranged into extremely organized structures to control cell responses [51].

For tissue regeneration applications, the alignment of the fibres can be a critical feature since the cells cultured on such scaffolds are able to recognize the geometry and then align themselves along the fibres [51]. There are two major methods that can be used to accomplish aligned electrospun fibres: high speed rotating drum collector and stationary gap collector.

The use of the rotating drum collector is a simple and mechanical method of aligning the fibres along the circumference of the cylindrical drum. Basically, the collector (grounded or negatively charged) rotates at a high surface speed (over 1500 rpm) to make the electrospun fibres align along the rotating axis. Although it generates

fibres with good alignment, this technique does not offer control over the fibre placement or a high degree of alignment since the deposited fibres accumulate residual charge that will consequently interfere with the incoming ones [77,78,79].

On the other hand, by using the gap method, the alignment of the electrospun fibres is achieved through the manipulation of the electric field. The manipulation is provoked by two parallel conductive electrodes spaced apart that direct the electrospinning jet across the gap as the electric field lines are attracted towards the electrodes. In addition to this, the presence of charges on the deposited fibres will originate mutual repulsion and consequently enhance the parallel and even distribution of the fibres. The main disadvantage of the gap method is the limitation in fibre placement, since the alignment only occurs between the two electrodes; in fact, if the distance that separates the electrodes is too big, the fibres will be deposited on the top of the electrodes and not across the gap [77,78,79].

According to literature, the alignment of the electrospun fibres is particular relevant to the regeneration of skeletal muscle, ligaments, nerve and blood vessels. For example, Aviss et al.[80] have created a PLGA aligned electrospun scaffold able to provide contact guidance for C2C12 myoblast adhesion, elongation and differentiation. In a similar way, a PLLA aligned electrospun scaffold was able to provide better guidance and growth for both neurite and ganglia than random PLLA fibres [81]. A study developed by Xu et al. [82] has described a favourable interaction between an aligned poly(l-lactid-co-e-caprolactone) [P(LLA-CL)] with human coronary artery smooth muscle cells (SMCs). The results showed that the SMCs cultured on the aligned scaffolds had better adhesion and proliferation rate than the ones cultured on plane polymer films; in addition to this, the fibres alignment has influenced the cell migration and the orientation of the cytoskeleton proteins inside the cells, which were parallel to the direction of the nanofibre.

Fibre diameter is other topographic feature of the electrospun fibres that can highly influence certain behaviors of cells such as adhesion, spreading, migration, proliferation and differentiation [51,83]. The investigation developed by Chen et al. [84] showed that the diameter of the PCL fibres affects the adhesion and proliferation of the NIH 3T3 fibroblast cell line. Indeed, the cell adhesion and growth kinetics decreased as a function of increasing diameter when the average fibre diameter was in the nano range; on the other hand, when the fibre diameter was in the micro range, cell adhesion and kinetics showed no variation. These cell behaviors can be either due to the larger surface area-to-volume ratio in the scaffolds with a smaller fibre diameter, which leads consequently to a more efficient growth factors adsorption; or it can be because the cells need less force to migrate within and over the fibres with smaller diameter than the fibres which present a larger diameter.

### 3. Aim

PolyActive is a well known FDA approved copolymer with adaptable surface energy and mechanical properties. Thus, it is commonly used as a biomaterial to create complex scaffolds for several tissue engineering applications and the upgrade of its abilities to mimic the natural extracellular matrix can be accomplished via the electrospinning process.

In this way, the overall motivation of this project was to develop bioactive fibrous scaffolds able to provide selective guidance for cells via topographic and biochemical cues. The topographic cues were accomplished by using the gap method in a controlled environment, allowing the alignment and a controlled deposition of the fibres. For biochemical cues, two distinct surface modification techniques were investigated with the purpose of ensure the immobilization of specific biomolecules.

In one approach, the influence of the UV irradiation in the appearance of new functional groups on the surface of both PA 300 and PA 1000 was studied. The purpose of this strategy was to induce the modification of the fibre surface chemistry with a spatially defined UV exposure, and consequently adjust the degree of biomolecule adsorption.

In the second strategy, two different blend solution of PA 300 + (bis)PEG-SVA and PA 300 + (bis)PEG-Alkyne were electrospun with the intention of incorporate chemical groups on the surface of the fibres, respectively NHS-esters and alkynes, for further functionalization. The concept behind this innovative approach is that depending on the selected PEG linker, it will be possible to induce adsorption of different biomolecules without the need of a previous surface treatment (e.g. plasma or UV). In fact the success of this strategy can open the door for more simple and original methodologies to develop functionalized electrospun scaffolds.

## 4. Materials and methods

The polymer used in this study was PolyActive (PA) copolymer (PolyVation BV, The Netherlands) with a composition of 300PEOT55PBT45 (PA 300) and 1000PEOT70PBT30 (PA 1000), where 300 and 1000 are the molecular weight in  $\text{g mol}^{-1}$  of the starting poly(ethylene glycol) blocks used in the copolymerization, 55 and 70 are the weight ratios of the PEOT segment and the 45 and 30 are the weight ratios of the PBT block.

### 4.1. Electrospinning

#### 4.1.1. PA 300

For electrospinning, a 20% (w/v) solution of PA 300 was prepared in a mixture of chloroform ( $\text{CHCl}_3$ ) and 1, 1, 1, 3, 3, 3-hexafluoro-2-propanol (HFIP) with an 80/20 % v/v. All these solvents were purchased from Sigma-Aldrich. Before use, the solution was left to stir for a minimum period of 12 hours at room temperature. Then, a syringe containing the described solution was pumped at a controlled flow rate (1ml/hour) using a syringe pump (KDS 100, KD Scientific). Polytetrafluoroethylene (PTFE) tubing was used to connect the syringe tip (diameter = 0.8 mm) and the electrospinning nozzle to which a high voltage was applied (Gamma High Voltage Research Inc., FL, USA). The electrospun fibres were aligned on a glass coverslip (diameter = 14 mm) due the presence of two parallel electrodes that were able to modulate the electric field. The electrodes were aligned to the centre of the coverslip and spaced 1 cm from it.

The PA 300 scaffolds were electrospun with a working distance (distance from the collector to the spinneret) of 20 cm and a voltage of 20 kV during 1 minute. The temperature during the spinning was 25°C and the humidity varied between 30% and 35%.

#### 4.1.2. PA 300 + (bis)PEG-SVA

The PA 300 and the (bis)PEG-SVA (SVA-PEG-SVA, MW 5 000, Laysan Bio Inc.) polymers were mixed together with a proportion of 4:1 in a 15% (w/v) solution. The solvents used were chloroform ( $\text{CHCl}_3$ ) and 1, 1, 1, 3, 3, 3-hexafluoro-2-propanol (HFIP) with an 80/20 % v/v.

The PA 300 + (bis)PEG-SVA scaffolds were electrospun with a working distance of 25 cm and a voltage of 25 kV during 1 minute. The temperature during the spinning was 25°C and the humidity varied between 30% and 35%. The electrospinning set up was similar to the one described in the previous section (4.1.1.).



### **4.1.3. PA 300 + (bis)PEG-Alkyne**

The PA 300 and the (bis)PEG-Alkyne (Alkyne-PEG-Alkyne, MW 5 000, Laysan Bio Inc.) polymers were mixed together with a proportion of 4:1 in a 15% (w/v) solution. The solvents used were chloroform ( $\text{CHCl}_3$ ) and 1, 1, 1, 3, 3, 3-hexafluoro-2-propanol (HFIP) with an 80/20 % v/v.

The PA 300 + (bis)PEG-Alkyne scaffolds were electrospun with a working distance of 25 cm and a voltage of 25 kV during 1 minute. The temperature during the spinning was 25°C and the humidity varied between 30% and 35%. The electrospinning set up was similar to the one described in the section 4.1.1.

### **4.1.4. PA 1000**

The PA 1000 solution (15% (w/v)) was prepared in a mixture of chloroform ( $\text{CHCl}_3$ ) and 1, 1, 1, 3, 3, 3-hexafluoro-2-propanol (HFIP) with an 80/20 % v/v. The solution was electrospun in the same set up described before (section 4.1.1.), with a working distance of 25 cm and a voltage of 25 kV during 1 minute. The temperature during the spinning was 25°C and the humidity varied between 30% and 35%.

## **4.2. UV treatment**

PA 300 and PA 1000 electrospun scaffolds were treated with UV irradiation using an UV Crosslinker (UltraLum, model CEX-800) with a wavelength of 254 nm and energy of 1200 mJ. The samples were positioned at a 20 cm from the UV source and the treatment was performed for 5, 10, 20, 40, 90 or 180 minutes.

An auxiliary pattern on the fibrous scaffold surface was produced by a nickel mask with outer dimensions of 2.5 cm X 2.5 cm. The mask was placed on the surface of the scaffold before UV exposure in order to selectively activate specific areas. Indeed, the irradiation only interacts with the surface through 140 rectangles (1.9 cm of high and 21.05  $\mu\text{m}$  of width) spaced by 103.76  $\mu\text{m}$ .

## **4.3. Analysis techniques**

### **4.3.1. NMR**

Nuclear Magnetic Resonance (NMR) spectroscopy is a technique based on the magnetic nuclear spin of isotopes (e.g.  $^1\text{H}$  and  $^{13}\text{C}$ ) and it is commonly used to identify and analyze organic compounds. Basically, the sample is placed in a magnetic field and subjected to a radiofrequency radiation, which, depending on the frequency used, can be absorbed by the nuclei of the sample. This energy absorption promotes a transition between nuclear energy levels (spin flip) and it is highly influenced by the local electronic environment surrounding the nucleus, which can shield the nucleus from

the externally applied magnetic field (nuclear shielding) and therefore modify the difference between the energy levels. These differences in the electron distribution can be due the differences in bond lengths and angles, bonding different atoms or bond types, and they are relative to a standard reference: tetramethylsilane. The association between the resonance frequency of a nucleus and the standard signal is called chemical shift and it is measured in parts per million (ppm). The chemical shifts allow you to indentify different chemical environments that can be determined by Fourier transforming the NMR signal. The resultant spectrum shows the different chemical environments (x-axis is given in ppm) associated with a peak, which area is directly proportional to the number of nuclei in that chemical environment [85,86,87,88].

The  $^1\text{H}$  NMR spectra (Bruker Avance 400 MHz) of the PA 1000 and PA 300 electrospun scaffolds (chapter 5) as well as the (bis)PEG-SVA and (bis)PEG-Alkyne (chapter 6) were recorded using solutions of the indicated polymers in d-chloroform purchased from Sigma-Aldrich. The analysis of the spectra was based on the chemical shifts tables from the Handbook of Basic Tables for Chemical Analysis [89].

#### **4.3.2. ATR-FTIR**

Fourier transform infrared spectroscopy (FTIR) is a spectroscopy technique based on the interaction between the infrared radiation (IR) with a material, in which its molecular vibrations are analyzed. These vibrations are provoked by restricted radiation absorption since each molecule only absorbs the radiation at frequencies that match its unique fundamental modes of vibration. The peaks of the FTIR spectra are associated to the frequencies which radiation is absorbed and consequently to the specific chemical bonds and chemical functional groups present on the material [90]. Besides the identification of the functional groups, it is also possible to do a quantitatively analysis of the sample since the area of one IR peak is an indicator of the specific molecules concentration [91].

As the main goal of the project is to functionalize the surfaces of electrospun scaffolds, a modality of FTIR was selected which is commonly used in surface or near-surface composition characterization: Attenuated Total Reflectance Fourier Transform Infrared (ATR-FTIR). For analysis, the ATR-FTIR process involves a close contact between an internal reflection element (e.g. zinc selenide or germanium crystals) with the sample. As this crystal has a high refractive index, the IR beam is reflected internally and consequently creates an evanescence wave that penetrates in the immediate environment above the crystal. As a result of that, the sample absorbs some energy from the evanescent wave that becomes a signal that later gets converted by Fourier transform to a defined spectrum [90,92]. The main advantage of this technique is that it does not require sample preparation, so the PA 1000 and PA

300 (chapter 5) as well as the PA 300 + (bis)PEG-SVA and PA 300 + (bis)PEG-Alkyne fibrous scaffolds (chapter 6) were analyzed immediately after the electrospinning process. The spectra were recorded (Bruker ALPHA FT-IR Spectrometer) at a resolution of  $4\text{ cm}^{-1}$  and average of 64 scans.

The qualitative analysis of the ATR-FTIR spectra (chapters 5 and 6) was made by using the tables from the Handbook of Basic Tables for Chemical Analysis [89]. Relatively to the quantitative analysis, the areas underneath the peaks were calculated using Microsoft Excel (Microsoft. Microsoft Excel. Redmond, Washington: Microsoft, 2007. Computer Software.) by the trapezoidal rule [93]. In the chapter 5, the chemical changes due the UV irradiation were calculated relatively to the peak areas from the untreated scaffolds.

### **4.3.3. XPS**

X-ray Photoelectron Spectroscopy (XPS) is a highly surface specific technique able to provide qualitative and quantitative information on the atomic composition of a solid's outer surface down to a depth of typically between 0.5 and 10 nm. It is a technique based on a photo-electronic effect: the sample is exposed to X-ray with the purpose of exciting the core-level electrons from the specific type of atoms/ions present on the surface. The energy of the emitted photoelectrons, which is specific for each element, is then analyzed by the electron spectrometer and the data displayed as a spectra of intensity versus electron energy. Besides elemental composition, the photoelectron peaks can also provide useful information about the quantification of the surface composition by calculating their areas [90,92].

XPS was performed by Gerard Kip to determine the chemical composition of the scaffolds (Chapters 5 and 6) and also to calculate any change in the chemical composition due either UV irradiation (chapter 5) or addition of functionalized PEG linkers (chapter 6). The process was carried out on a Quantera SXM (scanning XPS microprobe, 1e 2.6 mA, power 24.8 W, working pressure  $\sim 2\text{e-}8$  Torr, Physical Electronics). The measurements were carried out on electrospun scaffolds either after UV treatment (chapter 5) or after the electrospinning process (chapter 6), on four points per sample with monochromatic Al-K $\alpha$  radiation at 1486.6 eV. The main peak of C1s peak was set at 284.8 eV and Multipak v.9.0.0 was used for data reduction.

## **4.4. Protein adsorption tests**

Albumin-fluorescein isothiocyanate conjugate from bovine (FITC-BSA, Sigma Aldrich) was used as model protein to evaluate the adsorption on UV treated and untreated surfaces of both PA 1000 and PA 300 electrospun scaffolds (chapter 5). FITC-BSA was also used to test the adsorption properties of the PA 300 + (bis)PEG-SVA scaffold (section 6.1.). The scaffolds were incubated in a FITC-BSA / phosphate

buffered saline (PBS) (10 µg / 1 ml) solution at room temperature during 2 hours. After the incubation period, the samples were washed with PBS to remove any non-adherent proteins. The further analysis was carried out via fluorescent microscope observations in a Fluorescence/Histology microscope (NIKON ECLIPSE E600).

Some scaffolds were tested with the complex 1-Ethyl-3-(3-dimethylaminopropyl)carbodiimide / N-Hydroxysuccinimide (EDC/NHS). Scaffolds were immersed in a NHS/EDC (200mM/100mM) PBS solution for 1h at room temperature before the incubation in a FITC-BSA / PBS solution. The EDC and the NHS were purchased from Sigma-Aldrich.

## 4.5. Click Chemistry tests

The click chemistry reaction between the PA 300 + (bis)PEG-Alkyne electrospun scaffold and a model Azide (Azide MegaStokes dye 673, Sigma-Aldrich) was investigated in order to simulate the ability of the scaffold's surface to adsorb azide modified biomolecules. The scaffolds were incubated in an Azide / phosphate buffered saline (PBS) (10 µg / 1 ml) solution at room temperature during 2 hours. After the incubation period, the samples were washed with PBS to remove any non-adherent azide biomolecules. The further analysis was carried out via fluorescent microscope observations in a Microscope Fluorescence Nikon.

## 4.6. Cell culture

The *in vitro* experiments were performed with rat Schwann cells. Before the cell culture experiments, the electropun scaffolds (PA 300 and PA 1000 untreated and treated with UV) were placed on a non-treated well plate (NUNC) and soaked in 70% ethanol for 30 minutes in order to sterilize them. Then, the scaffolds were rinsed with PBS and incubated at 37 °C in a humid atmosphere with 5% CO<sub>2</sub> for 4h in a cell culture medium (Dulbecco's Modified Eagle Medium (DMEM) + 10% Fetal Bovine Serum (FBS) + 1% Penicillin-Streptomycin (pen-strep)) to allow protein adhesion from the medium. To ensure that the electrospun scaffolds would stay in place, rubber O-rings (Eriks BV, The Netherlands) were used to secure them.

15 000 cells (in 200 µl culture medium) were seeded on to each scaffold after removing the medium used for incubation. It was added more culture medium to a volume of 2 ml per well and the scaffolds were incubated for 12h. After the incubation period, the scaffolds were rinsed with PBS and fixed in 10% formalin for 20 min, upon removal of the medium. After that, the membranes of the cells were permeabilized in a 0.5% triton-X solution for 10 min between PBS washing steps. Then, to reduce the nonspecific background staining, the fixed cells were incubated in a PBS solution containing 1% of BSA for 25 minutes. Finally, the actin filaments of the cells were

stained with phalloidin (Sigma-Aldrich) and their nuclei were stained with DAPI (Sigma-Aldrich) for further fluorescent microscope observations in a fluorescence microscope (NIKON ECLIPSE E600).

## **5. Functionalization of PolyActive electrospun fibres by UV exposure**

The structural and functional properties of the surfaces of both PA 1000 and PA 300 electrospun scaffolds were modified via UV irradiation in order to improve protein adsorption and consequently to enhance cell adhesion.

The chemical changes induced by UV irradiation proved to be dependent on the PEOT/PBT wt % and on the molecular weight of PEG. Indeed, after 40 minutes of UV exposure, the PA 1000 electrospun fibres showed a high content of carboxyl and hydroxyl groups on their surface. On the other hand, the higher weight percentage of PBT on the PA 300 fibres provoked the generation of benzoquinones on their surface after 40 minutes of UV treatment. The chemical characterization of the electrospun scaffolds was made via NMR and the analysis of the untreated and treated surfaces was performed by ATR-FTIR and XPS techniques.

The FITC-BSA was used as model protein to evaluate the protein adsorption on untreated and surface treated scaffolds, which showed a considerable enhance in protein immobilization comparing with the UV non-treated surfaces. In terms of cell response, the Rat Schwann Cells successfully attached to both untreated and treated surfaces of PA 1000 and PA 300 scaffolds. However, the larger number of cells attached on the UV treated surfaces indicated the presence of a superior quantity of functional groups able to immobilize adhesion proteins from the culture medium. It was also noticed that the specific chemical composition of PA 300 and PA 1000 induced morphological differences in the cells. A spatially defined surface functionalization was also accomplished in both scaffolds by the use of a UV mask that allowed a preferential protein adsorption on the activated areas. As a consequence of the spatial definition of protein adsorption, the cell attachment occurred mostly on the sites of the electrospun scaffolds that were exposed to UV irradiation.

### **5.1. Scaffolds characterization**

The ATR-FTIR spectrum of PA 1000 samples displayed approximately the same characteristic bands as PA 300 (Figure 11); these results are not surprising since the only differences between the two polymers are the percentages of the PEOT and PBT segments as well as the initial PEG molecular weight.

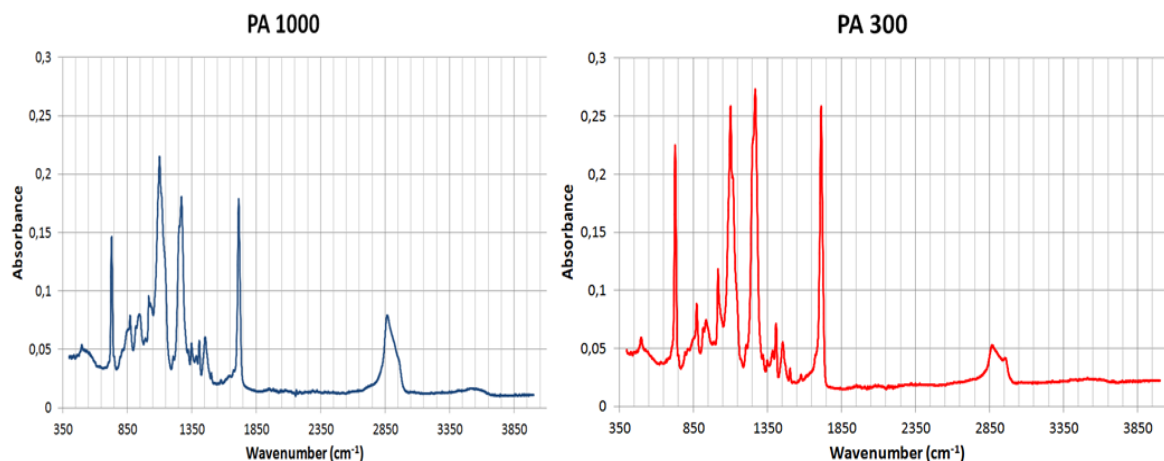


**Figure 11.** ATR-FTIR spectra of PA 1000 (blue) and PA 300 (red).

The FTIR spectrum of PA 1000 fibres shows a more intense absorbance in the C-H stretch region ( $2840 - 3000 \text{ cm}^{-1}$ ) than the PA 300. This is due to the higher PEO content and the longer chains present in the PA 1000. On the other hand, the PA 300 confirms the tendency to be more crystalline than PA 1000 because of the higher absorbance in the aromatic C-H out of plane bending region ( $715 - 735 \text{ cm}^{-1}$ ).

In both cases there are bands at  $1102 \text{ cm}^{-1}$ ,  $1270 \text{ cm}^{-1}$  and  $1714 \text{ cm}^{-1}$ , that are related with the C-O-C stretch of the ether and with the C-O and C=O stretches of the ester, respectively.

The comparison between the  $^1\text{H}$ -NMR spectra of the two polymers showed a similar chemical composition, only with slightly differences because of the dissimilarity in the PEOT/PBT contents. In fact, the higher hydrophilicity of the PA 1000 fibres compared to the PA 300 is illustrated in the Figure 12 as well as the differences in the PBT content. These two features are showed by the peaks at 1.56 ppm (higher in the PA 1000 spectrum) and 8.15 ppm (higher in the PA 300 spectrum), which are related to the water content in the sample (impurity) and with the hydrogen linked to the aromatic ring respectively.

The other peaks present in both spectra are associated with the  $\text{CH}_2$  located on the PEO backbone chain (3.70 ppm), the connection between the ethylene oxide residues connected to the terephthalate unit (3.90 ppm) and with the  $\text{CH}_2$  positioned in the butanediol component of the PBT (2.00 and 4.45 ppm). The  $^1\text{H}$ -NMR results reported here corroborate the results accomplished by Deschamps et al. [18].

One of the reasons why the peaks 2, 3, 4 and 5 are smaller in the PA 1000 spectrum could be because of the hydrolysis process induced by the high water content in this scaffold. The water molecules presented in the PA 1000 fibres could have been absorbed from the atmosphere during the electrospinning process due to the hydrophilicity properties of this polymer.

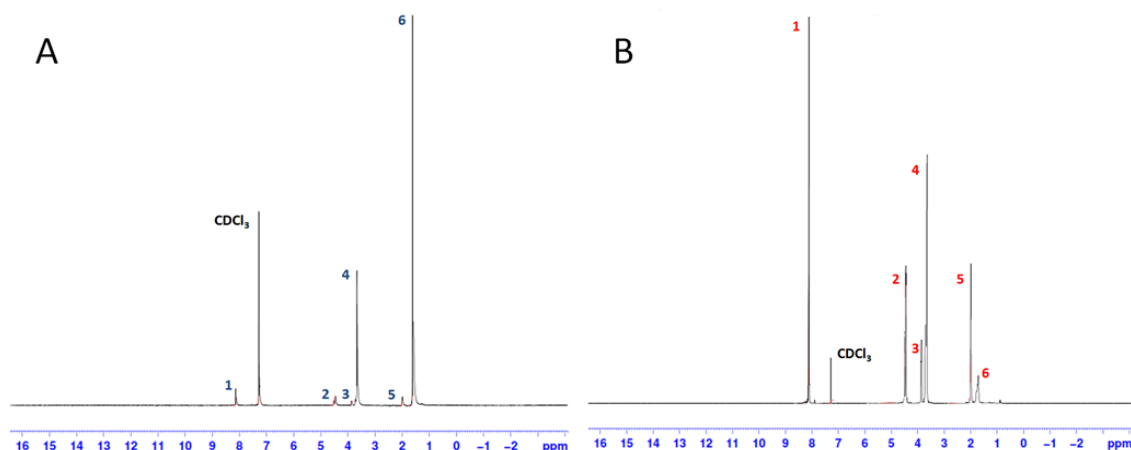


**Figure 12.**  $^1\text{H}$ -NMR spectra of PA 1000 (**A**) and PA 300 (**B**). Legend: 1- Aromatic; 2- Butylene ( $\text{CH}_2$ ); 3 – PEO ( $\text{CH}_2$ ); 4 – PEO backbone chain ( $\text{CH}_2$ ); 5 – Butylene ( $\text{CH}_2$ ); 6 – Water. The solvent peak for  $\text{CDCl}_3$  is located at 7.25 ppm.

The effect of the UV treatment on the surface of the PA 1000 and PA 300 fibres is resumed in the figures 10 and 11, that describe the time evolution of the surfaces chemistry composition during UV exposure. The changes are result of the degradation processes (both hydrolysis and oxidation) that provoke the rearrangement of the molecular structure and the formation of a new region between  $3100$  and  $3700\text{ cm}^{-1}$ . This new region is related to the O-H stretch and it indicates the formation of the new products that are originated during the several stages of the oxidation process (Figure 13).

The UV irradiation of the PA 1000 fibres leads to important modifications in the FTIR spectrum. In fact, during the first 10 minutes of exposure there is an increase in the absorbance bands of the C=O, C-O and C-O-C stretches and at the  $715 - 735\text{ cm}^{-1}$  region, which is due to the aromatic C-H out of plane bends. At the same time, a decrease in the C-H stretch peak and the O-H stretch region is noted. This data can be associated to the consumption of OH and H of the polymer chain for the production of both esters and formates (see Figure 4). The increasing in the  $715 - 735\text{ cm}^{-1}$  region is not related to the aromatic part, but instead to the C-H rocking of the oxidation products.

After this initial irradiation period, the increase of temperature in the system leads to the formation of the alcohols and the degradation of the PBT starts. Indeed, as the photo-oxidation starts in the amorphous phase because of the easy oxygen diffusion [23], it is plausible that the formation of mono and di-hydroxy-substituted compounds starts later then the formate and ester production. The decrease in the other absorbance bands is because of scission chain events originated by both oxidation and hydrolysis ( $\text{H}_2\text{O}$  is also formed during the formates production); The Figure 13 also shows the rise of a shoulder at  $1185\text{ cm}^{-1}$  (C-C-O stretch), which is related to the continuous production of formates [23].



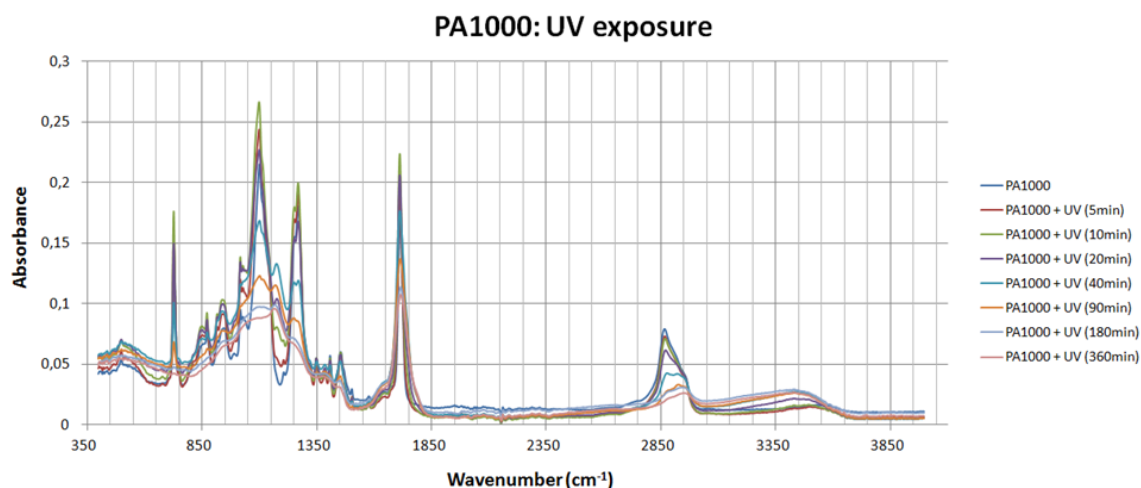


**Figure 13.** FTIR spectra of PA 1000 at various UV exposure times.

A similar analysis can be made for the PA 300 scaffold, and as expected the high PBT content in the fibres has a critical influence in the polymer degradation. Like it was illustrated in the PA 1000, the formation of esters and formates occurs in the first 10 minutes of UV irradiation with an increase in the C-O-C, C-O and C=O stretches and in the C-H rocking absorbance region. The Figure 14 also shows the decrease in the C-H stretch of the backbone chain related to the hydrogen abstraction reactions involved in the PEO segment photo-oxidation. Subsequent to this initial period, comes the decrease of these absorbance bands because of chain scission events.

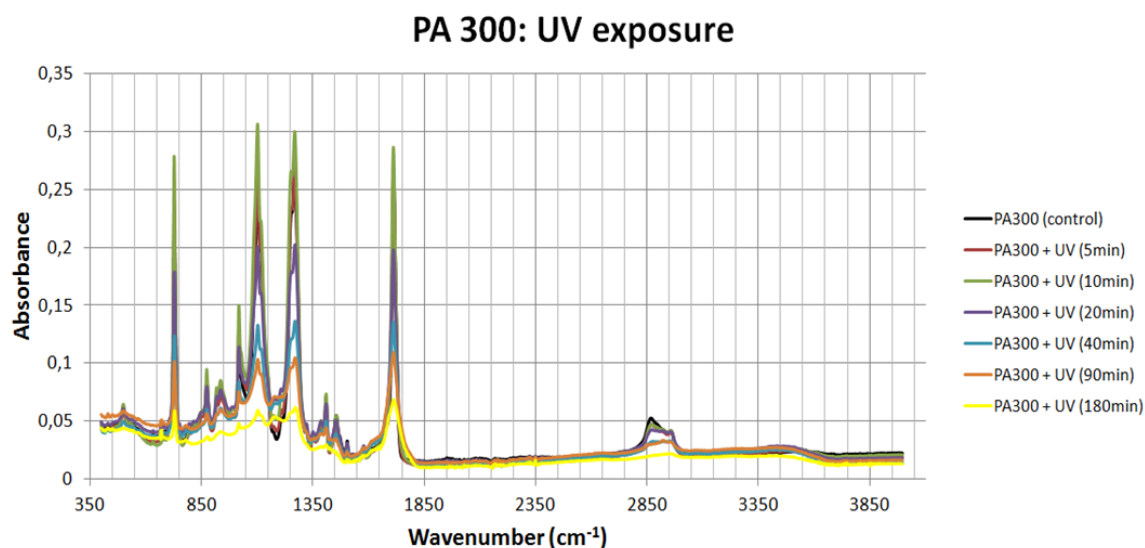


**Figure 14.** FTIR spectra of PA 300 at various UV exposure times.

The degradation of the PBT segment is mainly related with the changes in the O-H peak during UV exposure and with the decrease in the 715 – 735  $\text{cm}^{-1}$  region

(degradation of the aromatic ring). Contrary to the other absorbance bands, the behavior of the O-H region in the PA 300 scaffold isn't similar to the PA 1000 fibres: through the first 5 minutes there is a slight decrease in the O-H peak related to the production of formates and esters, followed by a boost until 20 minutes of exposure time. At this point there is a further decrease until the 40 minutes of UV exposure, when the O-H peak starts to increase again. Finally, during the next 50 minutes of UV irradiation the O-H absorbance region reaches its maximum intensity and then decreases until the end of the treatment.

The behavior of the O-H absorbance region in the PA 300 is mainly because of the high amount of mono and di-hydroxy-substituted compounds, formed during the PBT segment degradation, which are also susceptible to interact with the UV light and consequently originate a new chain of reactions. One possibility pathway is based on the photo-degradation of phenol under UV irradiation (Figure 15) [94,95]. As schematized in Figure 15, a hydroquinone can originate a P-benzonquinone by a reversible redox reaction, which is plausible because of the yellowing of the scaffold during UV exposure. Further irradiation leads to ring cleavage and formation of low mass compounds such as carboxylic acids (acetic acids, etc) and finally CO<sub>2</sub> [95,96].

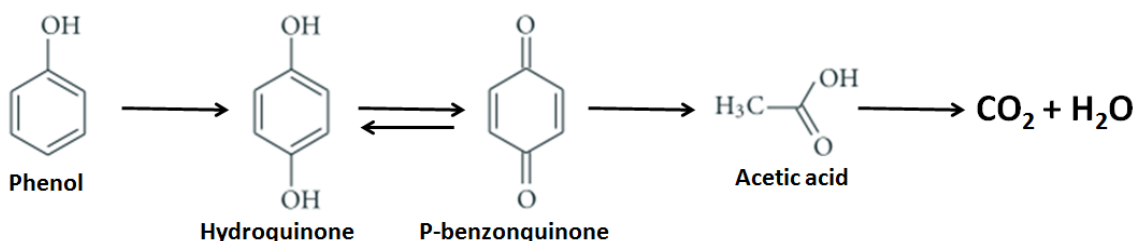


**Figure 15.** Degradation pathways of phenol under the UV irradiation.

The differences between the two scaffolds can be further analyzed by comparing the areas underneath each absorbance peak. In this way, it will be possible to evaluate the relative changes that occur on the PA 1000 and PA 300 surfaces composition during UV exposure.

As described above, the peak area between 715 cm<sup>-1</sup> and 735 cm<sup>-1</sup> is related not only with the C-H out of plane bending region, but also with the C-H rocking of the main chain. The higher crystallinity of the PA 300 is the reason why the peak area is bigger in this polymer compared with PA 1000. However, as the long PEO chain of the PA 1000 is able to produce more formates and esters than the small PEO segment in the PA 300, PA 1000 will show a superior gain in the peak area during the first 10 minutes of UV irradiation. The following peak area decreasing is related with scission chain events and aromatic ring degradation. The results are summarized in Table 2 and Figure 16.

Exposure time (min)	<i>C-H (Aromatic): 715 – 735 cm<sup>-1</sup></i>			
	PA 1000		PA 300	
	Area	Relative Changes (%)	Area	Relative Changes (%)
0	2.08	0	3.11	0
5	2.28	9.62	3.13	0.64
10	2.48	19.23	3.55	14.15
20	2.19	5.29	2.55	-18.01
40	1.64	-21.15	1.87	-39.87
90	1.26	-39.42	1.67	-46.30
180	0.99	-52.40	1.01	-67.52

**Table 2.** Relative Changes in the C-H aromatic peak area for PA1000 (blue) and PA 300 (red) during UV exposure.

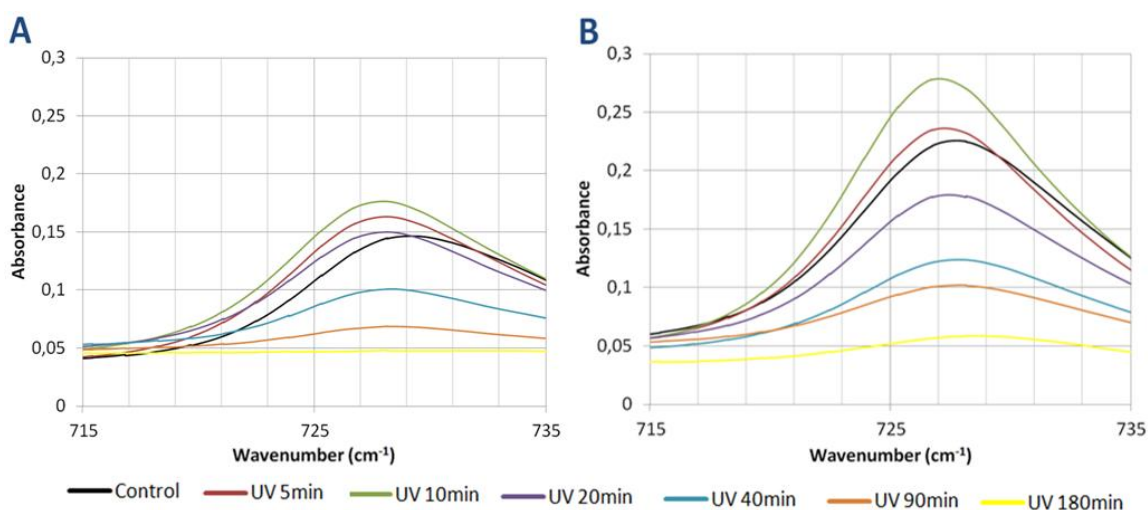


**Figure 16.** FTIR spectra of the C-H aromatic zone after various UV exposure times. **A)** PA 1000 ; **B)** PA 300.

The PA 1000 and PA 300 C-O-C stretches show similar peak areas before UV irradiation because of the high PEO content in one case and the repetition of the PBT chains in other. In a similar way as the C-H aromatic, the formation of formates and esters in the first 10 minutes occurs in both polymers, resulting in an increasing of the peak area. Again, the area increasing is more noticeable in the PA 1000 and the decreasing in both scaffolds is due to the effect of oxidation and hydrolysis (Table 3 and Figure 17).

Exposure time (min)	C-O-C: 1085 – 1150 cm <sup>-1</sup>			
	PA 1000		PA 300	
	Area	Relative Changes (%)	Area	Relative Changes (%)
0	11.14	0	11.24	0
5	12.26	10.05	11.54	2.67
10	13.47	20.92	12.96	15.30
20	12.18	9.34	9.42	-16.19
40	10.14	-8.98	6.71	-40.30
90	7.85	-29.53	5.63	-49.91
180	6.45	-42.10	3.48	-69.04

**Table 3.** Relative Changes in the C-O-C peak area for PA1000 (blue) and PA 300 (red) during UV exposure.

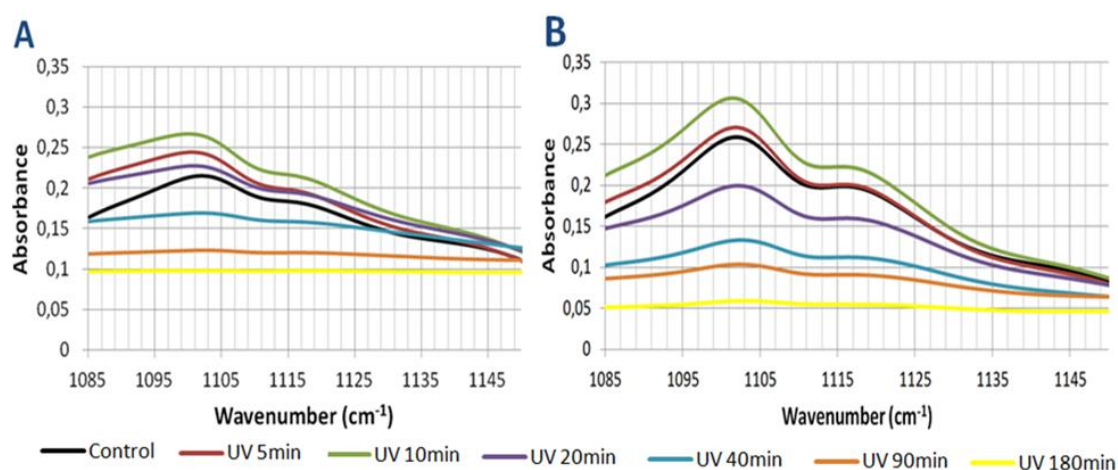


**Figure 17.** FTIR spectra of the C-O-C zone after various UV exposure times. **A)** PA 1000 ; **B)** PA 300.

The analysis of the Tables 4 and 5 and the Figures 18 and 19 confirm a higher concentration of C=O and C-O stretches in the PA 300 scaffold because of its PBT content. However, during the UV irradiation, the formation of esters and formates occurs and the gain in the peak area of these elements becomes superior in the PA 1000. The reason for that is the molecular structure of the PEO's oxidation products, which are formed in larger amounts in PA 1000 than in PA 300. Again, the peak areas decrease after the initial 10 minutes of UV irradiation.

Exposure time (min)	C-O: 1200 – 1300 cm <sup>-1</sup>			
	PA 1000		PA 300	
	Area	Relative Changes (%)	Area	Relative Changes (%)
0	10.32	0	14.17	0
5	11.39	10.37	14.82	4.59
10	12.50	21.12	16.76	18.28
20	11.74	13.76	12.86	-9.24
40	10.56	2.33	9.56	-32.53
90	8.41	-18.51	8.30	-41.43
180	7.10	-31.20	5.30	-62.60

**Table 4.** Relative Changes in the C-O peak area for PA1000 (blue) and PA 300 (red) during UV exposure.

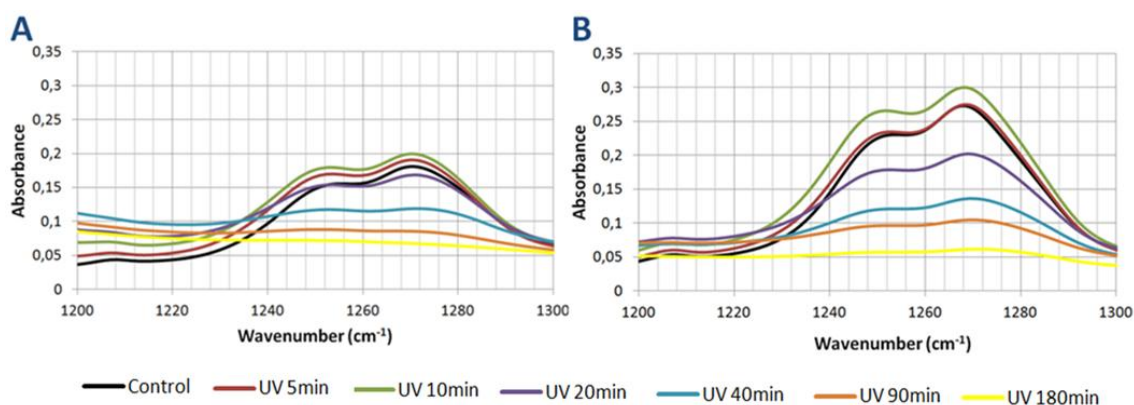


**Figure 18.** FTIR spectra of the C-O zone after various UV exposure times. **A)** PA 1000 ; **B)** PA 300.

Exposure time (min)	C=O: 1700 – 1730 cm <sup>-1</sup>			
	PA 1000		PA 300	
	Area	Relative Changes (%)	Area	Relative Changes (%)
0	3.91	0	5.50	0
5	4.53	15.86	5.63	2.36
10	5.22	33.50	6.11	11.09
20	5.19	32.74	4.66	-15.27
40	5.04	28.90	3.43	-37.64
90	4.10	4.86	2.96	-46.18
180	3.45	-11.76	1.95	-64.55

**Table 5.** Relative Changes in the C=O peak area for PA1000 (blue) and PA 300 (red) during UV exposure.

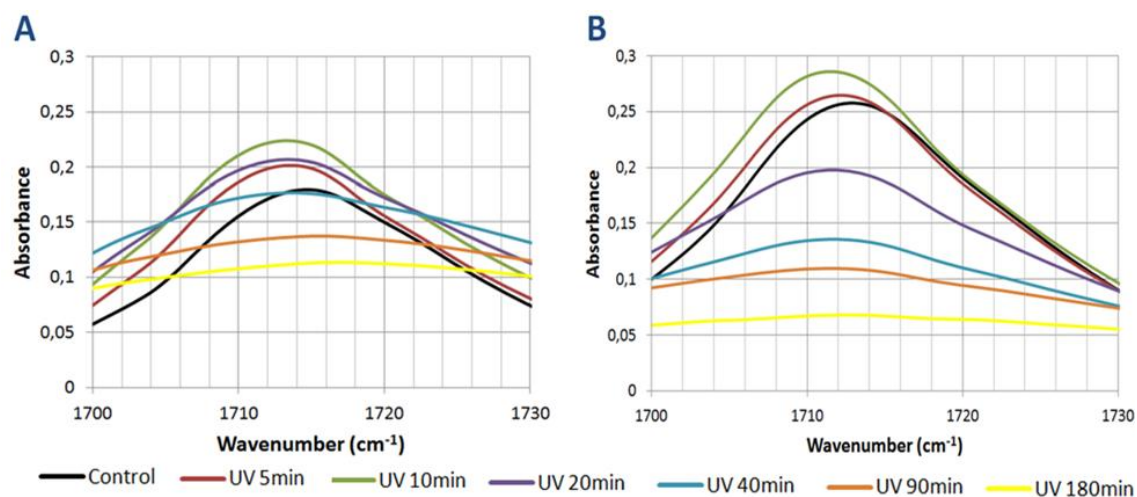


**Figure 19.** FTIR spectra of the C-O zone after various UV exposure times. **A)** PA 1000 ; **B)** PA 300.

The analysis of the C-H stretch related with the backbone chain of the polymers (Table 6 and Figure 20) shows a higher peak area in the PA 1000 before starting the UV treatment. This is because the large PEO chains that characterizes the molecular structure of these fibres. As the hydrogens presented in the main chains of both PA 1000 and PA 300 are deeply involved in the hydrogen abstraction reactions during UV degradation, the peak area in this region starts decreasing from the beginning of the process.

Exposure time (min)	C-H: 2840 – 3000 cm <sup>-1</sup>			
	PA 1000		PA 300	
	Area	Relative Changes (%)	Area	Relative Changes (%)
0	8.27	0	6.63	0
5	7.54	-8.83	6.22	-6.18
10	7.56	-8.59	6.31	-4.83
20	7.08	-14.39	6.08	-8.30
40	5.75	-30.47	4.97	-25.04
90	4.42	-46.55	4.93	-25.64
180	4.40	-46.80	3.35	-49.47

**Table 6.** Relative Changes in the C-H peak area for PA1000 (blue) and PA 300 (red) during UV exposure.

Contrary to the other regions of interest, the temporal evolution under UV irradiation of the O-H stretch is not similar for PA 1000 and PA 300. In fact, the relative gains and losses of this peak area in the PA 1000 are mainly related with the formation of alcohols and carboxylic acids. As it was explained above, the photo degradation of the PEO segments is the most dominant degradation process in PA 1000. In this way, the consumption of OH during the first minutes of UV irradiation leads to the formation of PEO oxidation products; these products (Figure 4) originate the following

boost in the peak area (Table 7 and Figure 21). Although the PBT degradation also occurs in the PA 1000, it has little influence in the ATR-FTIR spectra because of its modest amount in comparison with the PEO present in the PEOT segment.

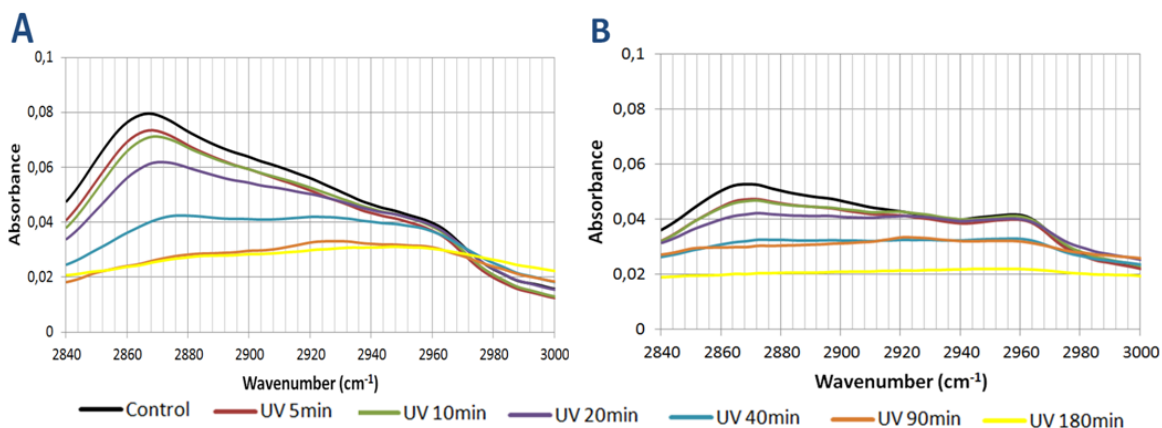


**Figure 20.** FTIR spectra of the C-H zone after various UV exposure times. **A)** PA 1000 ; **B)** PA 300.

On the other hand, the relative changes in the O-H peak area of the PA 300 are related with the photo-oxidation of PBT and with the low PEO content on this polymer. The formation of PEO oxidation products has a diminutive impact in the OH peak area evolution; nevertheless it is possible that this process contributes for the small loss in the absorbance region during the first 5 minutes of UV irradiation. Besides that, the first increasing of the peak area can be due to the formation of the mono and di-hydroxy-substituted compounds in the aromatic ring. Following the scheme in the Figure 7 it is possible that the formation of intermediate compounds like benzoquinones leads to the decreasing between the 20 and 40 minutes of UV exposure; the further degradation of the PA 300 scaffold can originate both substituted phenols and low mass products such as carboxylic acids, leading to a new peak area increasing during the next 50 minutes. Then, the absorbance band decreases again because of the collapse of the aromatic ring and the degradation of the low mass compounds. These results are summarized in Table 7 and Figure 21.

The analysis of the Table 7 also shows that the low molecular weight polymer (PA 300) presents a higher concentration of hydroxyl groups (OH) before UV exposure. This property is related to the chain folding of the PEO segment and it is correlated by Bigger et al. [97].



Exposure time (min)	O-H: 3100– 3700 cm <sup>-1</sup>			
	PA 1000		PA 300	
	Area	Relative Changes (%)	Area	Relative Changes (%)
0	8.33	0	13.32	0
5	6.63	-20.41	13.16	-1.20
10	7.16	-14.05	13.87	4.13
20	9.36	12.36	14.52	9.01
40	11.39	36.73	13.33	0.08
90	11.24	34.93	14.55	9.23
180	13.53	62.42	10.95	-17.79

**Table 7.** Relative Changes in the O-H peak area for PA1000 (blue) and PA 300 (red) during UV exposure.

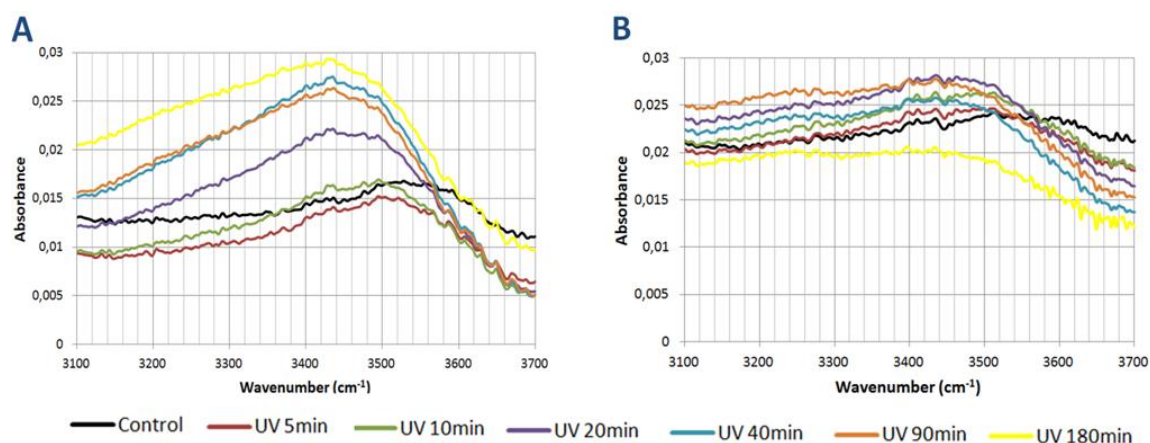


**Figure 21.** FTIR spectra of the O-H zone after various UV exposure times. **A)** PA 1000 ; **B)** PA 300.

The spectra presented in Figure 22 and 23 resume the relative changes in the peak areas during UV irradiation and for both PA 1000 and PA 300. As explained above, the different time evolutions of both polymers under UV exposure are related to their molecular structure and consequently with the competition between the production of lower molecular weight species and polymer chain/aromatic ring scission events that occur on their surface. In fact, the relative changes in the peak areas illustrate modifications on surface properties such as wettability and presence of functional groups that can largely influence the accessible surface area for protein binding.

Based on this, it is possible to say that the surfaces of both PA 1000 and PA 300 are able to offer a considerable number of scenarios to investigate protein adsorption and cell attachment, depending on the UV exposure time. Two scenarios were chosen for both polymers: untreated and 40 minutes of UV exposure. In the case of PA 1000, the UV irradiation will introduce reactive hydroxyl and carboxyl groups on the surface, improving the adhesion of proteins because of the hydrogen bond forming capability of these chemical groups [98,99]; on the other hand, the benzoquinones present on



the surface of PA 300 after 40 minutes of UV exposure will act as crosslinkers for proteins (equations 6, 7 and 8) [100,101,102].

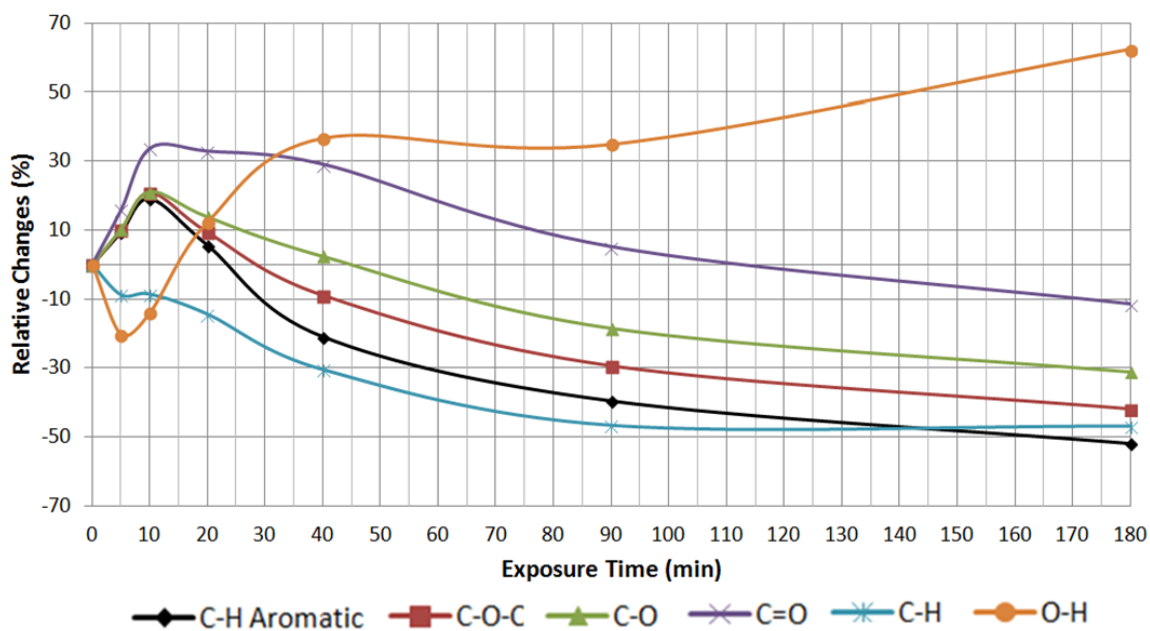


**Figure 22.** Spectra of the relative changes in different peak areas of the PA 1000 after various UV exposure times.

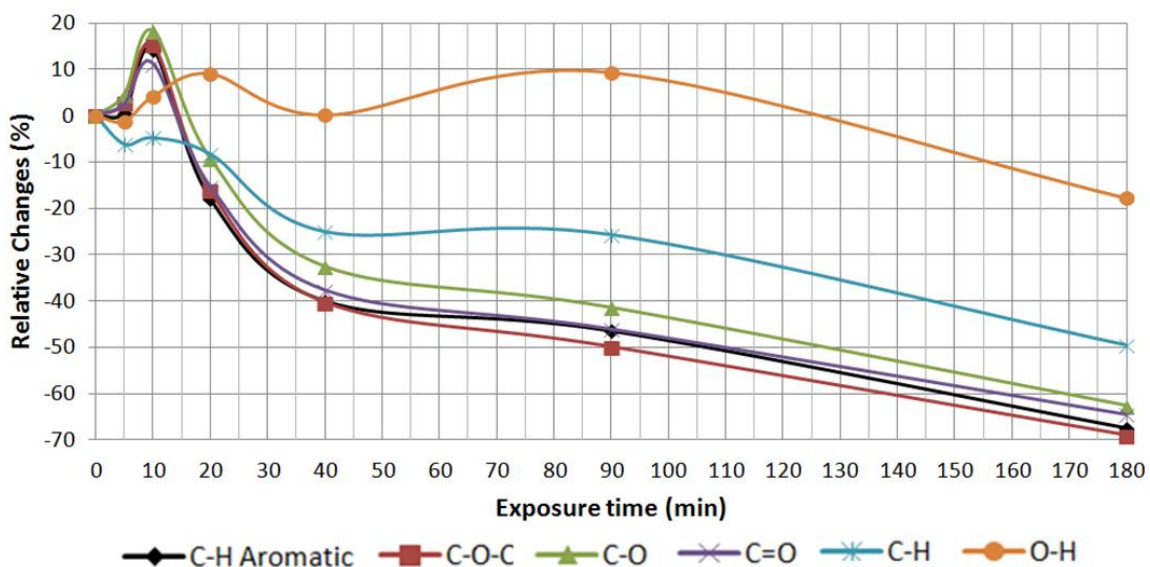
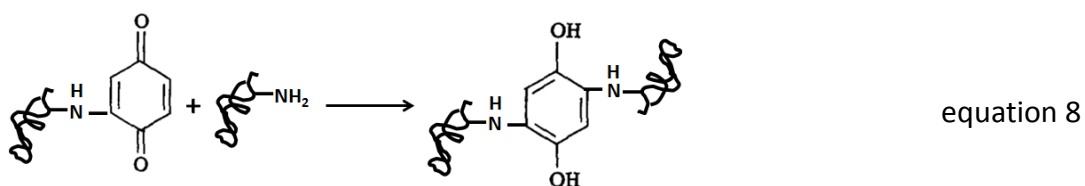
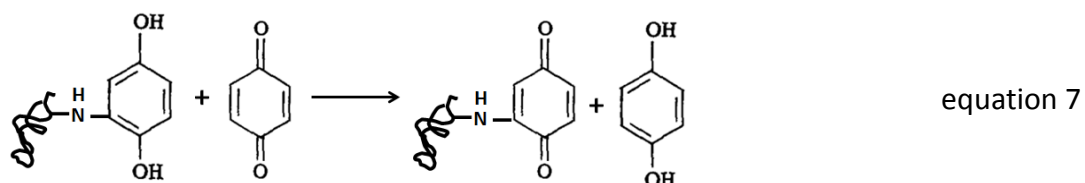
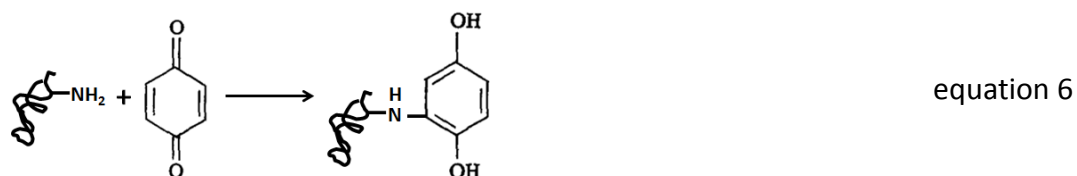


**Figure 23.** Spectra of the relative changes in different peak areas of the PA 300 after various UV exposure times.



The changes on the surface of each scenario were also monitored by XPS. The elemental compositions of PA 1000 and PA 300 before and after UV irradiation are presented in the Tables 8 and 9 respectively. It can be noted that the carbon and oxygen are the dominant species on both PA 1000 and PA 300 surfaces, however it is also observed some impurities like nitrogen on both PA 300 and PA 1000 and additional elements like potassium and silicon on the PA 1000 surface. These impurities are due to sample storage and handling during processing and UV treatment.

<i>PA 1000</i>	C	N	O	Other elements	O/C
<b>Untreated</b>	53.39%	0.37%	34.45%	11.79%	0,65
<b>40 min UV</b>	42.69%	0.81%	44.29%	12.21%	1,04

**Table 8.** PA 1000 elemental composition before and after 40 minutes of UV irradiation.

<i>PA 300</i>	C	N	O	O/C
<b>Untreated</b>	45.89%	0.44%	53.67%	1.17
<b>40 min UV</b>	52.99%	0.25%	46.76%	0.88

**Table 9.** PA 300 elemental composition before and after 40 minutes of UV irradiation.

The results in Table 8 show an increase in the oxygen/carbon ratio after UV irradiation provoked by the increase of hydroxyl and carboxyl functionalities and the chain scission events described before. In contrast, the Table 9 shows a decrease in the ratio O/C due the high OH content on the surface of untreated PA 300 and the

presence of the native oxide layer before UV treatment, the further formation of benzoquinones after 40 minutes of UV irradiation can also influence the lower amount of oxygen. The increasing of carbon after UV exposure on the PA 300 surface can be due the high probability of recombination caused by the strong attachment of chains in crystalline regions [103].

The C1s region analyses are presented in the Tables 10 and 11 for PA1000 and PA 300, respectively.

For both polymers, the C1s analysis of the untreated scaffolds showed four different peaks (Figures 24 and 25). The peak at 284.8 eV is attributed to C-H aromatic bonds and to the aliphatic carbon (C-C-C) bonds; the second and third peaks (286.2 eV and 287.3 eV) are associated with the C-C-O and C-C=O from the ether and ester groups, correspondingly. A four peak is located at 288.9 eV and it is related with the O-C=O bond, also from the ester group. These results are comparable with the results of Riekerink et al. [104] and Nandakumar et al. [98].

	BE = 284.8 eV	BE = 286.2 eV	BE = 287.3 eV	BE = 288.9 eV
<b>PA 1000</b>	C*-H (Aromatic); C-C*-C	C-C*-O; C*-O-H	C-C*=O	O-C*=O; C*-O-O-H
<b>Untreated</b>	62	29	6	3
<b>40 min UV</b>	48	33	9	10

**Table 10.** Fractions of various functional groups from PA 1000 C1s peaks.

	BE = 284.8 eV	BE = 286.2 eV	BE = 287.3 eV	BE = 288.9 eV
<b>PA 300</b>	C*-H (Aromatic); C-C*-C	C-C*-O; C*-O-H	C-C*=O	O-C*=O; C*-O-O-H
<b>Untreated</b>	63	25	8	4
<b>40 min UV</b>	60	23	7	10

**Table 11.** Fractions of various functional groups from PA 300 C1s peaks.

The changes in the C1s peaks after 40 minutes of UV irradiation (Figure 24 B and 25 B) are deeply related with the competition between scission chain events and formation of new products.

On the PA 1000 surface, the fracture of the polymer backbone chain is associated to the decreasing at 284.8 eV and the formation of esters, formates and carboxylic acids is the origin of the boost in the 288.9 eV after UV exposure. The apparent no effect of the UV treatment at 286.2 eV and 287.3 eV can be related to the formation of alcohols and other PEO photo-oxidation products (esters, formates and carboxylic acids) that balance respectively with the degradation of the originals ethers and esters.

A different behavior is observed on the PA 300 surface, where the PEO degradation is balanced with the high amount of aromatic structures and the ability of chains recombination, resulting in the preservation of the peak area at 284.8 eV. According to Solomon et al [105], the C1s peaks of C=O of benzoquinones and C-OH of phenols are located at 286.2 eV and 287.3 eV respectively. This means that the production of benzoquinones can be related with the no apparent effect of UV irradiation at 286.2 eV, despite the ether degradation; the same reasoning can be applied at 287.3 eV, where the UV irradiation seems to have no effect on the peak area. In this case the formation of the mono and di-hydroxy-substituted compounds during PBT photo-oxidation opposes to the degradation of the original esters. The boost in the last peak (288.9 eV) can be related to the oxidation products originated from the PEOT degradation and to the formation of carboxylic acids from benzoquinone degradation.

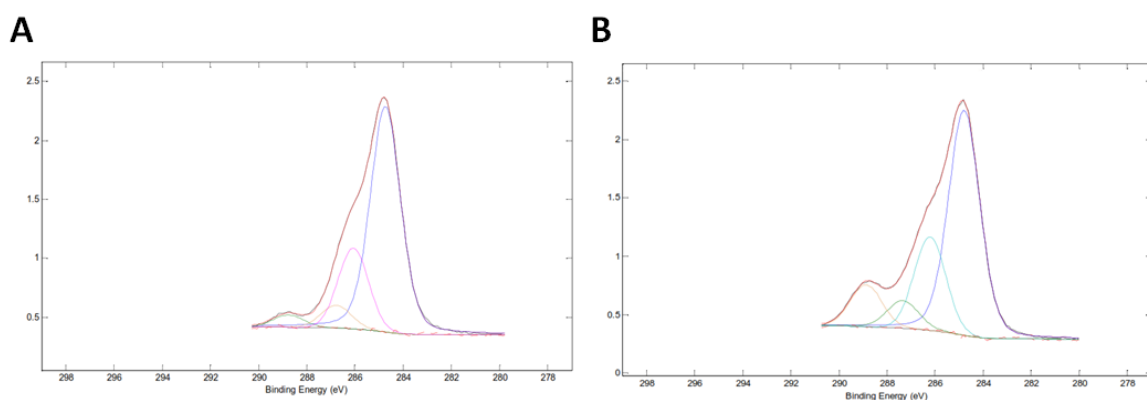


**Figure 24.** C1s peaks of PA 300. A) Untreated; B) after 40 minutes of UV exposure.

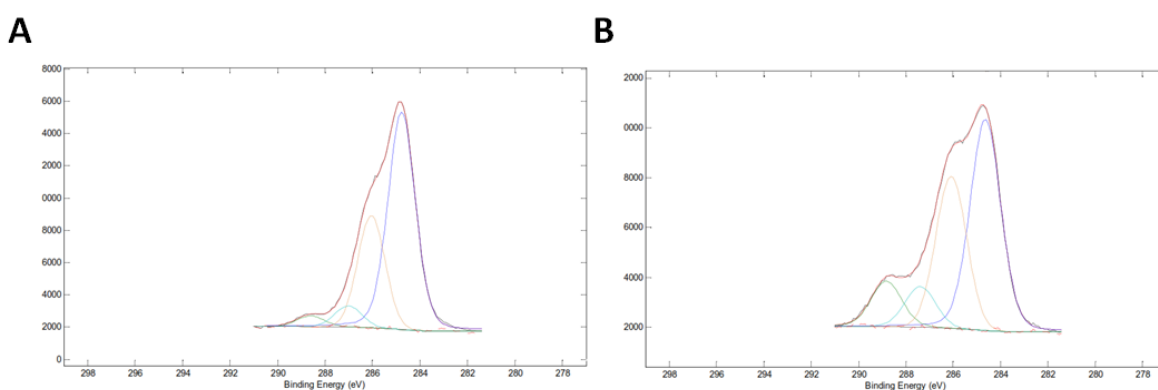


**Figure 25.** C1s peaks of PA 1000. A) Untreated; B) after 40 minutes of UV exposure.

## 5.2 Protein adsorption tests

The protein adsorption on the PA 1000 and PA 300 surfaces is directly dependent to the chemical and structural surface changes reported in the previous section. In fact, the molecular rearrangements on the surfaces due the UV irradiation can lead to substantial modifications in the amount, type and conformation of the adsorbed proteins.

Papenburg et al. [106] have suggested that the swelling ability and the two phase separation of untreated PEOT/PBT copolymers are significant in the protein adsorption process. The swelling ability opens the possibility for additional protein adsorption within the polymer sheet; on the other hand, the singular characteristics of each phase can lead to the adsorption of different kinds of proteins that express affinity to either of the phases. So, these and other properties of the material such as wettability, roughness, topography and the functional groups located on the surface are able to influence the protein adsorption and consequently the cell attachment via these proteins.

The ability of untreated and UV treated PA 1000 and PA 300 scaffolds adsorb the proteins of the serum-enriched medium was tested using FITC-BSA as a model protein. Besides the four initial scenarios (PA 1000; PA 1000 + UV; PA 300 and PA 300 + UV), it is possible create a fifth scenario for the protein adsorption test by adding the 1-ethyl-3-(3-dimethylaminopropyl)carbodiimide hydrochloride / *N*-Hydroxysuccinimide (EDC/NHS) complex to a UV treated scaffold.

In fact, the carboxylic acids present on the surface of both polymers after UV irradiation can be converted to active intermediates (*o*-acylisourea) by EDC; these reactive complexes react relatively slowly with amines, so they can be hydrolyzed in aqueous solutions before the coupling occurs. Because of that, NHS can be added to react with the active intermediate and form a stable amine-reactive NHS ester that will be nucleophilically attacked by the protein to form an amide bond, leading to covalent linkage to the polymer's surface (Figure 26) [107,108].

Theoretically the carboxylic acids should be mainly produced during PA 1000 degradation because of its large amount of PEO, however, the ATR-FTIR and XPS have showed that there is also a substantial amount of carboxylic acids on the surface of PA 300 after 40 minutes of UV irradiation. In this way, both possibilities (PA 1000 + UV and PA 300 + UV) were explored with the adding of the NHS/EDC complex. Relative to the untreated samples of PA 300 (Figure 27) and PA 1000 (Figure 28), there is no detectable fluorescence before or after incubation in a FITC-BSA / PBS solution. This information excludes respectively auto-fluorescence and protein absorption interference in the fluorescence microscope images.

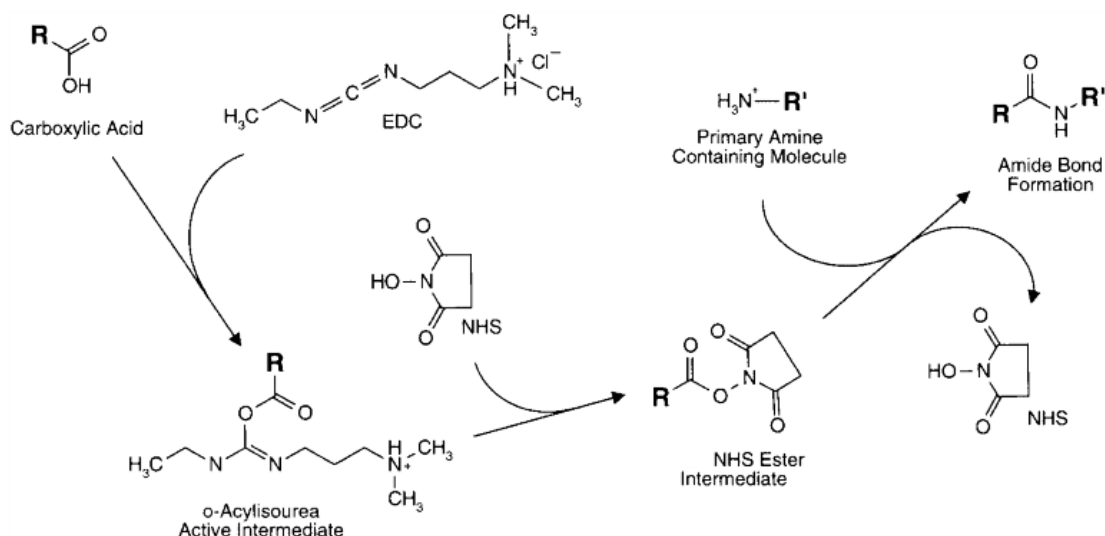


**Figure 26.** Mechanism of covalent attachment of carboxylic acid with protein via EDC/NHS complex. Adapted from

On the other hand, after 40 minutes of UV irradiation, the fibres of both electrospun scaffolds show fluorescence in the blue channel. This fact can be related with the degradation of superficial chromophores and with the photo / thermo oxidation of the PBT segment. The effect of the UV exposure on the surface of PA 1000 and PA 300 can also be proved by the detection of fluorescence proteins after incubation in a FITC-BSA / PBS solution.

According to the Figures 29 and 30, the addition of the EDC/NHS complex seems to produce no visible difference in the protein adsorption process. This means that the modifications that occur on the surface of the PA 1000 and PA 300 fibres during UV irradiation are sufficient to expand the availability of the surface areas to protein adsorption. It is also true that the process of functionalization became simpler without the introduction of this complex.

In order to have a better control on the spatial distribution of the functional groups on the surface of the fibres, we used a mask (linear patterning) between the surface and the UV light source before the FITC-BSA / PBS incubation period. As expected, the results show activate areas (green) regularly separated by non active areas. The results are illustrated in the Figure 31.

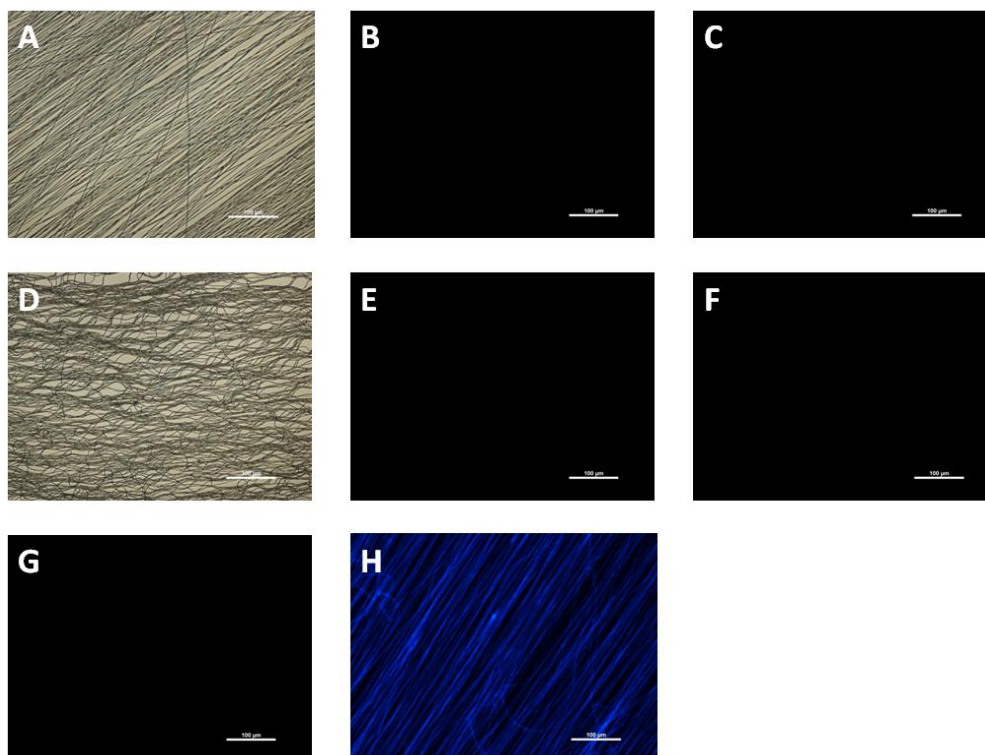


**Figure 27.** Representative fluorescence microscope images of PA 300. **A)** PA 300: bright field; **B)** PA 300: green channel; **C)** PA 300: blue channel; **D)** PA 300 + BSA: bright field; **E)** PA 300 + BSA: green channel; **F)** PA 300 + BSA: blue channel; **G)** PA 300 + UV (40min): green channel; **H)** PA 300 + UV (40min): blue channel.

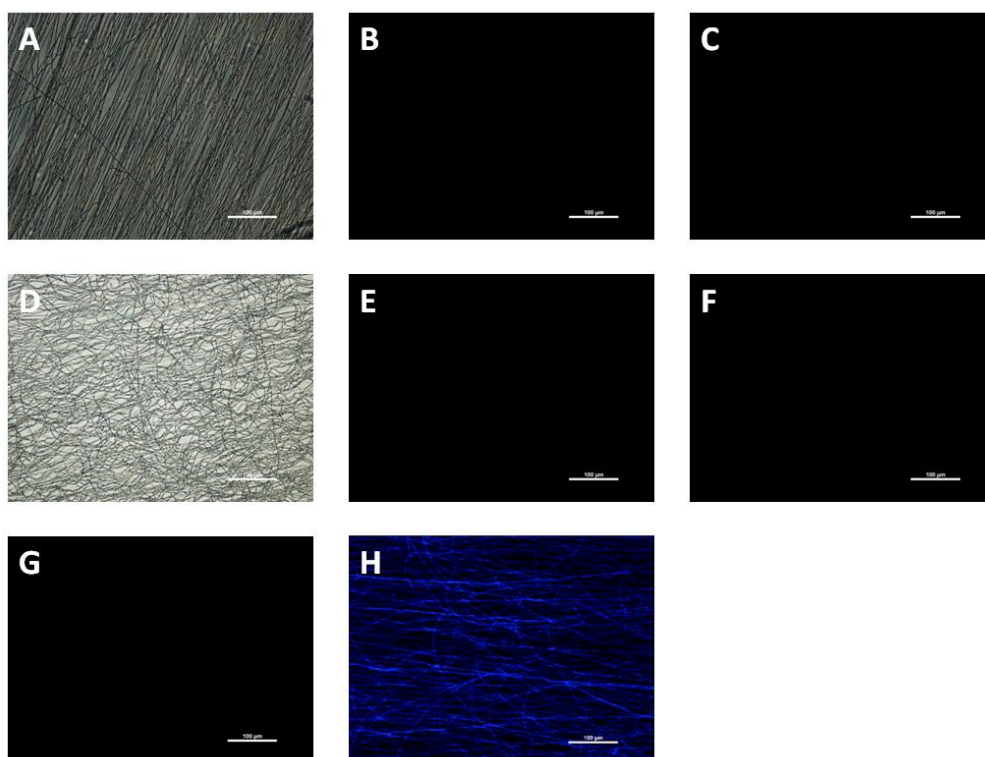


**Figure 28.** Representative fluorescence microscope images of PA 1000. **A)** PA 1000: bright field; **B)** PA 1000: green channel; **C)** PA 1000: blue channel; **D)** PA 1000 + BSA: bright field; **E)** PA 1000 + BSA: green channel; **F)** PA 1000 + BSA: blue channel; **G)** PA 1000 + UV (40min): green channel; **H)** PA 1000 + UV (40min): blue channel.



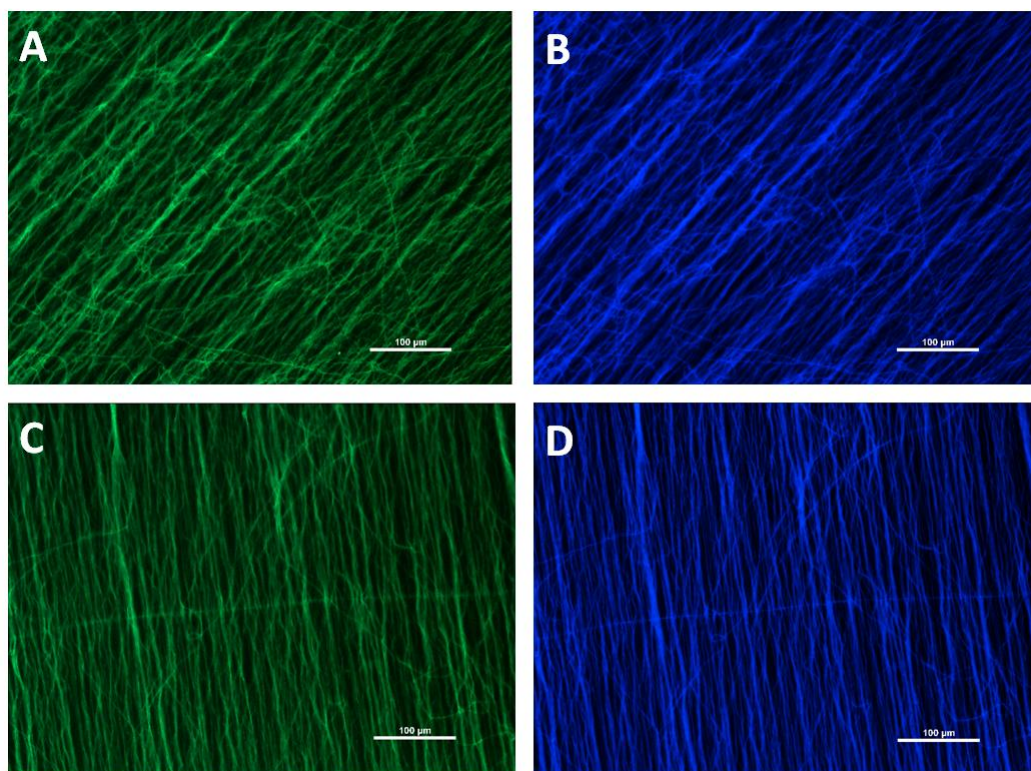


**Figure 29.** Fluorescent microscope observations of PA 300. **A)** PA 300 + UV (40min) + FITC-BSA (green channel); **B)** PA 300 + UV (40min) + FITC-BSA (blue channel); **C)** PA 300 + UV (40min) + EDC/NHS + FITC-BSA (green channel); **D)** PA 300 + UV (40min) + EDC/NHS + FITC-BSA (blue channel).

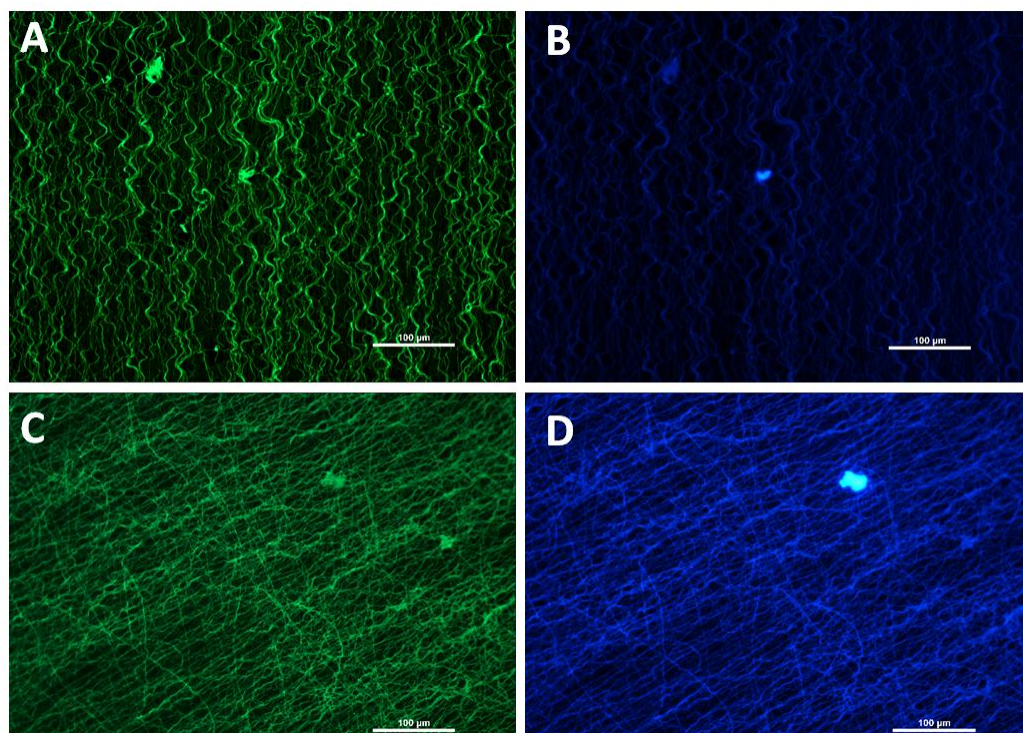


**Figure 30.** Fluorescent microscope observations of PA 1000. **A)** PA 1000 + UV (40min) + FITC-BSA (green channel); **B)** PA 1000 + UV (40min) + FITC-BSA (blue channel); **C)** PA 1000 + UV (40min) + EDC/NHS + FITC-BSA (green channel); **D)** PA 1000 + UV (40min) + EDC/NHS + FITC-BSA (blue channel).



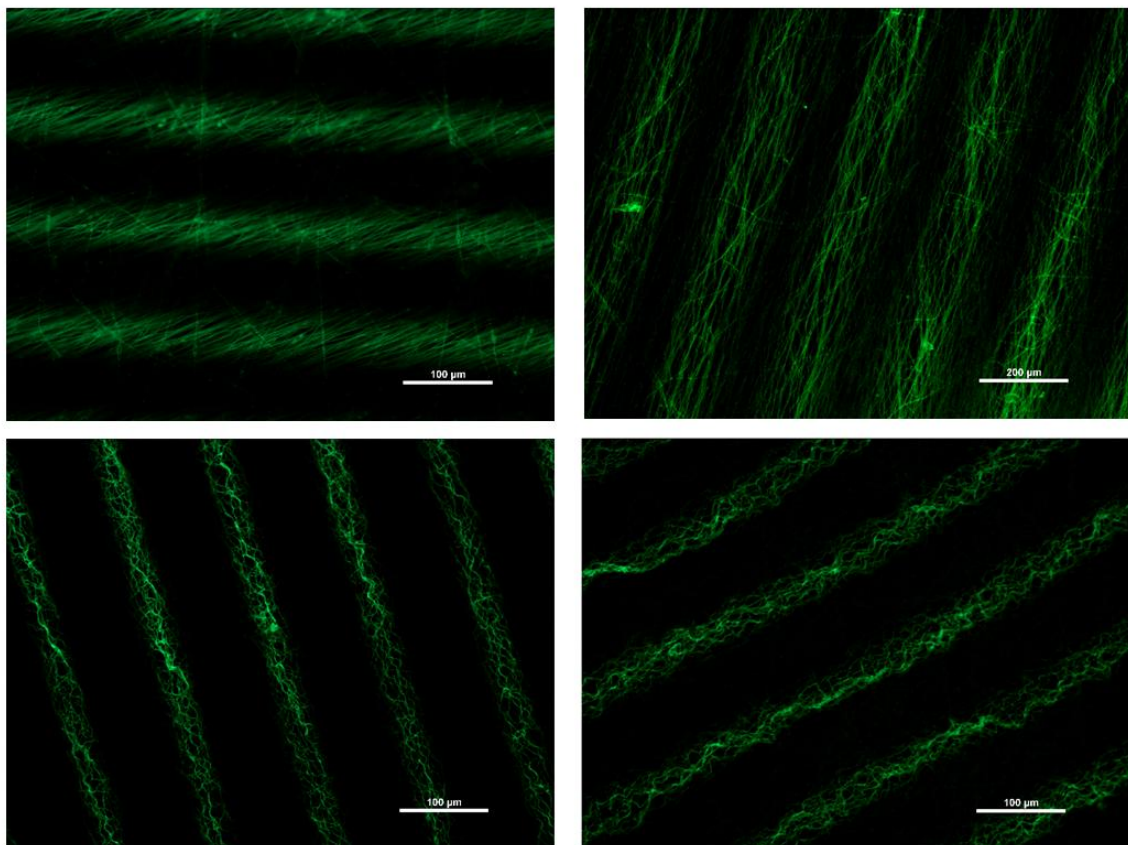


**Figure 31.** Fluorescent microscope observations of PA 300 + UV (40min / Mask) + BSA (**top**) and PA 1000 + UV (40min / Mask) + BSA (**bottom**).

### 5.3. Cell response

Adhesion is a cell type dependant process that involves a complex network of sequential events including attachment, spreading and growth, followed by other process like cell differentiation, migration and production of extra-cellular matrix (ECM) molecules [109,110]. This chain of physical interactions, chemical binding and biological signaling processes is highly influenced by the polymeric surface properties.

In fact, Arima et al. [111] have separated the cell-polymeric substrate interactions into four phases: adsorption of proteins from the medium to the surface, approach of cells to the surface, cell attachment and cell spreading. As explained before, the functional groups present on the surface of both PA 1000 and PA 300 determine the amount and the rate of the protein adsorption from the culture medium.

Initially, the cells approach the surface due to electrostatic, van der Waals and steric forces and also because of the gravity since the cells are denser than the culture medium. The more specific interactions that include the interaction between the transmembrane linking protein integrin and the proteins located on the polymer surface will then control the cell attachment. Adding to the proteins primarily

adsorbed from the culture medium, the cells themselves can start to secrete binding proteins such as fibronectin and collagen that will be also adsorb by the surface of the polymers, contributing to the cell adhesion process [110,111]. The fibronectin produced by the cells has a very important role in supporting the cell spreading [111,112].

The influence of the changes provoked by UV irradiation on the surfaces of both PA 1000 and PA 300 in the cell attachment process was tested with Rat Swann Cells, which are glial cells of the peripheral nervous system usually used for nerve tissue regeneration applications [113,114]. In culture, this cell line can show either a flat morphology or a spindle-shaped morphology with an oval nucleus and long process [115]. In fact, the results (Figures 32 - 37) show these two types of morphology in untreated and UV treated scaffolds; however it seems that the flattened pattern is more dominant in the PA 1000 samples.

The UV irradiated samples show a larger number of cells than the untreated scaffolds. This can be related to the increasing in the number of functional groups available after UV exposure, which consequently leads to an increase in the protein adsorption from the culture medium. This fact is also proved when the PA 1000 and PA 300 are patterned by the UV mask because the attachment of the Rat Schwann Cells occurs mostly on the UV activated areas.

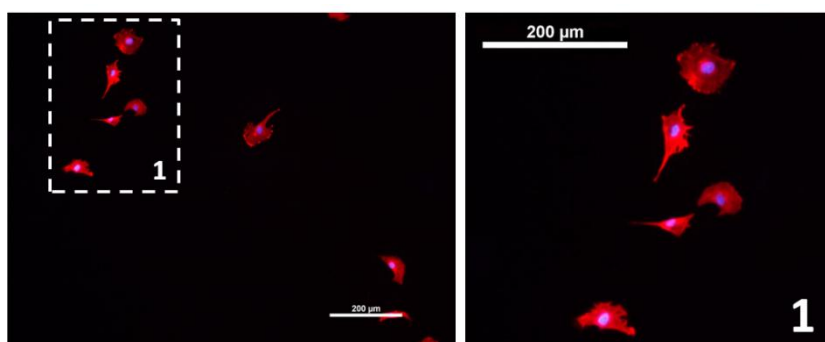


**Figure 32.** Rat Schwann Cells staining: PA 1000. Scale Bar: 200  $\mu\text{m}$ .

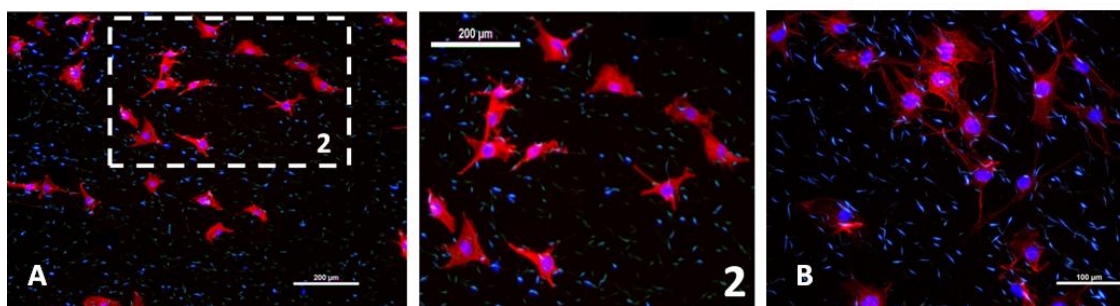


**Figure 33.** Rat Schwann Cells staining: PA 1000 + 40min UV irradiation. **A)** Scale Bar: 200  $\mu\text{m}$ ; **B)** Scale Bar: 100  $\mu\text{m}$ .

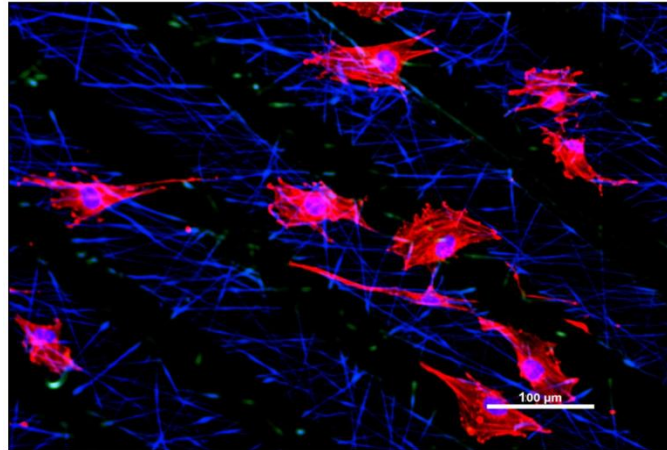


**Figure 34.** Rat Schwann Cells staining: PA 1000 + 40min UV irradiation (UV Mask). Scale Bar: 100  $\mu$ m.

The examination of the areas 1 and 2 corresponding to PA 1000 untreated and UV treated respectively shows no obvious differences in the cells morphology. In both cases, the cells show a predominant flat shape with several extensions. A similar analysis can be made by observing the areas 3 (untreated PA 300) and 4 (UV treated PA 300), since it is also possible to see no considerable change of cell morphology in both conditions: bipolar and tri-polar extensions with spindle shaped morphology.

Similarly to other studies [113,116], the aligned fibres of the electrospun scaffolds work as guidance cues for the Rat Schwann cells grow. In fact, it is possible that the aligned nanofibres influence the organization of the Rat Schwann Cells into columns called bands of Büngner during the proliferation stage [116]. Although it is unlikely to Rat Schwann Cells proliferation takes place during the culture period used in this experiment (12h), it is possible to see cell columns in both PA 1000 (Figure 28 B) and PA 300 (Figure 31, zone 4) after UV irradiation.

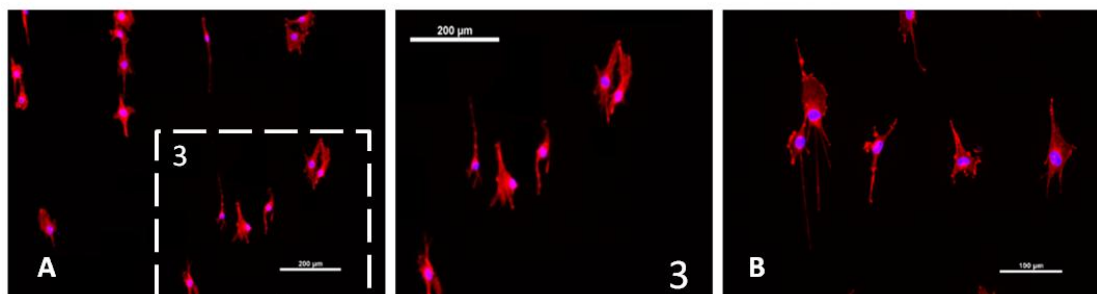


**Figure 35.** Rat Schwann Cells staining: PA 300. **A)** Scale Bar: 200  $\mu$ m; **B)** Scale Bar: 100  $\mu$ m.

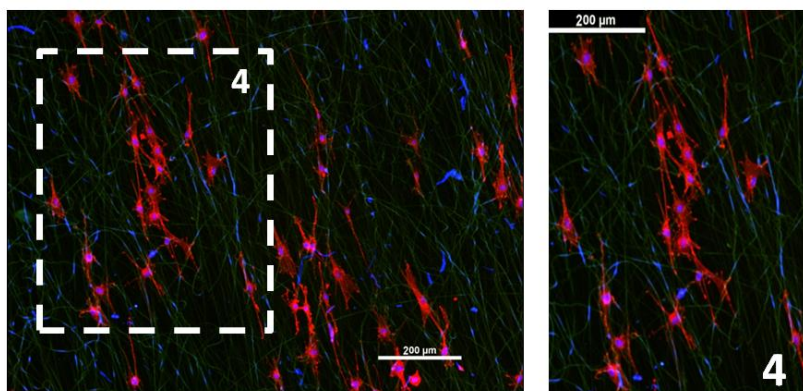


**Figure 36.** Rat Schwann Cells staining: PA 300 + 40min UV irradiation. Scale Bar: 200  $\mu\text{m}$ .

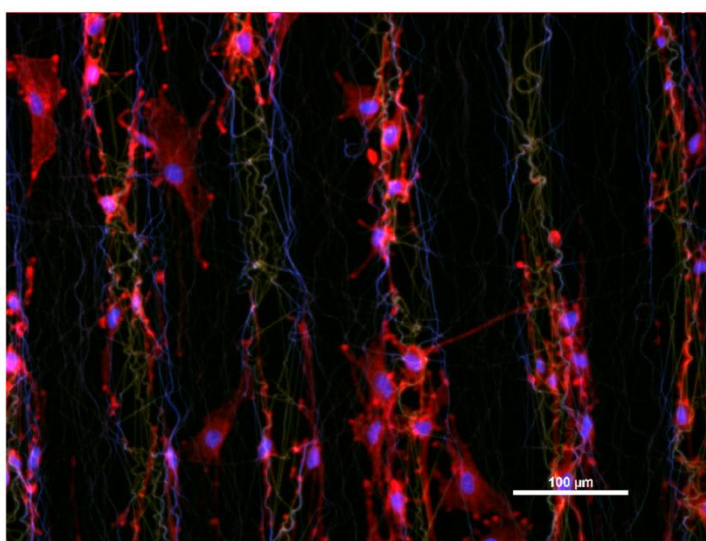


**Figure 37.** Rat Schwann Cells staining: PA 300 + 40min UV irradiation (UV Mask). Scale Bar: 100  $\mu\text{m}$ .

The more circular shape of the Rat Schwann Cells cultured on the PA 1000 scaffolds could be an outcome of a weaker fibre alignment [81] that difficult the cell elongation parallel to the fibres. On the other hand, the PA 300 fibres strong alignment is reflected in the narrow morphology presented by the Rat Schwann Cells [81].

## 6. Electrospinning PA fibres with functional groups

Although the mechanical and chemical properties of the PA 300 already show good levels of biocompatibility and biodegradability, they do not allow a selective adsorption process able to permit the immobilization of specific biomolecules on the surface. In order to accomplish that, blend solutions of PA 300 and functionalized PEG linkers were electrospun in order to place chemical groups on the surface of the fibres for further functionalization without the need of surface modification techniques like Plasma treatment or UV irradiation. The success of this concept can instigate new scaffold design methodologies for tissue engineering applications at same time that is able to originate innovative strategies for control cell behaviour (attachment, proliferation and differentiation) and migration.

### 6.1. PolyActive + (bis)PEG-SVA electrospun fibres

A blend solution of PA 300 and (bis)PEG-SVA was successfully electrospun with the purpose of placing NHS-esters on the surface of the fibres to promote protein adhesion. The presence of the functional groups on the surface of the PA 300 + (bis)PEG-SVA scaffold was confirmed via ATR-FTIR and XPS spectroscopy and the scaffold ability to immobilize proteins was investigated by using FTIC-BSA as a model protein. The chemical composition of the (bis)PEG-SVA was also investigated via NMR analysis.

#### 6.1.1. (bis)PEG-SVA/Amine reaction

The Succinimidyl valerate poly(ethylene glycol) succinimidyl valerate (SVA-PEG-SVA or (bis)PEG-SVA) is an amino (-NH<sub>2</sub>) homobifunctional reactive PEG derivate that can be used for the PEGylation of substances with available amino groups such as proteins (Figure 38).

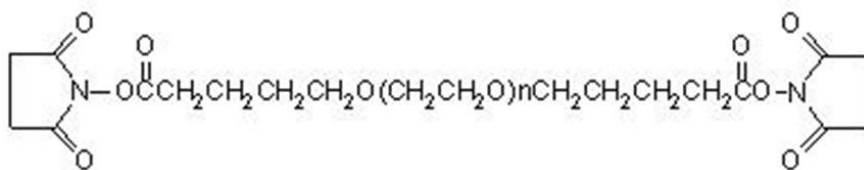


**Figure 38.** Molecular structure of (bis)PEG-SVA.



Indeed, due the presence of N-hydroxysuccinimide (NHS) esters on SVA-PEG-SVA molecular structure allows a nucleophilic attack and consequently the formation of stable amide linkage with NHS loss (Figure 39). This reaction competes with the hydrolysis of the NHS esters and because of that it should occur near physiological conditions (pH between 7 and 8.5) [107,117].

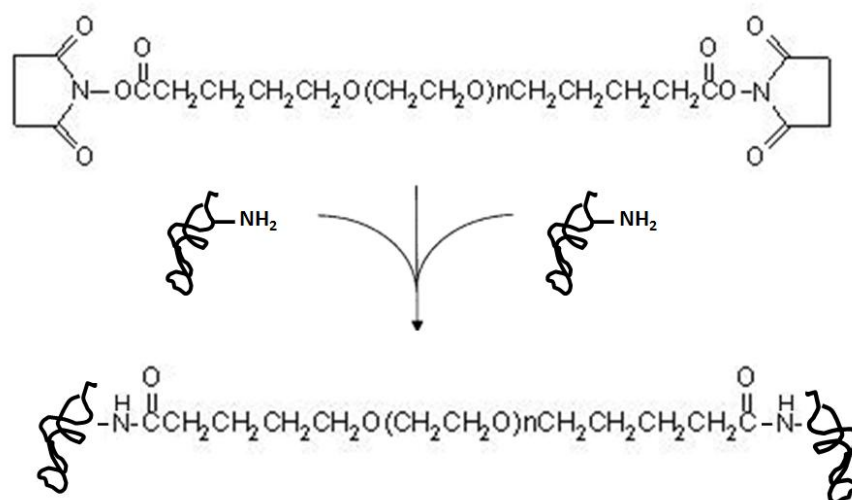


**Figure 39.** Reaction of (bis)PEG-SVA with amines on proteins.

The selectivity of PEG-NHS polymers towards primary amine terminals is commonly used in drug delivery applications because the attachment of PEG to therapeutic proteins leads to an increase in drug efficiency by reducing immunogenicity and enzymatic digestion, at same time that also induces an increasing in solubility and in the serum half life. In fact, several PEGylated protein conjugates were already FDA approved and are commercially available [118,119]. In addition to this, the PEG-NHS / PEG SVA polymers can be also employed in the incorporation of adhesion peptides or proteins on the scaffolds surfaces in order to modulate cell-surface interaction. Some tissue engineering applications include surface gradients [120], generation of protein adherent and non adherent areas [121,122], construction of hydrogel scaffolds [123] and nanoparticles surface customization [124]. Another example was reported by Delong et al. [125] that build a system able to immobilize basic fibroblast growth factor to hydrogel scaffolds via acryloyl-PEG-NHS in order to study protein gradient effects on vascular smooth muscle cell behavior and direct their migration.

The chemical composition of the (bis)PEG-SVA described above was confirmed by the  $^1\text{H}$ -NMR spectrum of (bis)PEG-SVA (Figure 40). The peak related to the C-H bond of the PEG backbone chain (3.70 ppm) is clearly the most intense because of its huge proportion in the molecular structure relatively to the NHS ester. The tiny peaks at 2.90 ppm, 2.70 ppm and 1.8 ppm are associated with the  $\text{CH}_2$  in the  $\alpha$  position, with the  $\text{CH}_2$  present on the NHS and with the C-H bond in the  $\beta$  position, respectively.

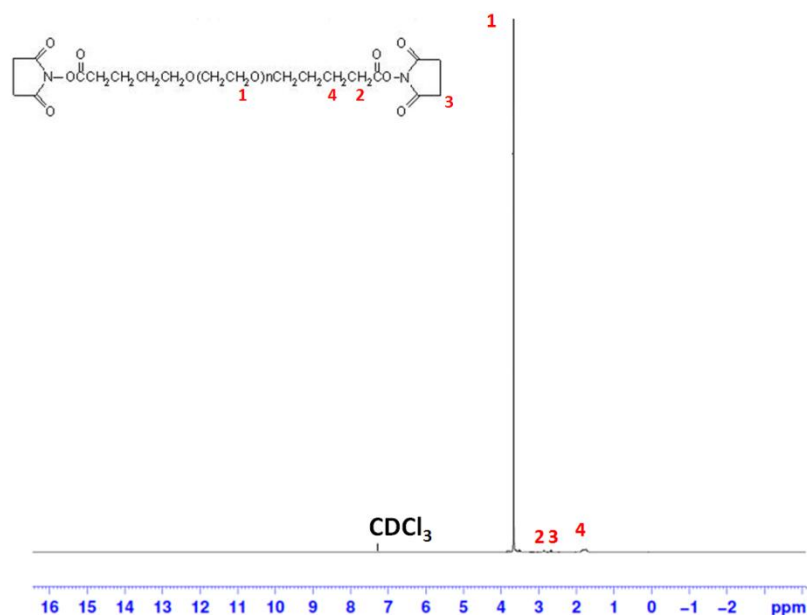


**Figure 40.** H-NMR spectrum of (bis)PEG-SVA. Legend: **1**- CH<sub>2</sub> (PEG backbone chain); **2**- CH<sub>2</sub> (α position); **3** - CH<sub>2</sub> (NHS); **4** - CH<sub>2</sub> (β position). The solvent peak for CDCl<sub>3</sub> is located at 7.25 ppm.

### 6.1.2. Scaffold characterization

The ATR-FTIR spectra of the PA 300 + (bis)PEG-SVA (Figure 41) shows a dominance of the PEOT/PBT components over the functional PEG. This situation is not completely unexpected since the proportion of this components is 4 times higher than the (bis)PEG-SVA component.

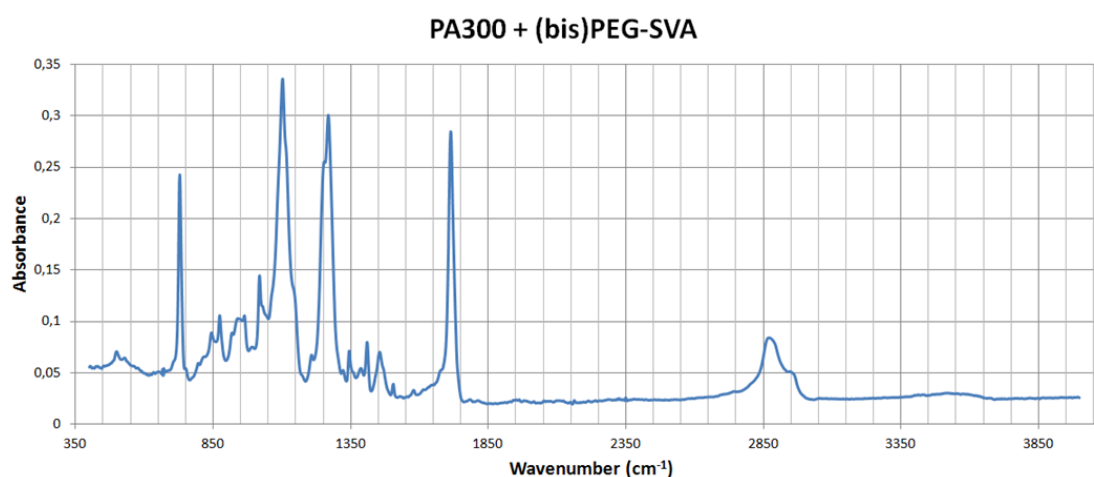


**Figure 41.** ATR-FTIR spectrum of PA300 + (bis)PEG-SVA.

There is a intense absorbance peak in the C-H stretch region associated with the Backbone chain of PEO (2840 – 3000 cm<sup>-1</sup>), it is also possible to see the ether C-O-C stretch band at 1102 cm<sup>-1</sup> and the ester C-O and C=O absorbance peaks at 1270 cm<sup>-1</sup>

and  $1714\text{ cm}^{-1}$ , respectively. The aromatic C-H out of plane region is located between  $715 - 735\text{ cm}^{-1}$  and the O-H region ( $3100$  and  $3700\text{ cm}^{-1}$ ) is nearly negligible.

Indeed, the spectrum of PA 300 + (bis)PEG-SVA is almost similar to the spectrum of PA 300 showed before (section 5.1.): both spectra present the same absorbance bands, with their only difference being the peak areas (Figures 42 – 44 and Table 12). In fact, the addition of (bis)PEG-SVA before the electrospinning process cause the increasing of the polymer backbone chain and consequently a boost in the C-O-C, C-O and C-H (main chain) regions. The PEG content is also responsible for the high water absorption during the electrospinning and consequently for the increasing of the O-H region. As expected, there is no significant change in the aromatic C-H region.

Theoretically, the NHS terminals should present three characteristic bands at  $17019\text{ cm}^{-1}$ ,  $1745\text{ cm}^{-1}$  and  $1818\text{ cm}^{-1}$  related respectively with the symmetric and asymmetric C=O stretches of NHS and with the carbonyl stretch of the NHS ester [126,127]. Although since none of these peaks are identified individually, it is possible that the increasing of the C=O peak area is due the presence of NHS-esters on the surface of the fibres.

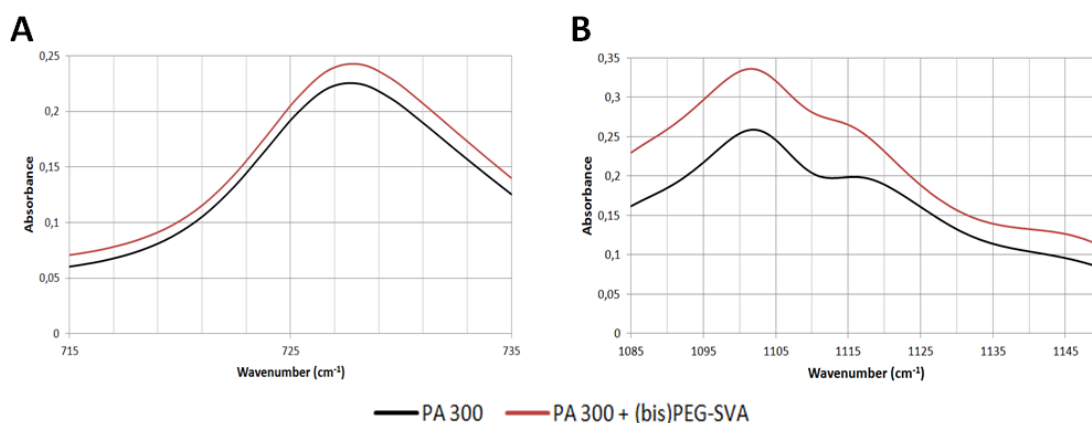


**Figure 42.** Comparison between the ATR-FTIR spectra of PA 300 and PA 300 + (bis)PEG-SVA. **A)** aromatic C-H region; **B)** C-O-C region.

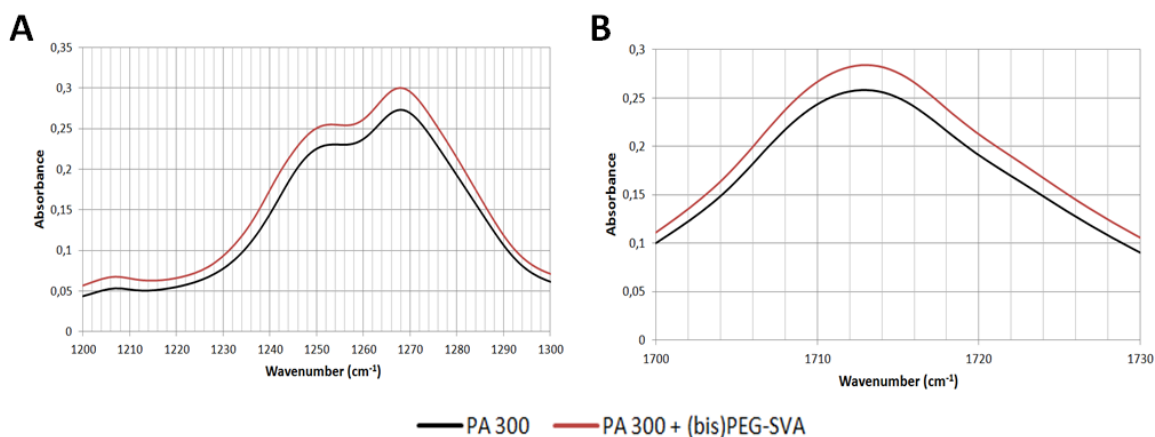


**Figure 43.** Comparison between the ATR-FTIR spectra of PA 300 and PA 300 + (bis)PEG-SVA. **A)** C-O region; **B)** C=O region.



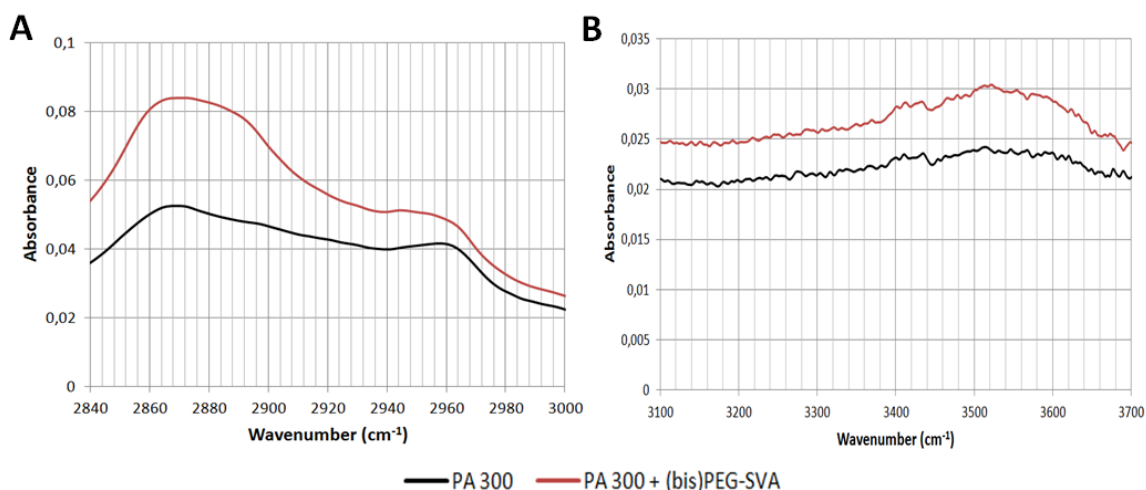


**Figure 44.** Comparison between the ATR-FTIR spectra of PA 300 and PA 300 + (bis)PEG-SVA. **A)** backbone chain C-H region; **B)** O-H region.

	Peak area: PA 300	Peak area: PA 300 + (bis)PEG-SVA
<b>C-H (aromatic)</b>	3.11	3.31
<b>C-O-C</b>	11.24	14.85
<b>C-O</b>	14.17	16.10
<b>C=O</b>	5.50	6.17
<b>C-H (main chain)</b>	6.63	9.32
<b>O-H region</b>	13.32	16.10

**Table 12.** Comparison between the ATR-FTIR peak areas of PA 300 and PA 300 + (bis)PEG-SVA.

The elemental composition of the PA 300 + (bis)PEG-SVA surface by XPS confirmed the ATR-FTIR analysis (Table 13). So, the carbon and oxygen are the dominate species on the scaffold's surface and there is a vestigial trace of nitrogen. These results make sense because it was not expectable to see a huge percentage of nitrogen on the surface due the proportion between PA 300 and (bis)PEG-SVA used; however the presence of the (bis)PEG-SVA is reflected in the higher amount of carbon and nitrogen on the surface comparing with PA 300 (Table 9).

<b>PA 300 + (bis)PEG-SVA</b>	<b>C</b>	<b>N</b>	<b>O</b>	<b>O/C</b>
	65.47%	0.53%	34%	0.52

**Table 13.** PA 300 + (bis)PEG-SVA elemental composition.

The C1s analysis of the PA 300 + (bis)PEG-SVA fibres (Table 14 and Figure 45) show the same four peaks as both PA 1000 and PA 300: the first peak is located at 284.8 eV (C-H aromatic and aliphatic carbon C-C-C bonds), the second peak at 286.2 eV (C-C-O ether bond), the third peak at 287.3 eV (C-C=O ester bond) and finally, the last peak located at 288.9 eV (O-C=O ester bond). The comparison with PA 300 (Table 9 and Figure 24 A) reveals a huge increment in the peak area associated with the C-C-O ether bond, which is explained by the higher amount of PEG in the PA 300 + (bis)PEG-SVA scaffold; and in addition to this, it is also possible associate this peak with the C-N bond [122].

Furthermore, it was also made an N1s analysis to both PA 300 + (bis)PEG-SVA and PA 300 in order to compare their functional groups and identify the NHS-ester terminals on the surface of the PA 300 + (bis)PEG-SVA fibres. The results (Table 15) show a common peak at 399.2 eV, which can be associated to nitrogen contamination. On the other hand it is possible to observe a second peak at 401.5 eV that only exist in the PA 300 + PEG-SVA scaffold, indicating the presence of the NHS-esters [128] on the surface of the fibres.

	BE = 284.8 eV	BE = 286.2 eV	BE = 287.3 eV	BE = 288.9 eV
<i>PA 300 + (bis)PEG-SVA</i>	C*-H (Aromatic); C-C*-C	C-C*-O; C*-O-H ; C*-N	C-C*=O	O-C*=O; C*-O-O-H
	39	53	6	2

**Table 14.** Fractions of various functional groups from PA 300 + (bis)PEG-SVA C1s peaks.

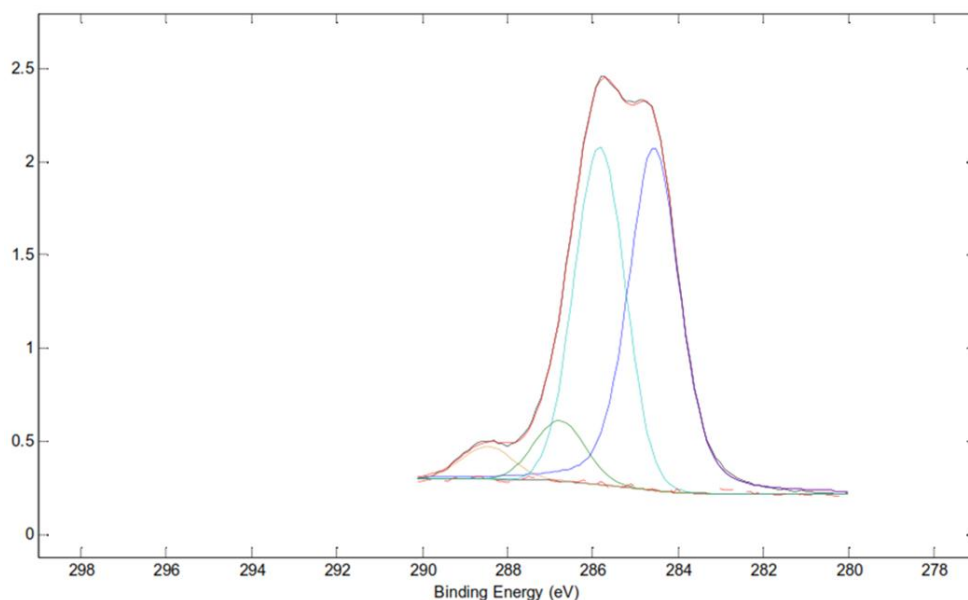


**Figure 45.** C1s peaks of PA 300 + (bis)PEG-SVA.

	BE = 399.2 eV	BE = 401.5 eV
	N*-H; N*-C	N of the NHS-ester
<b>PA 300</b>	100	-
<b>PA 300 + (bis)PEG-SVA</b>	58	42

**Table 15.** Comparison between PA 300 and PA 300 + (bis)PEG-SVA functional groups from N1s peaks.

### 6.1.3. Protein adsorption

As explained previously (section 5.2), the protein adsorption success is highly dependent on the surface characteristics, so the changes promoted by the adding of (bis)PEG-SVA to PA 300 should increase substantially the ability of the electrospun fibres adsorb the proteins.

In addition to the ATR-FTIR and XPS results that already have showed the presence of NHS-esters on the surface of the PA 300 + (bis)PEG-SVA fibres, the scaffold was also tested using FITC-BSA as a model protein to simulate the adsorption of the serum-enriched medium before cell seeding.

The results presented in Figure 46 confirm that only the PA 300 + (bis)PEG-SVA after incubation in a FITC-BSA / PBS solution was able to show detectable fluorescence. This means that the functional groups are indeed present on the surface of scaffold, contributing to protein adsorption. Similarly to the PA 300 fluorescence microscope images showed in section 5.2, the PA 300 + (bis)PEG-SVA didn't show any auto-fluorescence.

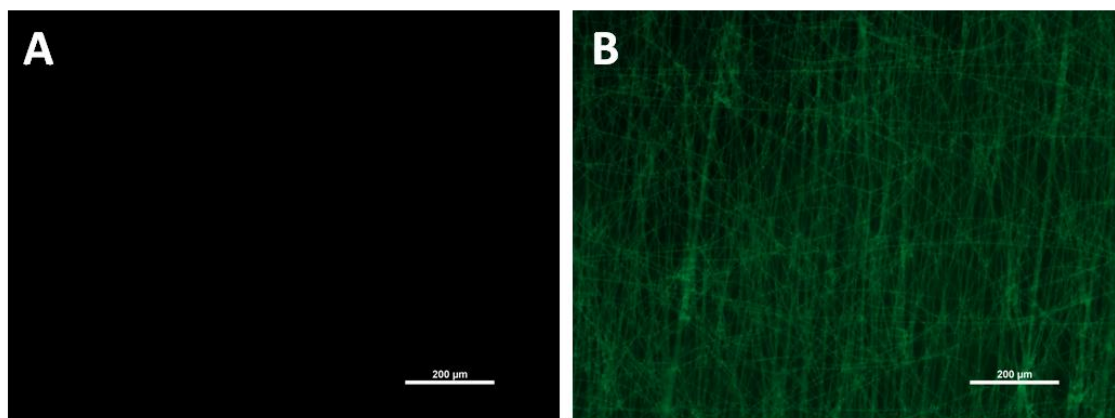


**Figure 46.** Fluorescent microscope observations of PA 300 + (bis)PEG-SVA **(A)** and PA 300 + (bis)PEG-SVA after incubation in a FITC-BSA / PBS solution **(B)**.

## 6.2. PolyActive + (bis)PEG-Alkyne electrospun fibres

A blend solution of PA 300 and (bis)PEG-Alkyne was successfully electrospun with the purpose of placing terminal alkynes on the surface of the fibres to promote click chemistry reactions with azide functionalized biomolecules. Although the presence of alkynes was not totally confirmed via ATR-FTIR and XPS spectroscopy, the PA 300 + (bis)PEG-Alkyne scaffold was able to successfully immobilize an azide dye and consequently prove the existence of alkyne functional groups on the surface of the fibres. The chemical composition of the (bis)PEG-Alkyne was investigated via NMR analysis.

### 6.2.1. (bis)PEG-Alkyne/Azide reaction

The reaction between an azide and an alkyne terminals of the (bis)PEG-Alkyne is one example of the click chemistry cycloaddition reactions, that are included in a larger group of chemical processes denominated Click Chemistry. The concept behind Click Chemistry is mainly related with the creation of substances by exploring simple reactions that are efficient at link two components under simple reaction conditions and fast reaction times [129,130].

The most popular cycloaddition reaction is referred as the Huisgen 1,3-dipolar cycloaddition reaction, which can occur through either of two alternative pathways described in Figure 47 in order to produce 1,2,3-triazoles. The more classical approach is purely thermal and produce both 1,4- and 1,5-regioisomers in a ratio 1:1, however because of the elevated temperatures and long reaction time required it is not very practical. So, Sharpless et al. [131] have described a variant of the original process to accelerate the cycloaddition reaction by using Cu(I) as catalyst. In fact, the addition of Cu(I) dramatically accelerates the kinetics of the reaction and allows it to be almost solvent insensitive and occur under ambient pressures and room temperature. As it is possible to see in the Figure 47, the Cu(I) catalyzed variation of the Huisgen 1,3-dipolar cycloaddition of azides and alkynes improves the regioselectivity to generate only the 1,4-regioisomer [107,129,130,132].

The simplicity of the click chemistry reactions has led to its application in tissue engineering strategies and materials science, mainly with the conjugation of polymers with biological entities such as peptides, proteins, viruses and cells [129]. In this way, the molecular structure of the (bis)PEG-Alkyne (Figure 48) transform this polymer into a suitable candidate for many applications of the azide-alkyne click approach, such as synthesis of hydrogels [133] and polymer surface functionalization [134,135].

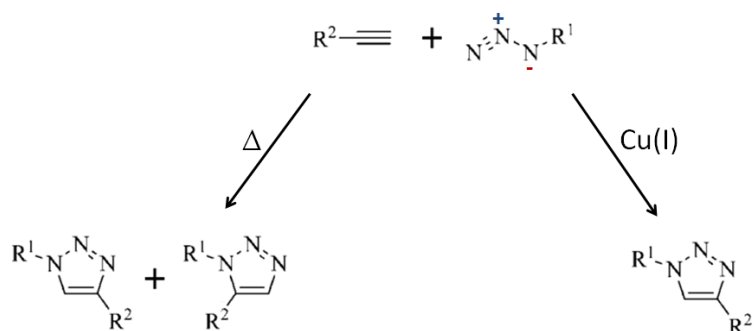


**Figure 47.** Two alternative pathways to the Huisgen 1,3-dipolar cycloaddition reaction: thermal and Cu(I) catalyzed.

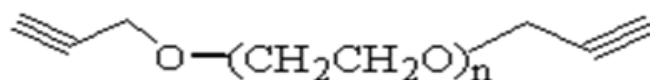


**Figure 48.** Molecular structure of (bis)PEG-Alkyne.

The chemical composition of the (bis)PEG-Alkyne was evaluated by a H-NMR analysis (Figure 49). The more intense peak is located at 3.70 ppm and it is related with the dominant presence of the PEG backbone chain ( $\text{CH}_2$ ) at the molecular structure. The peaks at 1.90 ppm and 2.4 ppm are related respectively with the alkyne proton and with  $\text{CH}_2$  adjacent to the triple bond carbon. Finally, the peak located at 4.2 ppm is probably related with the methylene protons of 4-pentynoic acid that is used during the Alkyne-PEG-Alkyne synthesis [136].

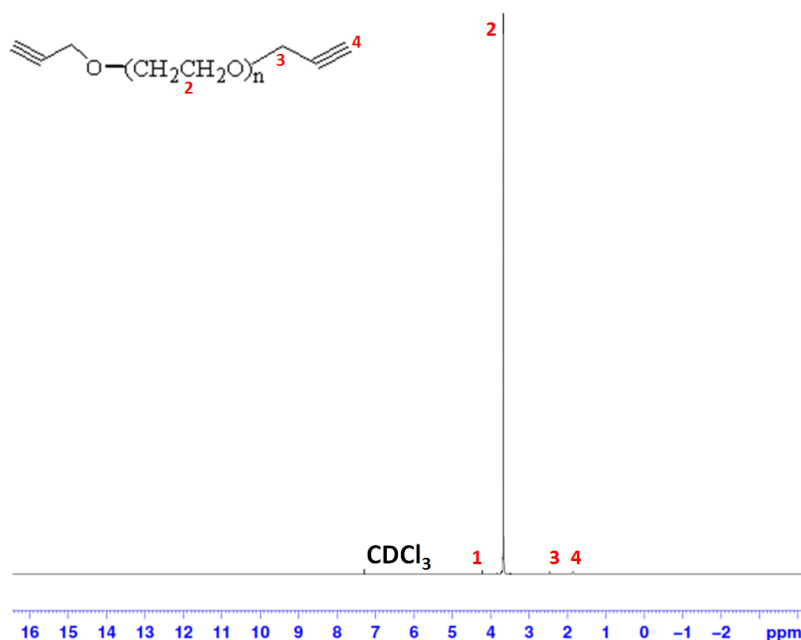


**Figure 49.** H-NMR spectrum of (bis)PEG-Alkyne. Legend: **1**-  $\text{CH}_2$  (polymer synthesis); **2**-  $\text{CH}_2$  (PEG backbone chain); **3** -  $\text{CH}_2$  (adjacent to the triple bond carbon); **4** - H-C (Alkyne terminal). The solvent peak for  $\text{CDCl}_3$  is located at 7.25 ppm.

### 6.2.2. Scaffold characterization

The PA 300 + (bis)PEG-SVA ATR-FTIR spectrum (Figure 50) presents the same peaks as the PA 300 by itself (section 5.1.): the region between  $2840\text{ cm}^{-1}$  and  $3000\text{ cm}^{-1}$  is dominated by the C-H stretch from the Backbone chain of PEO, the ether C-O-C stretch band is located at  $1102\text{ cm}^{-1}$ , the ester stretches C-O and C=O are situated respectively at  $1270\text{ cm}^{-1}$  and  $1714\text{ cm}^{-1}$ , the area between  $715\text{ cm}^{-1}$  and  $735\text{ cm}^{-1}$  is related with the aromatic C-H out of plane region and the O-H region ( $3100$  and  $3700\text{ cm}^{-1}$ ) is not significant. Indeed, the spectrum show a clearly dominance of the PEOT/PBT components that together with the PEG chain from the (bis)PEG-SVA suppress the characteristic bands of the Alkyne terminals. Theoretically these characteristic bands should be the C $\equiv$ C-H bend ( $610 - 700\text{ cm}^{-1}$ ), the C=C stretch ( $2100 - 2260\text{ cm}^{-1}$ ) and the C=C-H stretch ( $3270 - 3330\text{ cm}^{-1}$ ).

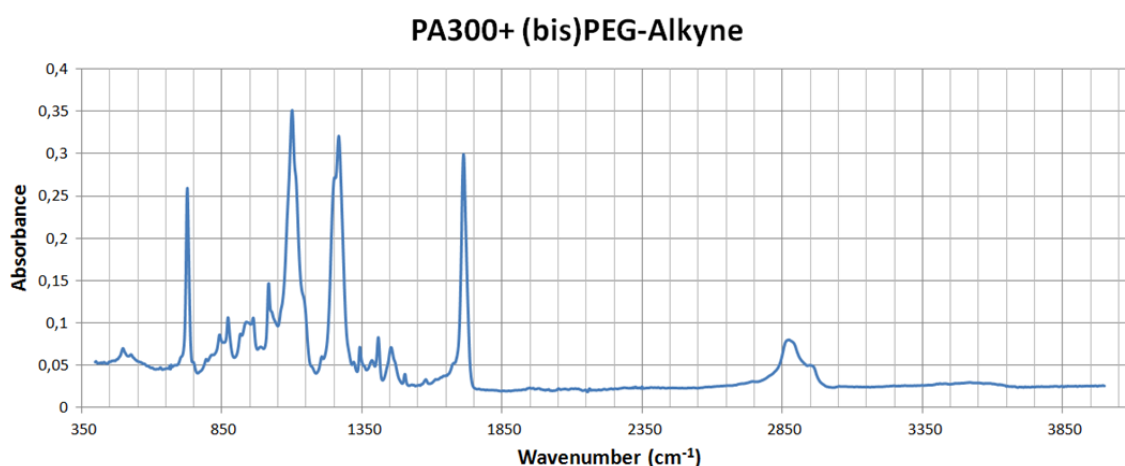


**Figure 50.** ATR-FTIR spectrum of PA300 + (bis)PEG-Alkyne.

The comparison between the PA 300 + (bis)PEG-Alkyne and the PA 300 scaffold has showed, as expected, some changes on the peak areas but not in the absorbance bands locations. It is possible to see from the Figures 51-53 and from the analysis of the Table 16, that the influence of the PEG during the scaffold fabrication is reflected in the increasing of the polymer backbone and therefore in the associated areas (C-O-C, C-O and C-H (main chain) regions). Similarly to what was explained for the PA 300 + (bis)PEG-SVA scaffold, the addition of PEG-Alkyne before the electrospinning process brings consequences for the hydrophilic properties of the fibres, that are then able to absorb more water than the PA 300 by itself. Then as consequence of the increase in the water absorption levels in the PA 300 + PEG-Alkyne scaffold, there is an increase in the O-H region comparing with the PA 300 scaffold.

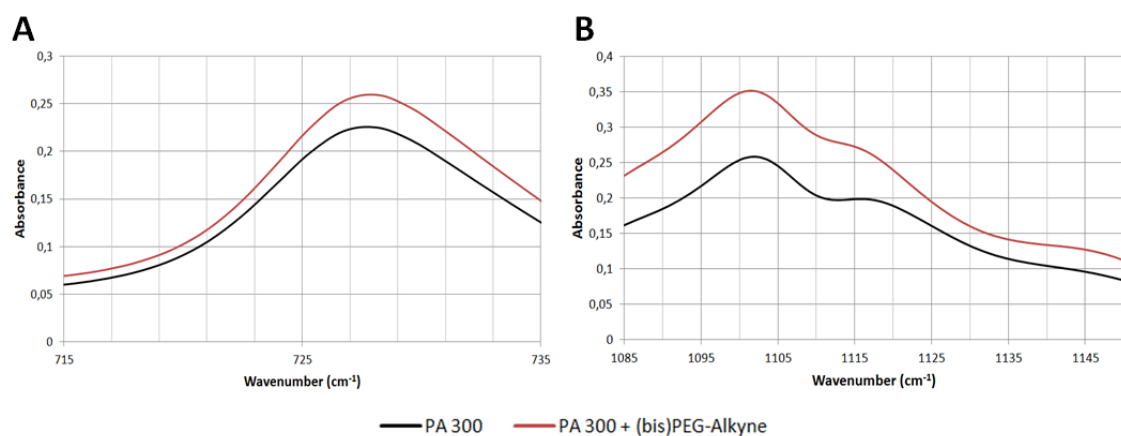


**Figure 51.** Comparison between the ATR-FTIR spectra of PA 300 and PA 300 + (bis)PEG-Alkyne. **A)** aromatic C-H region; **B)** C-O-C region.

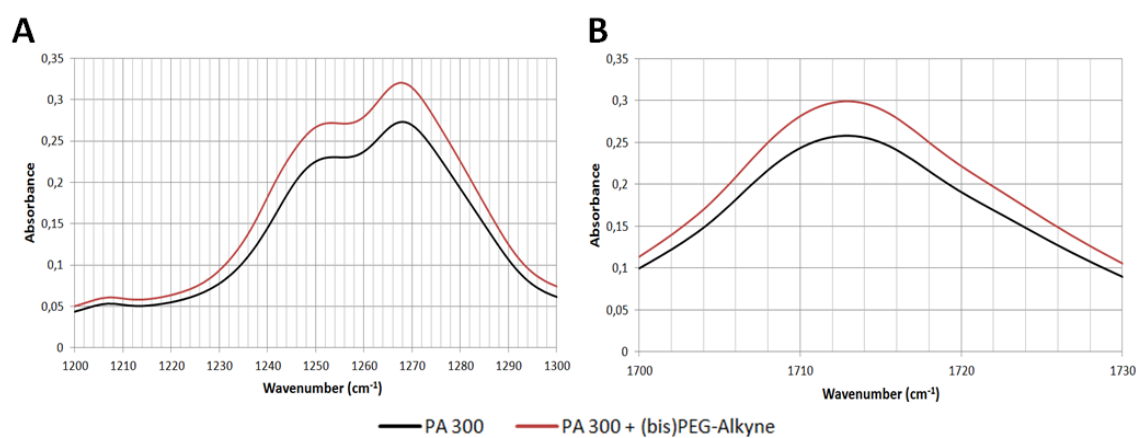


**Figure 52.** Comparison between the ATR-FTIR spectra of PA 300 and PA 300 + (bis)PEG-Alkyne. **A)** C-O region; **B)** C=O region.

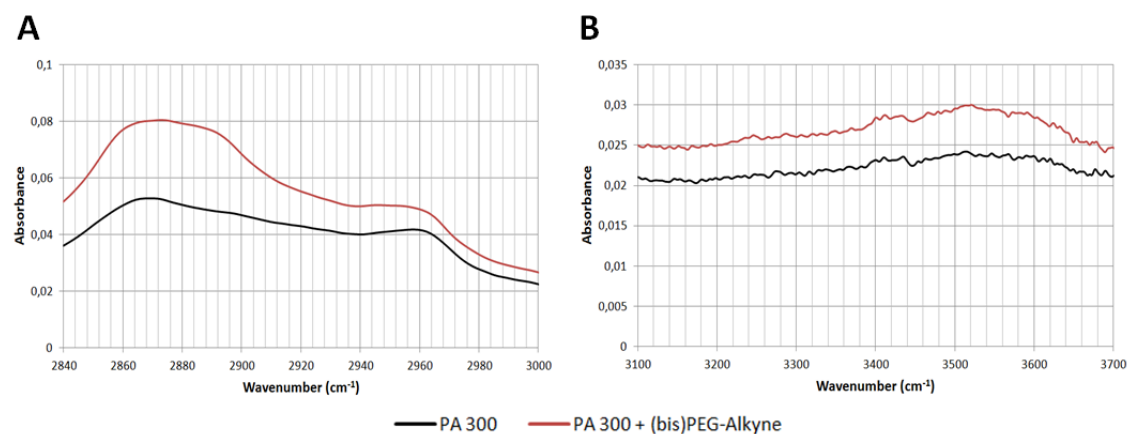


**Figure 53.** Comparison between the ATR-FTIR spectra of PA 300 and PA 300 + (bis)PEG-Alkyne. **A)** backbone chain C-H region; **B)** O-H region.

	Peak area: PA 300	Peak area: PA 300 + (bis)PEG-Alkyne
<b>C-H (aromatic)</b>	3.11	3.48
<b>C-O-C</b>	11.24	15.26
<b>C-O</b>	14.17	16.79
<b>C=O</b>	5.50	6.42
<b>C-H (main chain)</b>	6.63	9.11
<b>O-H region</b>	13.32	16.17

**Table 16.** Comparison between the ATR-FTIR peak areas of PA 300 and PA 300 + (bis)PEG-Alkyne.

The elemental composition of the surface of the PA 300 + (bis)PEG-Alkyne scaffold via XPS (Table 17) showed that carbon and oxygen are the two dominant components; it is also noticeable a vestigial amount of nitrogen impurities.

<i><b>PA 300 + (bis)PEG-Alkyne</b></i>	<b>C</b>	<b>N</b>	<b>O</b>	<b>O/C</b>
	65.67%	0.40%	38.93%	0.59

**Table 17.** PA 300 + (bis)PEG-Alkyne elemental composition.

Similarly to the ATR-FTIR results, the XPS analysis has not established clearly the existence of Alkyne functional groups on the surface of the PA 300 + (bis)PEG-Alkyne. Indeed, the C1s peaks (Figure 54) are located in the same places as the peaks from the other scaffolds analyzed previously (PA 1000, PA 300 and PA 300 + (bis)PEG-SVA): the peak centered at 284.8 eV is related with both C-H aromatic and aliphatic C-C-C bonds, the peak located at 286.2 eV is associated with the C-C-O ether bond and the last two peaks are related with the C-C=O (287.3 eV) and O-C=O (288.9 eV) from the ester group. The comparison between the PA 300 (section 5.1.) and the PA 300 + (bis)PEG-Alkyne (Table 18) shows, as expected, that there is a substantial increment in the C-C-O peak area in the PA 300 + (bis)PEG-Alkyne scaffold probably due the addition of the PEG segments before electrospinning. The high PEG content on the scaffold is also the motive for a small O/C ratio (0.59) showed in the element composition table.



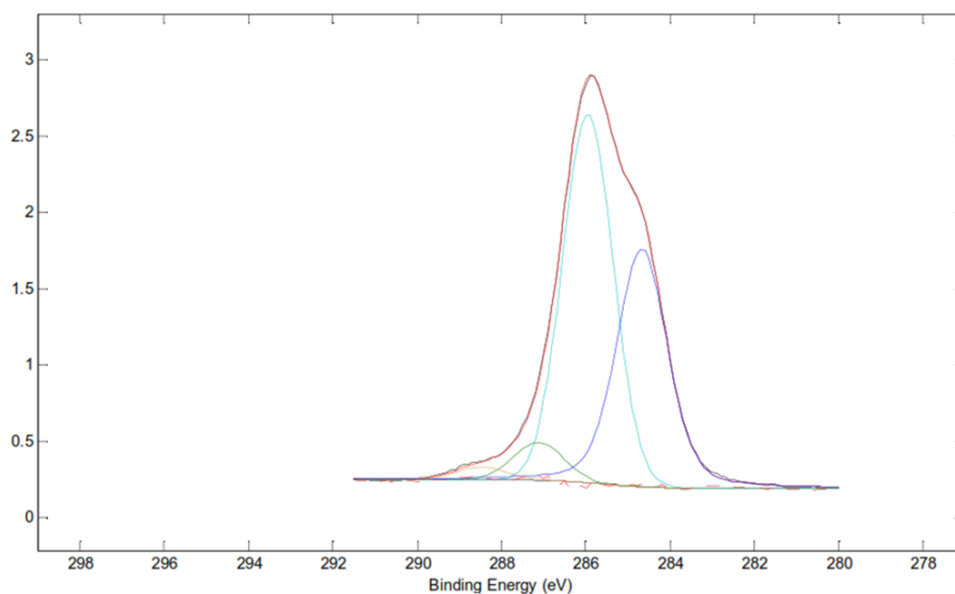


**Figure 54.** C1s peaks of PA 300 + (bis)PEG-Alkyne.

	BE = 284.8 eV	BE = 286.2 eV	BE = 287.3 eV	BE = 288.9 eV
<i>PA 300 + (bis)PEG-Alkyne</i>	C*-H (Aromatic); C-C*-C	C-C*-O; C*-O-H	C-C*=O	O-C*=O; C*-O-O-H
	48	41	7	4

**Table 18.** Fractions of various functional groups from PA 300 + (bis)PEG-Alkyne C1s peaks.

### 6.2.3. Click Chemistry tests

Since the ATR-FTIR and XPS results were not conclusive about the presence of alkyne functional groups on the surface of the PA 300 + (bis)PEG-SVA fibres, a new approach was followed by using a fluorescent azide in order to induce the azide-alkyne cycloaddition reaction and then locate the functional groups. Although the usual click chemistry approaches involved a Cu(I) catalyst, the protocol followed (section 4.5) did not include any catalyst. This was because, contrary to the (bis)PEG-Alkyne by itself, the alkynes on the surface of the PA 300 + (bis)PEG-Alkyne electrospun scaffold are influenced by neighboring electron-withdrawing functional groups such as the ester and the carbonyl groups from the PA 300, leading to the formation of the cycloaddition products at room temperature and in an aqueous medium [137]. In addition to this, the high local alkyne concentration present on the surface of the scaffold due to the proportion of PA 300:(bis)PEG-Alkyne (4:1) can also induce the Huisgen 1,3-dipolar cycloaddition reaction without the need of a catalyst [138]. Indeed, the properties of the PA 300 + (bis)PEG-Alkyne by inducing the alkyne-azide click chemistry reaction without Cu(I), can avoid the toxic nature of the copper catalysis [134,139].

As expected, the detectable fluorescence only occurs at the PA 300 + (bis)PEG-Alkyne fibres after azide incubation, indicating the existence of alkyne functional groups on its surface (Figure 55).

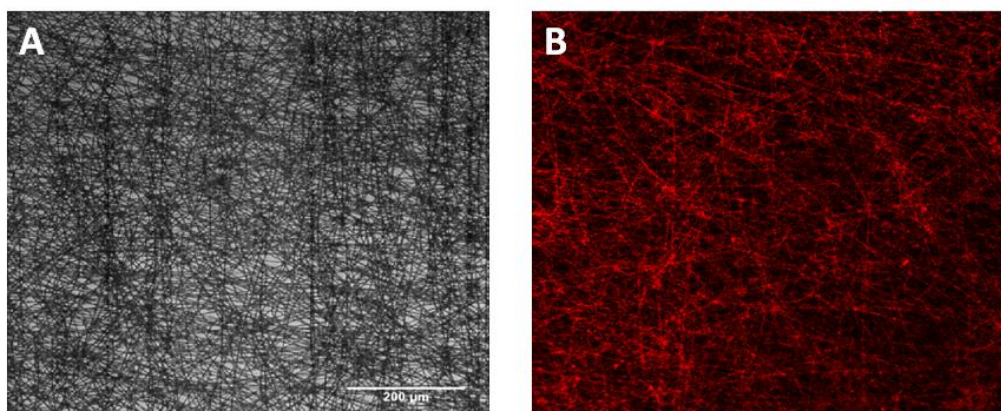


**Figure 55.** Fluorescent microscope observations of PA 300 + (bis)PEG-Alkyne after incubation in a Azide-dye / PBS solution **(A)** Bright Field **(B)** Far red channel. Scale bar = 200  $\mu\text{m}$ .

The adsorption process is also confirmed with the analysis of the negative controls, that showed no fluorescence properties under far-red light: the PA 300 scaffold after azide incubation (Figure 56) and the PA 300 + (bis)PEG-Alkyne scaffold before azide incubation (Figure 57). The first condition allows to exclude the relevance of the azide absorption process in the detectable fluorescence; on the other hand, as the PA 300 + (bis)PEG-Alkyne scaffold before azide incubation didn't show fluorescence, the auto-fluorescence process is also excluded.

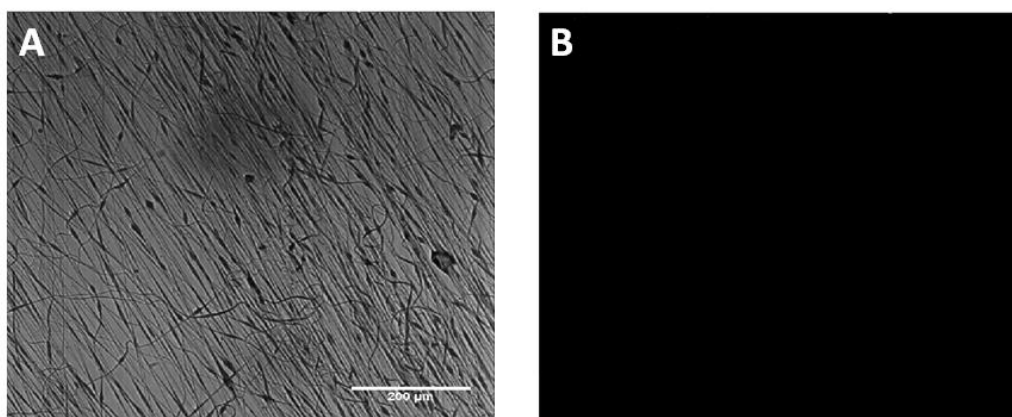


**Figure 56.** Fluorescent microscope observations of the negative control PA 300 after incubation in a Azide-dye / PBS solution **(A)** Bright Field **(B)** Far red channel. Scale bar = 200  $\mu\text{m}$ .

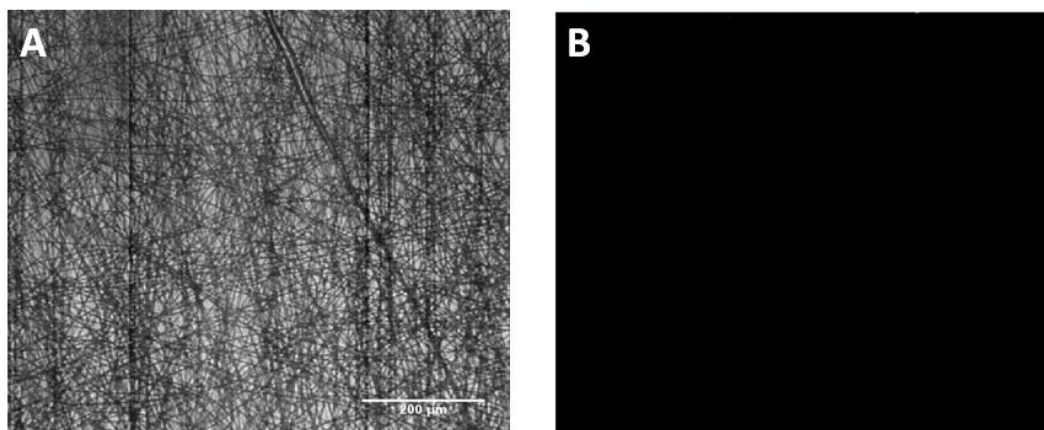


**Figure 57.** Fluorescent microscope observations of the negative control PA 300 + (bis)PEG-Alkyne before incubation in a Azide-dye / PBS solution **(A)** Bright Field **(B)** Far red channel. Scale bar = 200  $\mu\text{m}$ .

## 7. Discussion

The selection of PolyActive as biomaterial was made not only because of its physical and mechanical properties such as elasticity and toughness, but also because it is a well studied polymer with good levels of biocompatibility and biodegradability. Furthermore, this copolymer was already successfully electrospun and adapted for several tissue engineering applications due its versatility.

As explained in previous chapters, by shifting the weight ratios of the PEOT and PBT segments and the molecular weight of the PEG, a wide range of polymers with distinct mechanical, biological and physicochemical properties can be obtained. Papadaki et al. [19] have studied the effects of different PEGT/PBT weight percentages and two different molecular weights (300 Da and 1000 Da) of PEG in the behavior of two different cell lines: skeletal muscle cells and chondrocytes. The results have showed that the cell attachment, proliferation and differentiation depend not only on the copolymer composition, but also on the cell type used. In fact, the skeletal muscle cells exhibited maximum attachment, proliferation and differentiation on the 300PEGT55PBT45 substrate comparing with their response on the other scaffolds. On the other hand, chondrocytes exhibited a more pronounced cell response (attachment and proliferation) on the 1000PEGT70PBT30 substrate. The differences between the two scaffolds are more pronounced on the skeletal muscle cells behavior since their attachment is similar for 300PEGT55PBT45 and 1000PEGT55PBT45, but the proliferation is more accentuated on the 300PEGT55PBT45. This allows to conclude that for this particular cell line, the PEGT weight percentage is crucial for cell attachment purposes and the PEG molecular weight is important for proliferation. Generally, the scaffolds with higher percentage of PEOT (or PEGT) or higher PEG molecular weight present a more hydrophilic surface, which leads to a considerable higher water uptake and consequently to an elevated absorption of biomolecules and changes on the surface due swelling. The absorption process by annulling the adsorption of medium proteins and adhesion molecules on the surface of the scaffolds can reduce the attachment of cells that require a high level of adhesion biomolecules. In addition to this, longer PEG chains originate instability on the surface, leading to an inhibition of cell lines that exhibit high tensile stress.

The most popular PEOT/PBT copolymers combinations are 300PEOT55PBT45 and 1000PEOT70PBT30, and according to the literature, the PA 300 (55/45) induce superior cell responses and the PA 1000 (70/30) present better *in vivo* degradation. Although these scaffolds are commonly used in bone and skin tissue regeneration applications, modifications on their surfaces can help to optimize the advantages and reduce their weakness in order to produce more adaptable and suitable scaffolds for tissue engineering processes.

In the chapter 5 it was described that the introduction of oxygen containing functional groups to the PA 1000 surface via UV irradiation can influence protein adsorption and cell attachment. According to the ATR-FTIR analysis, there is a continuously increasing O-H peak area after the first 10 minutes of UV exposure, while there is a decrease in the ester, ether and aromatic associated peaks. This means that the functional groups are probably hydroxyl and carboxyl generated due the photo-oxidation of the PEO segment. The introduction of these oxygen groups are corroborated by the XPS results, which presents an increase on the O/C ratio after 40 minutes of UV irradiation.

Contrary to PA 1000, the modifications on the PA 300 electrospun fibres through UV exposure are mostly influenced by the degradation of the PBT segment, which results in the appearance of mono and di-hydroxy-substituted compounds on the aromatic rings. The instability of these compounds is visible in the evolution of the O-H ATR-FTIR peak area during 180 minutes of UV treatment: simultaneously to a decrease in the ATR-FTIR peak areas associated with the backbone main chain, the O-H region showed an oscillatory behavior during the first 90 minutes of UV exposure. This can be explained by the instability of the mono and di-hydroxy-substituted compounds, which can easily originate P-benzonquinones via a reversible redox reaction. After this period, a collapse of the aromatic ring is noticeable due to the decreasing O-H peak. The formation of P-benzonquinones is supported by the visible yellowing of the scaffolds and via XPS analysis by the decreasing on the O/C ratio after 40 minutes of UV exposure.

The scaffolds were treated by UV irradiation during 40 minutes with purpose of evaluating the influence that the oxygen containing functional groups on the PA 1000 surface and the presence of P-benzonquinones on the PA 300 surface have on the protein adsorption and cell attachment processes.

For both scaffolds, the fluorescent microscope observations were made by using the FITC-BSA protein as model protein. The comparison between untreated and treated samples showed that the detectable fluorescence only came from the UV treated scaffolds after FITC-BSA incubation, excluding the auto-fluorescence and the protein absorption phenomena influence on these observations. It was also tried an optimization of these results by adding the EDC/NHS complex in both scaffolds before FITC-BSA incubation; and, although the presence of carboxylic acids on the surface of both PA 1000 and PA 300 was observed after 40 minutes under UV irradiation, there was no detectable changes in the detectable fluorescent in the two cases. Because of that and to simplify the surface functionalization process, the EDC/NHS complex was eliminated from the methodology followed for the evaluation of the cell response. However, in the future, the influence of the EDC/NHS complex should be tested with a protein quantification process like the ninhydrin test. The protein adsorption tests also

included the modification of the fibre surface with a spatially defined UV exposure by using a mask for spatial patterning. The results show successfully and spatially controlled alterations in the degree of FITC-BSA adsorption on both UV treated scaffolds.

The results presented by the protein adsorption tests were confirmed by the interaction between the Rat Schwann Cells and the untreated and treated electrospun scaffolds. Although they had successfully attached on untreated and treated surfaces of both PA 1000 and PA 300 scaffolds, there was a clear preference for the activated areas on the surfaces treated with the UV mask, which means that there are more functional groups available after UV irradiation, and consequently more adsorbed adhesion proteins in these locations. This can be also validated by the higher number of cells on the UV treated scaffolds, comparing with the untreated samples.

The changes on the morphology of the cells were not noticeable between untreated and treated surfaces. However the PEG molecular weight and the percentage of the copolymers PEOT/PBT seem to affect Rat Schwann cells morphology. Indeed, when cultured on the PA 1000 samples, the cells showed a flattened pattern. On the other end, on the surface of the PA 300, the cells presented a spindle shaped morphology. Similar differences were reported by Chew et al. [140], that have studied the effects of aligned and random PCL fibrous scaffolds in the morphology of the Rat Schwann cells. The results showed that the cells were able to elongate unidirectionally along the fibre axes on aligned electrospun, but when cultured on a random fibrous scaffold, the cells adopted a random orientation and a spread-out morphology. Based on these results, there is a possibility that the variations in the cell morphology may occur due to slight differences in the alignment of the electrospun fibres in both PA 1000 and PA 300. One hypothesis is that, although the same electrospinning set up was used for both copolymers, the PA 1000 electrospinning jet was able to discharge its electric charge more efficiently to the water vapor molecules in the atmosphere, comparing with the PA 300 jet that is more hydrophobic. As a considerable portion of the charge from the PA 1000 jet is discharged during electrospinning, the generated fibres will be less charged and, consequently, the influence of the electrodes that are responsible for their alignment will be less significant. In addition to this, the long PEG chains and the high PEO content of the PA 1000 can easily be affected by the aqueous environment during the cell culture protocol, leading to an increasing instability on the polymer backbone chain that can originate deviations from the original fibre alignment. Finally, in order to complete the analysis described in the section 5.3, a Real-time PCR analysis can be done in the future with the purpose of study the maturation of the Rat Schwann cells on the PA 300 and PA 1000 untreated and treated scaffolds [140]; another possibility is using other cell line, such as skeletal muscle cells, that need more adhesion proteins on the surface to attach, than the rat Schwann cells [19]. In this way it would be easier to

observe differences in the attachment process between untreated and UV treated PolyActive samples.

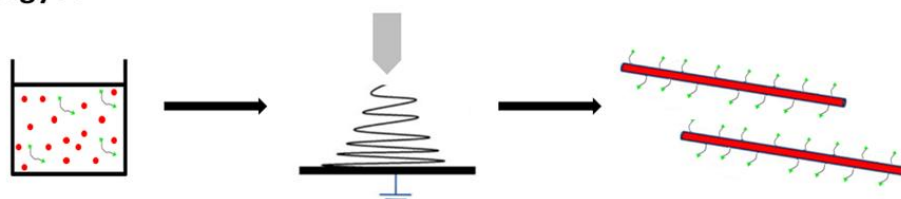
The modification of the PA 300 and PA 1000 surfaces by UV irradiation proved to be able to improve protein adsorption and it has also showed promising results in enhancing cell attachment. So, it is reasonable to consider UV treatment as a valid alternative to other PolyActive functionalization techniques such as plasma activation. Claase et al. [141] have exhaustively explored strategies to functionalize the surface of PA 1000 scaffolds: firstly, they used acidic and alkaline treatments to modify the surface, however the acidic treatment did not enhance cell attachment and growth and the alkaline treatment has resulted in severe surface degradation. In another approach, hydroxyapatite (HA) was incorporated on the PA 1000 scaffolds to augment the proteins adsorption and consequently increase the bone marrow stromal cell adhesion and growth. This methodology only showed positive results on particular areas of the scaffold because the cells were able to attach to the added HA but not to the copolymer. The same authors have explored the effects of the CO<sub>2</sub> gas plasma treatment on the surface of the PA 1000 films, and likewise what was described in chapter 5, it resulted in the generation of oxygen containing functional groups on the surface of the scaffold and in a subsequent increment of protein adsorption from the medium, leading to an effective attachment of the bone marrow stromal cells. In another approach, Nandakumar et al. [98] have successfully modify the surface of PA 300 electrospun scaffolds via oxygen plasma in order to optimize the human mesenchymal stromal cells (hMSC) adhesion and proliferation. It was demonstrated that the treated scaffolds showed higher oxygen content on their surface, comparing to the untreated ones, which is associated with the presence of functional groups like hydroxyl and carboxyl. These functional groups were able to enhance the medium protein adsorption process, leading to an improved attachment and proliferation of the hMSC.

The strategies described above can be optimized by incorporating functionalized PEG linkers on the surface with the purpose of having a preferential immobilization of functional biomolecules or nanostructures. In this way, a single scaffold is able to possess binding areas with specific affinities in order to selectively immobilize biomolecules on particular regions of the surface and consequently build a complex and organized cell guide system.

An innovative and original technique to modify the PA 300 (55/45) surface is suggested in the chapter 6. The strategy adopted in this chapter has the purpose of modifying the surface of the PA 300 electrospun scaffold by adding functionalized PEG in the polymer solution before the electrospinning process. The goal is endow the copolymer surface with specific functional groups without previous surface treatments or incubation periods. The Figure 58 compare the approach suggested on chapter 6

(strategy A) with the common procedure for incorporate functionalized PEG linkers on the surface of electrospun scaffolds (strategy B). Basically, the strategy A describes that the functionalized PEG should be mixed together with the polymer in a blending solution before the electrospinning process. At the end, the fibres should have incorporated the functional groups on their surface for further biomolecule immobilization. The success of this strategy will open the window for new surface modification methodologies since it is a much efficient and practical approach than the strategy B, which describes a complex approach: in the first phase of the process, the polymer of interest is electrospun; then, depending on the intrinsic characteristics of the fibrous scaffold, the resultant fibres can be treated by a specific surface modification technique, leading to the formation of functional groups able to crosslink with one terminal of the functionalized PEG during an incubation period. The other terminal of the functionalized PEG will then immobilize specific biomolecules. The strategy B was described in the section 5.2, when the complex NHS/EDC was incorporated on the surface of both PA 1000 and PA 300 electrospun fibres.

#### Strategy A



#### Strategy B

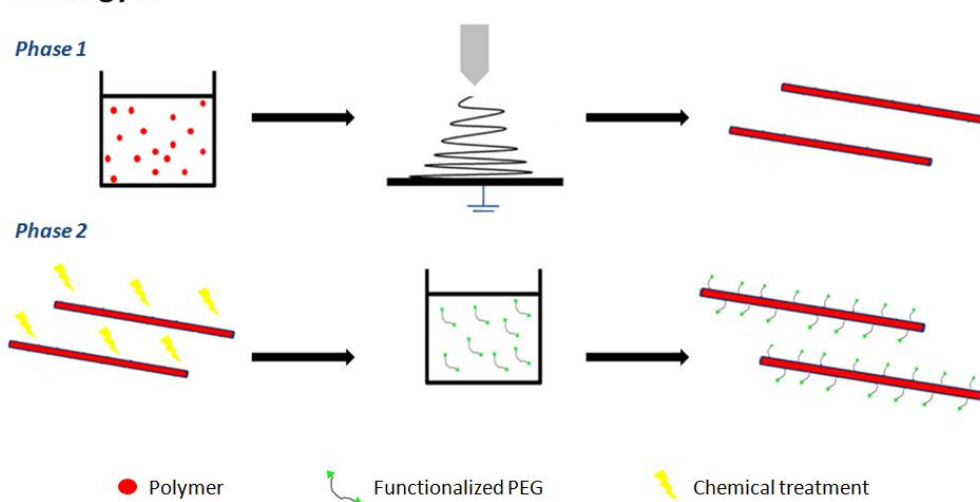


**Figure 58.** Incorporation of functionalized PEG linkers on the surface of electrospun scaffolds by two different strategies.

The incorporation of the functionalized PEG linkers can lead to an increase in the chain instability of the target polymer because augmenting its length also increases the hydrophilic properties of the polymer. Therefore, to avoid a fast degradation by



hydrolysis and to ensure a proper polymer length, the copolymer PA 300 was selected to test the viability of the strategy A. The (bis)PEG-SVA and (bis)PEG-Alkyne were chosen as functionalized PEG linkers because they allow to explore two different kinds of immobilization processes: by the NHS-ester – protein interaction (section 6.1.1.) and via the “click chemistry” approach (section 6.2.1.).

The PA 300 + (bis)PEG-SVA ATR-FTIR spectrum allowed to confirm a higher polymer backbone length, comparing with PA 300 by itself, but it was not conclusive about the presence of NHS on the surface of the fibres. However, this result is acceptable since the proportion of PA 300 per (bis)PEG-SVA is 4:1, and therefore it is plausible that the peaks originated from the NHS stretches, which are usually located at  $1719\text{ cm}^{-1}$ ,  $1745\text{ cm}^{-1}$  and  $1818\text{ cm}^{-1}$ , are barely noticeable. On the other hand, the XPS analysis was able to prove the presence of the NHS-ester on the surface of the fibres by the appearance of one peak at 401.5 eV, which can be associated with this functional group. The FITC-BSA was used as model protein to test the ability of the PA300 + (bis)PEG-SVA in immobilize proteins. The results have definitely confirmed the presence of the functional groups on the surface of the fibres since the only detectable fluorescence signal was originated from the PA300 + (bis)PEG-SVA scaffold after FITC-BSA incubation.

The ATR-FTIR and XPS analysis of the PA 300 + (bis)PEG-Alkyne scaffolds were only able to demonstrate the increase of the polymer chain due the adding of the (bis)PEG-Alkyne (section 6.2.2.), in fact none of the spectra have showed new peaks. However, the presence of the alkyne terminals on the surface of the fibres was confirmed by the click chemistry test (section 6.2.3.). Indeed, the fluorescent azides were immobilized only by the PA 300 + (bis)PEG-Alkyne electrospun scaffolds.

Although the presented results allow to conclude that the PEG linker functional groups were successfully incorporated on the surface of the scaffolds, it would be interesting, in the future, to test the cell response (adhesion, proliferation and differentiation) on similar scaffolds and also analyze the PA 300 + (bis)PEG-SVA and PA 300 + (bis)PEG-Alkyne electrospun scaffolds via TOF-SIMS, which is the most sensitive surface analysis technique.

In summary, the strategy followed in chapter 6 proved to be a simple and efficient approach to functionalize electrospun scaffolds. In fact, comparing to other surface modification techniques such as the one presented on chapter 5, this original approach avoids a large variety of disadvantages like degradation due photo-exposure or hydrolysis, as well as other problems related with energetic beams like wave diffraction, scattering and backscattering. One possible application for this surface modification technique is the fabrication of electrospun scaffolds with two different types of fibres, resulting in two incorporated chemical groups for later functionalization. This approach involves an adaptation of the traditional

electrospinning set up since it demands that two spinnerets electrospin the different bending solutions (Polymer A + functionalized PEG linker A and Polymer B + functionalized PEG linker B) at same time. Then, the right conformation of the electrodes will generate a scaffold divided by two different types of fibres with distinct functional groups. As each kind of fibre has affinity with one specific type of biomolecule, it will be possible to functionalize the electrospun scaffold with high spatial definition. This type of scaffold could be very helpful for tissue engineering applications that involve the segregation of a mixed cell population since different cell lines have affinity with different type of biomolecules (Figure 59).

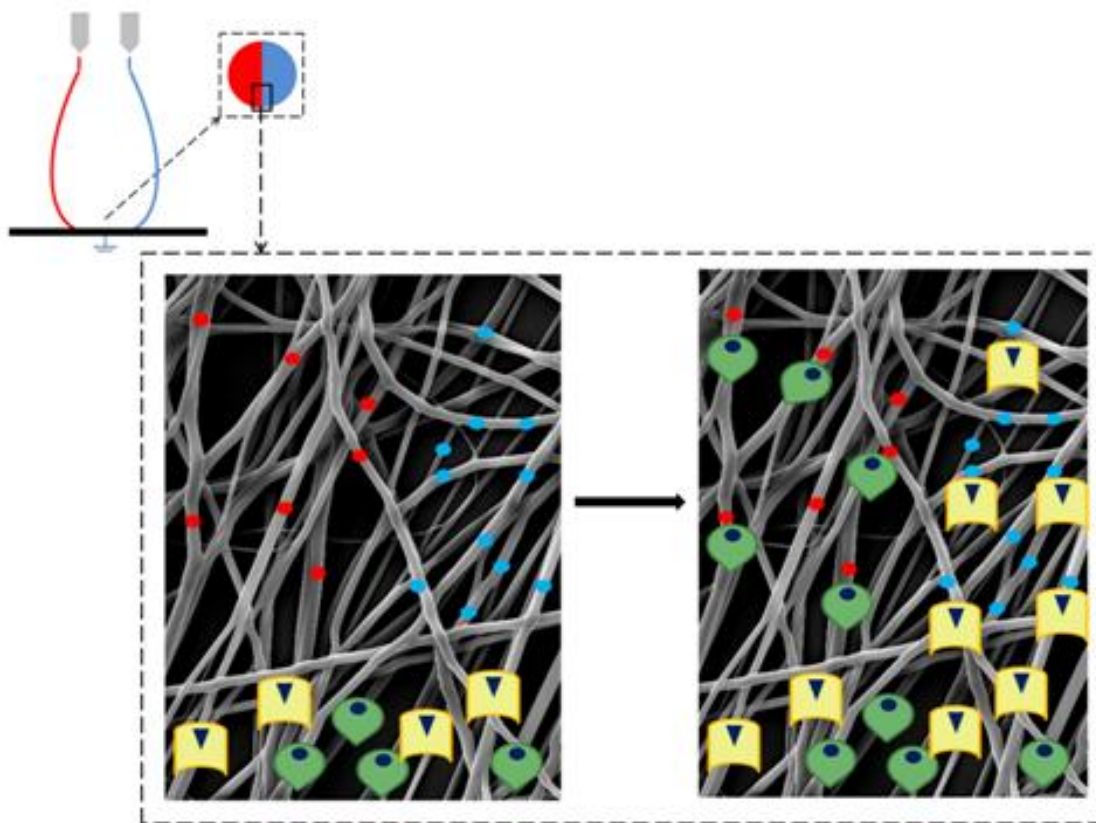


**Figure 59.** Segregation of a mixed cell population.

## 8. Conclusion

The design and fabrication of biofunctional tissue engineering scaffolds involve a wide range of challenges from the selection of the bulk material to the tailoring of the mechanical, physical and biological functionalities. So, towards developing the next generation of tissue regenerative interfaces, electrospun scaffolds of PEOT/PBT copolymers were successfully produced in order to provide topographical and biochemical cues for cell guidance. Indeed, the scaffolds were designed and fabricated to mimic the natural extracellular cell matrix by including aligned fibres and chemical functional groups on their surface for later biomolecules immobilization.

The alignment and deposition of the electrospun fibres were managed by using the gap method under a controlled environment and the biochemical cues were introduced on the surface after the application of two distinct surface modification techniques: UV irradiation and incorporation of functionalized PEG linkers.

In the study presented in the Chapter 5 it was shown that UV irradiation can be used to modify the surface properties of both PA 300 and PA 1000 electrospun scaffolds by introducing new functional groups onto the scaffolds surfaces in order to improve the protein adsorption from the culture medium and consequently increase the available areas for cell adhesion. These areas could be spatially controlled by using a UV mask able to modify the degree of protein adsorption on electrospun fibres and consequently provide different cell responses (cell attachment, proliferation, differentiation, migration) on the same scaffold, depending on the copolymer composition and on the cell type used. In addition to this, the UV treatment offers the opportunity to create complex surface compositions for both soft- and hard-tissue applications because it can enhance the immobilization of proteins independently of the variations in the PEOT/PBT weight percentage and in the PEG molecular weight present on the copolymer composition.

The innovative approach investigated in the Chapter 6 described the incorporation of the functional groups originated from specific PEG linkers on the surface of PA 300 electrospun scaffolds before the electrospinning process. To my knowledge, it was the first time that (bis)PEG-SVA and (bis)PEG-Alkyne were electrospun together with a copolymer, leading to the fabrication of functional fibres with NHS-esters and Alkynes on their surface, respectively. These incorporated functional groups are able to allow a selective immobilization of biomolecules onto the surface of the electrospun fibres, avoiding unspecific adsorption and giving to the scaffold a high degree of specificity. In reality, this original concept can be adopted for multiple tissue engineering applications since it presents a simple and efficient methodology to develop biofunctional electrospun scaffolds able to reproduce complex cell microenvironments.

## 9. References

1. Ji W, Sun Y, Yang F, van den Beucken JJ, Fan M, et al. (2011) Bioactive electrospun scaffolds delivering growth factors and genes for tissue engineering applications. *Pharm Res* 28: 1259-1272.
2. Williams D (2008) Chapter 9 - Biocompatibility. In: Clemens van B, Peter T, Anders L, Jeffrey H, David FW et al., editors. *Tissue Engineering*. Burlington: Academic Press. pp. 255-278.
3. Yang S, Leong KF, Du Z, Chua CK (2001) The design of scaffolds for use in tissue engineering. Part I. Traditional factors. *Tissue Eng* 7: 679-689.
4. Ma PX (2008) Biomimetic materials for tissue engineering. *Advanced Drug Delivery Reviews* 60: 184-198.
5. O'Brien FJ (2011) Biomaterials & scaffolds for tissue engineering. *Materials Today* 14: 88-95.
6. Heise U, Osborn JF, Duwe F (1990) Hydroxyapatite ceramic as a bone substitute. *Int Orthop* 14: 329-338.
7. Yoshikawa H, Myoui A (2005) Bone tissue engineering with porous hydroxyapatite ceramics. *J Artif Organs* 8: 131-136.
8. Brahatheeswaran Dhandayuthapani YY, Toru Maekawa, D Sakthi Kumar (2011) Polymeric Scaffolds in Tissue Engineering Application: A Review. *International Journal of Polymer Science* 2011.
9. Gomes M, Azevedo H, Malafaya P, Silva S, Oliveira J, et al. (2008) Chapter 6 - Natural Polymers in tissue engineering applications. In: Clemens van B, Peter T, Anders L, Jeffrey H, David FW et al., editors. *Tissue Engineering*. Burlington: Academic Press. pp. 145-192.
10. Khaing ZZ, Schmidt CE (2012) Advances in natural biomaterials for nerve tissue repair. *Neurosci Lett* 519: 103-114.
11. Venkatesan J, Kim SK (2010) Chitosan composites for bone tissue engineering--an overview. *Mar Drugs* 8: 2252-2266.
12. Dang JM, Leong KW (2006) Natural polymers for gene delivery and tissue engineering. *Adv Drug Deliv Rev* 58: 487-499.
13. Yoshimoto H, Shin YM, Terai H, Vacanti JP (2003) A biodegradable nanofiber scaffold by electrospinning and its potential for bone tissue engineering. *Biomaterials* 24: 2077-2082.
14. Bini TB, Gao S, Wang S, Ramakrishna S (2006) Poly(l-lactide-co-glycolide) biodegradable microfibers and electrospun nanofibers for nerve tissue engineering: an in vitro study. *Journal of Materials Science* 41: 6453-6459.
15. van Dijkhuizen-Radersma R, Moroni L, Apeldoorn Av, Zhang Z, Grijpma D (2008) Chapter 7 - Degradable polymers for tissue engineering. In: Clemens van B, Peter T, Anders L, Jeffrey H, David FW et al., editors. *Tissue Engineering*. Burlington: Academic Press. pp. 193-221.
16. Deschamps AA, Grijpma DW, Feijen J (2001) Poly(ethylene oxide)/poly(butylene terephthalate) segmented block copolymers: the effect of copolymer composition on physical properties and degradation behavior. *Polymer* 42: 9335-9345.
17. Moroni L, Licht R, de Boer J, de Wijn JR, van Blitterswijk CA (2006) Fiber diameter and texture of electrospun PEOT/PBT scaffolds influence human mesenchymal stem cell proliferation and morphology, and the release of incorporated compounds. *Biomaterials* 27: 4911-4922.
18. Deschamps AA, van Apeldoorn AA, Hayen H, de Bruijn JD, Karst U, et al. (2004) In vivo and in vitro degradation of poly(ether ester) block copolymers based on poly(ethylene glycol) and poly(butylene terephthalate). *Biomaterials* 25: 247-258.
19. Papadaki M, Mahmood T, Gupta P, Claase MB, Grijpma DW, et al. (2001) The different behaviors of skeletal muscle cells and chondrocytes on PEGT/PBT block copolymers are related to the surface properties of the substrate. *Journal of biomedical materials research* 54: 47-58.

20. Moroni L, de Wijn JR, van Blitterswijk CA (2005) Three-dimensional fiber-deposited PEOT/PBT copolymer scaffolds for tissue engineering: influence of porosity, molecular network mesh size, and swelling in aqueous media on dynamic mechanical properties. *Journal of biomedical materials research Part A* 75: 957-965.
21. Moroni L, Poort G, Van Keulen F, de Wijn JR, van Blitterswijk CA (2006) Dynamic mechanical properties of 3D fiber-deposited PEOT/PBT scaffolds: an experimental and numerical analysis. *Journal of biomedical materials research Part A* 78: 605-614.
22. Qian Z, Li S, He Y, Liu X (2004) Synthesis and in vitro degradation study of poly(ethylene terephthalate)/poly(ethylene glycol) (PET/PEG) multiblock copolymer. *Polymer Degradation and Stability* 83: 93-100.
23. Morlat S, Gardette J-L (2001) Phototransformation of water-soluble polymers. I: photo- and thermooxidation of poly(ethylene oxide) in solid state. *Polymer* 42: 6071-6079.
24. Gijssman P, Meijers G, Vitarelli G (1999) Comparison of the UV-degradation chemistry of polypropylene, polyethylene, polyamide 6 and polybutylene terephthalate. *Polymer Degradation and Stability* 65: 433-441.
25. Kaurav S (2011) *Engineering Chemistry with Laboratory Experiments*: PHI Learning.
26. Sharma BK (1981) *Spectroscopy*: Krishna Prakashan.
27. Rabek JF (1995) *Polymer Photodegradation: Mechanisms and Experimental Methods*: Chapman & Hall.
28. Howard JA, Ingold KU (1968) Self-reaction of sec-butylperoxy radicals. Confirmation of the Russell mechanism. *Journal of the American Chemical Society* 90: 1056-1058.
29. Han S, Kim C, Kwon D (1997) Thermal/oxidative degradation and stabilization of polyethylene glycol. *Polymer* 38: 317-323.
30. Hassouna F, Morlat-Thélias S, Mailhot G, Gardette JL (2007) Influence of water on the photodegradation of poly(ethylene oxide). *Polymer Degradation and Stability* 92: 2042-2050.
31. Fachine GJM, Rabello MS, Souto Maior RM, Catalani LH (2004) Surface characterization of photodegraded poly(ethylene terephthalate). The effect of ultraviolet absorbers. *Polymer* 45: 2303-2308.
32. Tabankia MH, Gardette J-L (1986) Photo-chemical degradation of polybutyleneterephthalate: Part 1—Photo-oxidation and photolysis at long wavelengths. *Polymer Degradation and Stability* 14: 351-365.
33. Rivaton A, Gardette J-L (1998) Photo-oxidation of aromatic polymers. *Die Angewandte Makromolekulare Chemie* 261-262: 173-188.
34. Carroccio S, Rizzarelli P, Scaltro G, Puglisi C (2008) Comparative investigation of photo- and thermal-oxidation processes in poly(butylene terephthalate). *Polymer* 49: 3371-3381.
35. Valk VG, Kehren ML, Daamen I (1970) Über die Photooxidation von Polyäthylenglykolteterephthalat-Fasern. *Die Angewandte Makromolekulare Chemie* 13: 97-107.
36. Gardette J-L, Mailhot B, Posada F, Rivaton A, Wilhelm C (1999) Photooxidative degradation of polyether-based polymers. *Macromolecular Symposia* 143: 95-109.
37. Vasita R, Katti DS (2006) Nanofibers and their applications in tissue engineering. *Int J Nanomedicine* 1: 15-30.
38. Dahlin RL, Kasper FK, Mikos AG (2011) Polymeric nanofibers in tissue engineering. *Tissue Eng Part B Rev* 17: 349-364.
39. Lu T, Li Y, Chen T (2013) Techniques for fabrication and construction of three-dimensional scaffolds for tissue engineering. *Int J Nanomedicine* 8: 337-350.
40. Hutmacher D, Woodfield T, Dalton P, Lewis J (2008) Chapter 14 - Scaffold design and fabrication. In: Clemens van B, Peter T, Anders L, Jeffrey H, David FW et al., editors. *Tissue Engineering*. Burlington: Academic Press. pp. 403-454.
41. Shin HJ, Lee CH, Cho IH, Kim YJ, Lee YJ, et al. (2006) Electrospun PLGA nanofiber scaffolds for articular cartilage reconstruction: mechanical stability, degradation and cellular responses under mechanical stimulation in vitro. *J Biomater Sci Polym Ed* 17: 103-119.

42. Alves da Silva ML, Martins A, Costa-Pinto AR, Costa P, Faria S, et al. (2010) Cartilage Tissue Engineering Using Electrospun PCL Nanofiber Meshes and MSCs. *Biomacromolecules* 11: 3228-3236.
43. Jeong SI, Krebs MD, Bonino CA, Samorezov JE, Khan SA, et al. (2011) Electrospun chitosan-alginate nanofibers with in situ polyelectrolyte complexation for use as tissue engineering scaffolds. *Tissue Eng Part A* 17: 59-70.
44. Pham QP, Sharma U, Mikos AG (2006) Electrospinning of polymeric nanofibers for tissue engineering applications: a review. *Tissue Eng* 12: 1197-1211.
45. Nezarati RM, Eifert MB, Cosgriff-Hernandez E (2013) Effects of humidity and solution viscosity on electrospun fiber morphology. *Tissue Eng Part C Methods* 19: 810-819.
46. Chan BP, Leong KW (2008) Scaffolding in tissue engineering: general approaches and tissue-specific considerations. *European Spine Journal* 17: 467-479.
47. Causa F, Netti PA, Ambrosio L (2007) A multi-functional scaffold for tissue regeneration: The need to engineer a tissue analogue. *Biomaterials* 28: 5093-5099.
48. Mukhatyar VJ, Salmeron-Sanchez M, Rudra S, Mukhopadaya S, Barker TH, et al. (2011) Role of fibronectin in topographical guidance of neurite extension on electrospun fibers. *Biomaterials* 32: 3958-3968.
49. Holland TA, Tabata Y, Mikos AG (2005) Dual growth factor delivery from degradable oligo(poly(ethylene glycol) fumarate) hydrogel scaffolds for cartilage tissue engineering. *Journal of Controlled Release* 101: 111-125.
50. Wang C, Wang M, Yuan X-Y (2012) Novel Electrospun Bicomponent Scaffolds for Bone Tissue Engineering: Fabrication, Characterization and Sustained Release of Growth Factor. *MRS Online Proceedings Library* 1418: null-null.
51. Rim NG, Shin CS, Shin H (2013) Current approaches to electrospun nanofibers for tissue engineering. *Biomed Mater* 8: 014102.
52. Agarwal S, Wendorff JH, Greiner A (2010) Chemistry on electrospun polymeric nanofibers: merely routine chemistry or a real challenge? *Macromol Rapid Commun* 31: 1317-1331.
53. Jacobs T, Morent R, Geyter N, Dubruel P, Leys C (2012) Plasma Surface Modification of Biomedical Polymers: Influence on Cell-Material Interaction. *Plasma Chemistry and Plasma Processing* 32: 1039-1073.
54. Yoo HS, Kim TG, Park TG (2009) Surface-functionalized electrospun nanofibers for tissue engineering and drug delivery. *Advanced Drug Delivery Reviews* 61: 1033-1042.
55. Siow KS, Britcher L, Kumar S, Griesser HJ (2006) Plasma Methods for the Generation of Chemically Reactive Surfaces for Biomolecule Immobilization and Cell Colonization - A Review. *Plasma Processes and Polymers* 3: 392-418.
56. He W, Ma Z, Yong T, Teo WE, Ramakrishna S (2005) Fabrication of collagen-coated biodegradable polymer nanofiber mesh and its potential for endothelial cells growth. *Biomaterials* 26: 7606-7615.
57. Duan Y, Wang Z, Yan W, Wang S, Zhang S, et al. (2007) Preparation of collagen-coated electrospun nanofibers by remote plasma treatment and their biological properties. *J Biomater Sci Polym Ed* 18: 1153-1164.
58. Koh HS, Yong T, Chan CK, Ramakrishna S (2008) Enhancement of neurite outgrowth using nano-structured scaffolds coupled with laminin. *Biomaterials* 29: 3574-3582.
59. Chen JP, Su CH (2011) Surface modification of electrospun PLLA nanofibers by plasma treatment and cationized gelatin immobilization for cartilage tissue engineering. *Acta Biomaterialia* 7: 234-243.
60. Park J, Kim J-M, Lee S, Lee S, Jeong Y-K, et al. (2007) Surface hydrolysis of fibrous poly( $\epsilon$ -caprolactone) scaffolds for enhanced osteoblast adhesion and proliferation. *Macromolecular Research* 15: 424-429.
61. Welle A (2004) Competitive plasma protein adsorption on modified polymer surfaces monitored by quartz crystal microbalance technique. *J Biomater Sci Polym Ed* 15: 357-370.

62. Welle A, Kroger M, Doring M, Niederer K, Pindel E, et al. (2007) Electrospun aliphatic polycarbonates as tailored tissue scaffold materials. *Biomaterials* 28: 2211-2219.
63. Son WK, Youk JH, Park WH (2006) Antimicrobial cellulose acetate nanofibers containing silver nanoparticles. *Carbohydrate Polymers* 65: 430-434.
64. Chua K-N, Chai C, Lee P-C, Ramakrishna S, Leong KW, et al. (2007) Functional nanofiber scaffolds with different spacers modulate adhesion and expansion of cryopreserved umbilical cord blood hematopoietic stem/progenitor cells. *Experimental Hematology* 35: 771-781.
65. Chua K-N, Lim W-S, Zhang P, Lu H, Wen J, et al. (2005) Stable immobilization of rat hepatocyte spheroids on galactosylated nanofiber scaffold. *Biomaterials* 26: 2537-2547.
66. Shin YM, Kim KS, Lim YM, Nho YC, Shin H (2008) Modulation of spreading, proliferation, and differentiation of human mesenchymal stem cells on gelatin-immobilized poly(L-lactide-co--caprolactone) substrates. *Biomacromolecules* 9: 1772-1781.
67. Shin Y, Shin H, Lim Y (2010) Surface modification of electrospun poly(L-lactide-co-ε-caprolactone) fibrous meshes with a RGD peptide for the control of adhesion, proliferation and differentiation of the preosteoblastic cells. *Macromolecular Research* 18: 472-481.
68. Lee K, Silva EA, Mooney DJ (2011) Growth factor delivery-based tissue engineering: general approaches and a review of recent developments. *J R Soc Interface* 8: 153-170.
69. Silva AK, Richard C, Bessodes M, Scherman D, Merten OW (2009) Growth factor delivery approaches in hydrogels. *Biomacromolecules* 10: 9-18.
70. Sahoo S, Ang LT, Goh JC, Toh SL (2010) Growth factor delivery through electrospun nanofibers in scaffolds for tissue engineering applications. *Journal of biomedical materials research Part A* 93: 1539-1550.
71. Goh Y-F, Shakir I, Hussain R (2013) Electrospun fibers for tissue engineering, drug delivery, and wound dressing. *Journal of Materials Science* 48: 3027-3054.
72. Nie H, Soh BW, Fu YC, Wang CH (2008) Three-dimensional fibrous PLGA/HAp composite scaffold for BMP-2 delivery. *Biotechnol Bioeng* 99: 223-234.
73. Nie H, Wang C-H (2007) Fabrication and characterization of PLGA/HAp composite scaffolds for delivery of BMP-2 plasmid DNA. *Journal of Controlled Release* 120: 111-121.
74. Kowalczyk T, Nowicka A, Elbaum D, Kowalewski TA (2008) Electrospinning of Bovine Serum Albumin. Optimization and the Use for Production of Biosensors. *Biomacromolecules* 9: 2087-2090.
75. Zhang YZ, Wang X, Feng Y, Li J, Lim CT, et al. (2006) Coaxial electrospinning of (fluorescein isothiocyanate-conjugated bovine serum albumin)-encapsulated poly(epsilon-caprolactone) nanofibers for sustained release. *Biomacromolecules* 7: 1049-1057.
76. Liu JJ, Wang CY, Wang JG, Ruan HJ, Fan CY (2011) Peripheral nerve regeneration using composite poly(lactic acid-caprolactone)/nerve growth factor conduits prepared by coaxial electrospinning. *Journal of biomedical materials research Part A* 96: 13-20.
77. Carnell LS, Siochi EJ, Holloway NM, Stephens RM, Rhim C, et al. (2008) Aligned Mats from Electrospun Single Fibers. *Macromolecules* 41: 5345-5349.
78. Usman Ali YZ, Xungai Wang, Tong Lin (2011) Electrospinning of Continuous Nanofiber Bundles and Twisted Nanofiber Yarns, *Nanofibers - Production, Properties and Functional Applications*. In: (Ed.) DTL, editor.
79. Ramakrishna S (2005) *An Introduction to Electrospinning and Nanofibers*: World Scientific.
80. Aviss KJ, Gough JE, Downes S (2010) Aligned electrospun polymer fibres for skeletal muscle regeneration. *Eur Cell Mater* 19: 193-204.
81. Corey JM, Lin DY, Mycek KB, Chen Q, Samuel S, et al. (2007) Aligned electrospun nanofibers specify the direction of dorsal root ganglia neurite growth. *Journal of biomedical materials research Part A* 83: 636-645.
82. Xu CY, Inai R, Kotaki M, Ramakrishna S (2004) Aligned biodegradable nanofibrous structure: a potential scaffold for blood vessel engineering. *Biomaterials* 25: 877-886.

83. Mo XM, Xu CY, Kotaki M, Ramakrishna S (2004) Electrospun P(LLA-CL) nanofiber: a biomimetic extracellular matrix for smooth muscle cell and endothelial cell proliferation. *Biomaterials* 25: 1883-1890.
84. Chen M, Patra PK, Warner SB, Bhowmick S (2007) Role of fiber diameter in adhesion and proliferation of NIH 3T3 fibroblast on electrospun polycaprolactone scaffolds. *Tissue Eng* 13: 579-587.
85. Balci M (2005) *Basic <sup>1</sup>H- and <sup>13</sup>C-NMR Spectroscopy*: Elsevier Science.
86. Richards SA, Hollerton JC (2010) *Essential Practical NMR for Organic Chemistry*: Wiley.
87. James TL (1998) *Fundamentals of NMR*. Department of Pharmaceutical Chemistry University of California San Francisco, CA 94143-0446 USA.
88. California Uo UC Davis ChemWiki.
89. Bruno TJ, Svoronos PDN (2011) *CRC Handbook of Basic Tables for Chemical Analysis*, Third Edition: Taylor & Francis.
90. Xu Z, Huang X, Wan L (2009) *Surface Engineering of Polymer Membranes*: Zhejiang University Press.
91. Sung L-P, Jasmin J, Gu X, Nguyen T, Martin J (2004) Use of laser scanning confocal microscopy for characterizing changes in film thickness and local surface morphology of UV-exposed polymer coatings. *JCT Research* 1: 267-276.
92. Stamm M (2008) *Polymer Surfaces and Interfaces: Characterization, Modification and Applications*: Springer.
93. Haggerty R (1999) *Numerical Integration Using Excel*.
94. Tao Y, Cheng ZL, Ting KE, Yin XJ (2013) Photocatalytic Degradation of Phenol Using a Nanocatalyst: The Mechanism and Kinetics. *Journal of Catalysts* 2013: 6.
95. Moctezuma E, Zermeño B, Zarazua E, Torres-Martínez L, García R (2011) Photocatalytic Degradation of Phenol with Fe-Titania Catalysts. *Topics in Catalysis* 54: 496-503.
96. Grabowska E, Reszczyńska J, Zaleska A (2012) Mechanism of phenol photodegradation in the presence of pure and modified-TiO<sub>2</sub>: A review. *Water Research* 46: 5453-5471.
97. Bigger SW, Scheirs J, Delatycki O, Billingham NC (1991) Effects of frequency, molecular weight and thermal oxidation on the dynamic mechanical response of poly (ethylene oxide). *Polymer International* 26: 181-186.
98. Nandakumar A, Tahmasebi Birgani Z, Santos D, Mentink A, Auffermann N, et al. (2013) Surface modification of electrospun fibre meshes by oxygen plasma for bone regeneration. *Biofabrication* 5: 015006.
99. Voger EA, Bussian RW (1987) Short-term cell-attachment rates: a surface-sensitive test of cell-substrate compatibility. *Journal of biomedical materials research* 21: 1197-1211.
100. Morrison M, Steele W, Danner DJ (1969) The reaction of benzoquinone with amines and proteins. *Archives of Biochemistry and Biophysics* 134: 515-523.
101. Wang A, Zhang F, Chen F, Wang M, Li H, et al. (2011) A facile technique to prepare cross-linked enzyme aggregates using p-benzoquinone as cross-linking agent. *Korean Journal of Chemical Engineering* 28: 1090-1095.
102. Nithianandam VS, Erhan S (1991) Quinone—amine polymers: 10. Use of calcium hypochlorite in the syntheses of polyamine—quinone (PAQ) polymers. *Polymer* 32: 1146-1149.
103. Friedrich J, Loeschcke I, Frommelt H, Reiner H-D, Zimmermann H, et al. (1991) Ageing and degradation of poly(ethylene terephthalate) in an oxygen plasma. *Polymer Degradation and Stability* 31: 97-114.
104. Olde Riekerink MB, Claase MB, Engbers GH, Grijpma DW, Feijen J (2003) Gas plasma etching of PEO/PBT segmented block copolymer films. *Journal of biomedical materials research Part A* 65: 417-428.
105. Solomon D, Lehmann J, Kinyangi J, Liang B, Heymann K, et al. (2009) Carbon (1s) NEXAFS Spectroscopy of Biogeochemically Relevant Reference Organic Compounds All rights reserved. No part of this periodical may be reproduced or transmitted in any form or by any means, electronic or mechanical, including photocopying, recording, or any information storage and



retrieval system, without permission in writing from the publisher. Permission for printing and for reprinting the material contained herein has been obtained by the publisher. *Soil Sci Soc Am J* 73: 1817-1830.

106. Papenburg BJ, Rodrigues ED, Wessling M, Stamatialis D (2010) Insights into the role of material surface topography and wettability on cell-material interactions. *Soft Matter* 6: 4377-4388.

107. Hermanson GT (2010) *Bioconjugate Techniques*: Elsevier Science.

108. Ju S, Yeo WS (2012) Quantification of proteins on gold nanoparticles by combining MALDI-TOF MS and proteolysis. *Nanotechnology* 23: 135701.

109. Delaittre G, Greiner AM, Pauloehrl T, Bastmeyer M, Barner-Kowollik C (2012) Chemical approaches to synthetic polymer surface biofunctionalization for targeted cell adhesion using small binding motifs. *Soft Matter* 8: 7323-7347.

110. Marcotte L, Tabrizian M (2008) Sensing surfaces: Challenges in studying the cell adhesion process and the cell adhesion forces on biomaterials. *IRBM* 29: 77-88.

111. Arima Y, Iwata H (2007) Effects of surface functional groups on protein adsorption and subsequent cell adhesion using self-assembled monolayers. *Journal of Materials Chemistry* 17: 4079-4087.

112. O'Keefe EJ, Woodley D, Castillo G, Russell N, Payne RE, Jr. (1984) Production of soluble and cell-associated fibronectin by cultured keratinocytes. *J Invest Dermatol* 82: 150-155.

113. Gupta D, Venugopal J, Prabhakaran MP, Dev VRG, Low S, et al. (2009) Aligned and random nanofibrous substrate for the in vitro culture of Schwann cells for neural tissue engineering. *Acta Biomaterialia* 5: 2560-2569.

114. Schlosshauer B, Muller E, Schroder B, Planck H, Muller H (2003) Rat Schwann cells in bioresorbable nerve guides to promote and accelerate axonal regeneration. *Brain Research* 963: 321-326.

115. Jung-Testas I, Schumacher M, Bugnard H, Baulieu E-E (1993) Stimulation of rat Schwann cell proliferation by estradiol: synergism between the estrogen and cAMP. *Developmental Brain Research* 72: 282-290.

116. Masaeli E, Morshed M, Nasr-Esfahani MH, Sadri S, Hilderink J, et al. (2013) Fabrication, characterization and cellular compatibility of poly(hydroxy alkanoate) composite nanofibrous scaffolds for nerve tissue engineering. *PLoS One* 8: e57157.

117. Roberts MJ, Bentley MD, Harris JM (2002) Chemistry for peptide and protein PEGylation. *Adv Drug Deliv Rev* 54: 459-476.

118. Lee H, Park TG (2003) A novel method for identifying PEGylation sites of protein using biotinylated PEG derivatives. *Journal of Pharmaceutical Sciences* 92: 97-103.

119. Cheng T-L, Chuang K-H, Chen B-M, Roffler SR (2012) Analytical Measurement of PEGylated Molecules. *Bioconjugate Chemistry* 23: 881-899.

120. Mougín K, Ham AS, Lawrence MB, Fernandez EJ, Hillier AC (2005) Construction of a tethered poly(ethylene glycol) surface gradient for studies of cell adhesion kinetics. *Langmuir* 21: 4809-4812.

121. Lu HB, Campbell CT, Castner DG (2000) Attachment of Functionalized Poly(ethylene glycol) Films to Gold Surfaces. *Langmuir* 16: 1711-1718.

122. Harbers GM, Emoto K, Greef C, Metzger SW, Woodward HN, et al. (2007) A functionalized poly(ethylene glycol)-based bioassay surface chemistry that facilitates bio-immobilization and inhibits non-specific protein, bacterial, and mammalian cell adhesion. *Chem Mater* 19: 4405-4414.

123. Sokic S, Papavasiliou G (2012) Controlled proteolytic cleavage site presentation in biomimetic PEGDA hydrogels enhances neovascularization in vitro. *Tissue Eng Part A* 18: 2477-2486.

124. Sun X, Zhang G, Patel D, Stephens D, Gobin AM (2012) Targeted cancer therapy by immunoconjugated gold-gold sulfide nanoparticles using Protein G as a cofactor. *Ann Biomed Eng* 40: 2131-2139.

125. DeLong SA, Moon JJ, West JL (2005) Covalently immobilized gradients of bFGF on hydrogel scaffolds for directed cell migration. *Biomaterials* 26: 3227-3234.
126. Lahiri J, Isaacs L, Tien J, Whitesides GM (1999) A Strategy for the Generation of Surfaces Presenting Ligands for Studies of Binding Based on an Active Ester as a Common Reactive Intermediate: A Surface Plasmon Resonance Study. *Analytical Chemistry* 71: 777-790.
127. Aguilera JM, Lillford PJ (2008) *Food Materials Science: Principles and Practice*: Springer.
128. Im J-E, Han J-A, Kim BK, Han JH, Park TS, et al. (2010) Electrochemical detection of estrogen hormone by immobilized estrogen receptor on Au electrode. *Surface and Coatings Technology* 205, Supplement 1: S275-S278.
129. Le Droumaguet B, Velonia K (2008) Click Chemistry: A Powerful Tool to Create Polymer-Based Macromolecular Chimeras. *Macromolecular Rapid Communications* 29: 1073-1089.
130. Binder WH, Sachsenhofer R (2008) 'Click' Chemistry in Polymer and Material Science: An Update. *Macromolecular Rapid Communications* 29: 952-981.
131. Rostovtsev VV, Green LG, Fokin VV, Sharpless KB (2002) A stepwise Huisgen cycloaddition process: copper(I)-catalyzed regioselective "ligation" of azides and terminal alkynes. *Angew Chem Int Ed Engl* 41: 2596-2599.
132. Bock VD, Hiemstra H, van Maarseveen JH (2006) CuI-Catalyzed Alkyne-Azide "Click" Cycloadditions from a Mechanistic and Synthetic Perspective. *European Journal of Organic Chemistry* 2006: 51-68.
133. van Dijk M, van Nostrum CF, Hennink WE, Rijkers DTS, Liskamp RMJ (2010) Synthesis and Characterization of Enzymatically Biodegradable PEG and Peptide-Based Hydrogels Prepared by Click Chemistry. *Biomacromolecules* 11: 1608-1614.
134. Johnson JA, Finn MG, Koberstein JT, Turro NJ (2008) Construction of Linear Polymers, Dendrimers, Networks, and Other Polymeric Architectures by Copper-Catalyzed Azide-Alkyne Cycloaddition "Click" Chemistry. *Macromolecular Rapid Communications* 29: 1052-1072.
135. Durmaz H, Dag A, Altintas O, Erdogan T, Hizal G, et al. (2006) One-Pot Synthesis of ABC Type Triblock Copolymers via in situ Click [3 + 2] and Diels-Alder [4 + 2] Reactions. *Macromolecules* 40: 191-198.
136. Durmaz YY, Sangermano M, Yagci Y (2010) Surface modification of UV-cured epoxy resins by click chemistry. *Journal of Polymer Science Part A: Polymer Chemistry* 48: 2862-2868.
137. Li Z, Seo TS, Ju J (2004) 1,3-Dipolar cycloaddition of azides with electron-deficient alkynes under mild condition in water. *Tetrahedron Letters* 45: 3143-3146.
138. Rozkiewicz DI, Jańczewski D, Verboom W, Ravoo BJ, Reinhoudt DN (2006) "Click" Chemistry by Microcontact Printing. *Angewandte Chemie International Edition* 45: 5292-5296.
139. Moses JE, Moorhouse AD (2007) The growing applications of click chemistry. *Chem Soc Rev* 36: 1249-1262.
140. Chew SY, Mi R, Hoke A, Leong KW (2008) The effect of the alignment of electrospun fibrous scaffolds on Schwann cell maturation. *Biomaterials* 29: 653-661.
141. Claase MB, Olde Riekerink MB, de Bruijn JD, Grijpma DW, Engbers GH, et al. (2003) Enhanced bone marrow stromal cell adhesion and growth on segmented poly(ether ester)s based on poly(ethylene oxide) and poly(butylene terephthalate). *Biomacromolecules* 4: 57-63.